UNCLASSIFIED

SECURITY CLASSIFICATION OF THIS PAGE *(When Data Entered)*

REPORT DOCUMENTATION PAGE		READ INSTRUCTIONS BEFORE COMPLETING FORM
1. REPORT NUMBER AFGL-TR-79-0285	2. GOVT ACCESSION NO.	3. RECIPIENT'S CATALOG NUMBER
4. TITLE *(and Subtitle)* PRELIMINARY ANALYSIS & MODELLING BASED UPON PROJECT OPAQUE PROFILE & SURFACE DATA		5. TYPE OF REPORT & PERIOD COVERED Scientific - Interim Scientific Report No. 12 6. PERFORMING ORG. REPORT NUMBER SIO Ref. 80-5
7. AUTHOR(s) Richard W. Johnson, Wayne S. Hering, Jacqueline I. Gordon, Bruce W. Fitch, Janet E. Shields		8. CONTRACT OR GRANT NUMBER(s) F19628-78-C-0200
9. PERFORMING ORGANIZATION NAME AND ADDRESS University of California, San Diego Visibility Laboratory La Jolla, California 92093		10. PROGRAM ELEMENT, PROJECT, TASK AREA & WORK UNIT NUMBERS 62101F 7670-14-01
11. CONTROLLING OFFICE NAME AND ADDRESS Air Force Geophysics Laboratory Hanscom AFB, Massachusetts 01731 Contract Monitor: Major Ted S. Cress/OPA		12. REPORT DATE November 1979 13. NUMBER OF PAGES 50
14. MONITORING AGENCY NAME & ADDRESS*(if different from Controlling Office)*		15. SECURITY CLASS. *(of this report)* UNCLASSIFIED 15a. DECLASSIFICATION/DOWNGRADING SCHEDULE

16. DISTRIBUTION STATEMENT *(of this Report)*

Distribution limited to U.S. Government agencies only; (Foreign Information); 16 November 1979. Other requests for this document must be referred to AFGL/OPA, Hanscom AFB, Massachusetts 01731

17. DISTRIBUTION STATEMENT *(of the abstract entered in Block 20, if different from Report)*

18. SUPPLEMENTARY NOTES

19. KEY WORDS *(Continue on reverse side if necessary and identify by block number)*

Atmospheric Optical Properties
Atmospheric Scattering Coefficients
Atmospheric Profile Models
Equilibrium Radiance
OPAQUE
Ground Level Optical & Meteorological Measurements
Sky-Ground Ratio

20. ABSTRACT *(Continue on reverse side if necessary and identify by block number)*

This report surveys portions of the optical and meteorological measurements collected during Program OPAQUE. Two sets of data are addressed, the first is surface data collected by the participating scientific teams associated with the NATO Research Study Group 8 of Panel IV, AC243, and the second represents vertical profile measurements made by Visibility Laboratory in cooperation with and under the sponsorship of the Air Force Geophysics Laboratory. Two reports closely related to this initial survey report are AFGL-TR-78-0011, Fenn (1978) and AFGL-TR-78-0286, Duntley, *et al.* (1978).

DD FORM 1 JAN 73 1473 EDITION OF 1 NOV 65 IS OBSOLETE
S/N 0102-014-6601

UNCLASSIFIED

SECURITY CLASSIFICATION OF THIS PAGE *(When Data Entered)*

20. ABSTRACT continued:

Data availability and its applicability to the general task of modelling atmospheric optical properties are discussed, as are recommendations for the most promising approaches to the modelling task. Samples of a model fit to the vertical profile of atmospheric volume scattering coefficient are included with discussion.

AFGL-TR-79-0285 SIO Ref. 80-5

PRELIMINARY ANALYSIS & MODELLING BASED UPON PROJECT OPAQUE PROFILE & SURFACE DATA

Richard W. Johnson, Wayne S. Hering, Jacqueline I. Gordon,
Bruce W. Fitch, and Janet E. Shields

Visibility Laboratory
University of California, San Diego
Scripps Institution of Oceanography
La Jolla, California 92093

Approved:

Roswell W. Austin, Acting Director
Visibility Laboratory

Approved:

William A. Nierenberg, Director
Scripps Institution of Oceanography

CONTRACT NO. F19628-78-C-0200
Project No. 7670
Task No. 7670-14
Work Unit No. 7670-14-01

Scientific Report No. 12
November 1979

Contract Monitor
Major Ted S. Cress, Atmospheric Optics Branch, Optical Physics Division

Prepared for
AIR FORCE GEOPHYSICS LABORATORY
AIR FORCE SYSTEMS COMMAND
UNITED STATES AIR FORCE
HANSCOM AFB, MASSACHUSETTS 01731

SUMMARY

This initial scientific survey report has been prepared under the terms of the Air Force Geophysics Laboratory Contract No. F19628-78-C-0200. It addresses the initial development of modelling procedures related to atmospheric optical/infra-red properties based upon the data collected during Program OPAQUE. The data base considered includes both the surface measurements made by the various participating members of the NATO Research Study Group 8 of Panel IV, AC243, and the vertical profile and multi-level airborne measurements made by the technical team representing the Visibility Laboratory and the Air Force Geophysics Laboratory.

The data availability within these two data bases is addressed, as is its applicability to the general modelling goals. The surface data is found to need additional editing and review prior to its general use in the determination of inter-parameter relationships. Selected sub-sets however appear to contain adequate information for immediate investigation, such as the study of surface layer directional scattering characteristics. The airborne data are found to contain data of adequate quantity and quality to formulate a preliminary model of visible spectrum volume scattering coefficient profiles based upon atmospheric temperature lapse rates. A discussion describing the utilization of the data in developing preliminary modelling of the directional scattering properties of the lower troposphere is also included.

General recommendations are presented for the development of selected sub-sets of carefully edited measurements for application to the modelling effort in both the visible and infra-red regimes.

TABLE OF CONTENTS

LIST OF ILLUSTRATIONS

1. INTRODUCTION

This survey report has been prepared for the Air Force Geophysics Laboratory under contract F19628-78-C-0200. It addresses the interpretation of an extensive set of optical and meteorological data collected mostly in northern Europe during the interval 1 April 1976 through 30 September 1978. These data fall basically into two subsets, the first being those airborne data collected by the Visibility Laboratory in cooperation with and under the sponsorship of the Air Force Geophysics Laboratory. This subset, described and summarized in AFGL-TR-78-0286, Duntley, *et al.* (1978c), will in general be referred to as the OPAQUE flight data. The second subset contains those data collected by several European, Canadian and U. S. scientific teams operating under the NATO Research Study Group 8 of Panel IV, AC 243. This ground based data set and its conceptual organization is fully described in AFGL-TR-78-0011, Fenn, (1978), and will normally be referred to as the OPAQUE surface data. In both cases the acronym OPAQUE designates the RSG-8 program for measuring OPtical Atmospheric QUantities in Europe.

The general European locale for both the airborne and surface measurements is illustrated in Fig. 1-1 which has been abstracted from Duntley, *et al.* (1978c). Within this geographical context and within the time frame associated with the surface measurement program, there were eighty-six sets of profile measurements accomplished, as illustrated in Table 1.1. The temporal relationship between these airborne data and the surface data which have been available for analysis during this

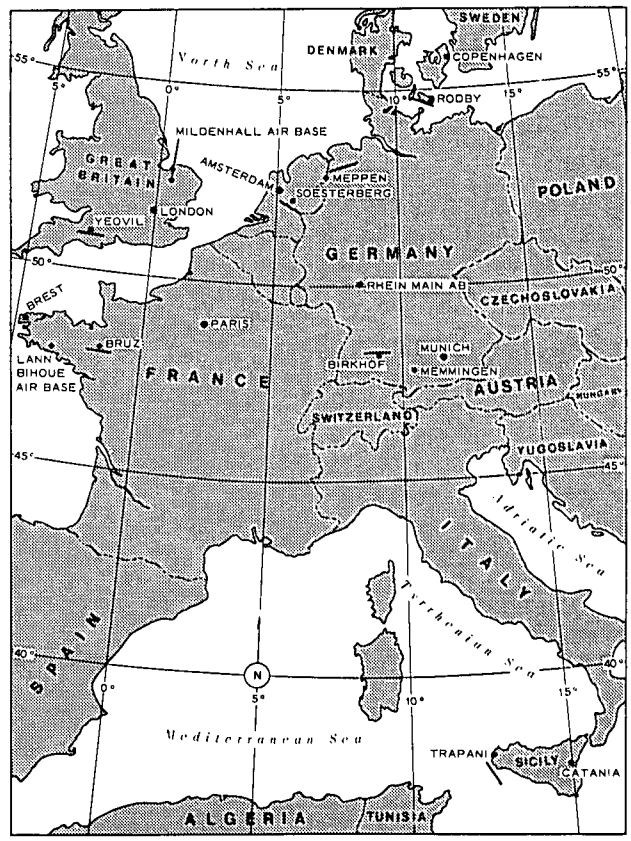

Fig. 1-1. Typical OPAQUE Flight Tracks & Surface Data Sites.

Table 1.1.

Geographical Distribution of Project OPAQUE Data Flights

Flight Track Ident	Attempted (and reported) Data Sequences					
	OPAQUE I Spring '76	OPAQUE II Fall '76	OPAQUE III Summer '77	OPAQUE IV Winter '78	OPAQUE V Summer '78	Total
Sigonella, Sicily*	0	0	0	2 (2)	0	2 (2)
Trapani, Sicily	0	0	0	3 (3)	4	7 (3)
Bruz, France	0	5 (5)	3 (3)	0	0	8 (8)
Birkhof, Germany	0	0	0	8 (7)	5	13 (7)
Yeovil, England	5 (3)	0	0	5 (5)	3	13 (8)
Soesterberg, Netherlands	1 (1)	0	1 (0)	2 (2)	2	6 (3)
Mildenhall, England*	0	0	0	2 (2)	0	2 (2)
Ahlhorn, Germany*	0	0	2 (2)	0	0	2 (2)
Meppen, Germany	5 (2)	4 (3)	3 (3)	3 (3)	4	19 (11)
Rodby, Denmark	2 (2)	4 (4)	4 (4)	2 (2)	2	14 (12)
TOTAL	13 (8)	13 (12)	13 (12)	27 (26)	20	86 (58)

*These track locations, while not specifically anticipated for use during the OPAQUE program, were flown as "tracks of opportunity" during several instances when local weather conditions rendered the initially planned track unuseable.

initial study interval is illustrated in Fig. 1-2. In this composite figure, the OPAQUE surface data availability is represented by heavily shaded horizontal bars in the seven horizontal rows, one row for each of the seven participating data stations. In this representation, each month long block of data is identified with a "1" or a "2", to identify the source tape from which it was extracted. The lightly shaded vertical bars represent the interval during which the airborne measurements were being conducted and the symbol "c" indicates the approximate time at which coincident airborne and surface measurements should occur within the two data sets. For data processed as of September 1979, no instances of coincident flight data and surface data were available for analysis. However, as this data processing proceeds, many sets of coincident data will become available for direct comparison and study.

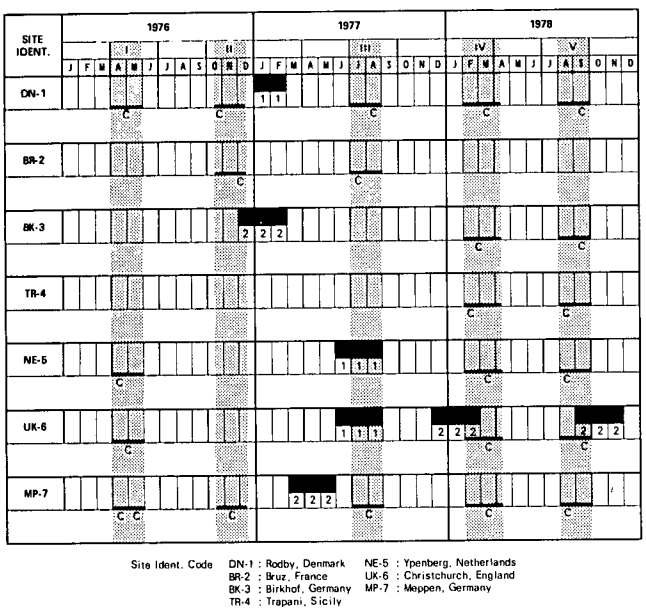

Fig. 1-2. OPAQUE Airborne & Surface Data Availability.

This report summarizes preliminary investigations based upon the OPAQUE data that have been addressed during the initial phase of this contract interval, and identifies those considered most promising to yield the predictive correlations and models desired for improving optical forecasting capability.

The general experimental procedure around which these studies have been oriented is illustrated in Fig. 1-3. In this schematic diagram the overall approach to the prediction of atmospheric aerosol effects upon optical/infra-red transmissions from ground level observations is indicated. As illustrated, the more immediately addressable goal of approaching this capability is via the airborne profile data collected by the C-130 system. In either of the illustrated procedures, the direct anticlockwise route or the indirect clockwise route, the key element is the existence of the comprehensive surface data base generated by the OPAQUE program. This unique data set with its near simultaneous measurements within the three regimes required for technique development, *i.e.* the visible and infra-red optical regimes plus the surface meteorological regime, represents the surface layer Rosetta stone through which the desired inter-regime relationships can be established. The subsequent air to surface link can be addressed via the visible spectrum optical measurements produced by the C-130 flight program in conjunction with their contemporary sets of surface data. As the optical-meteorological relationships illustrated within these two data sets become more clearly established, then the integration of the aerosol size distribution measurements which have accompanied both sets should provide the guidance required for closing the experimental loop between the visible and infra-red optical effects.

The following sections of this report discuss the progress made in establishing this analytic approach, and recommend the direction in which the continuing effort might most fruitfully be directed.

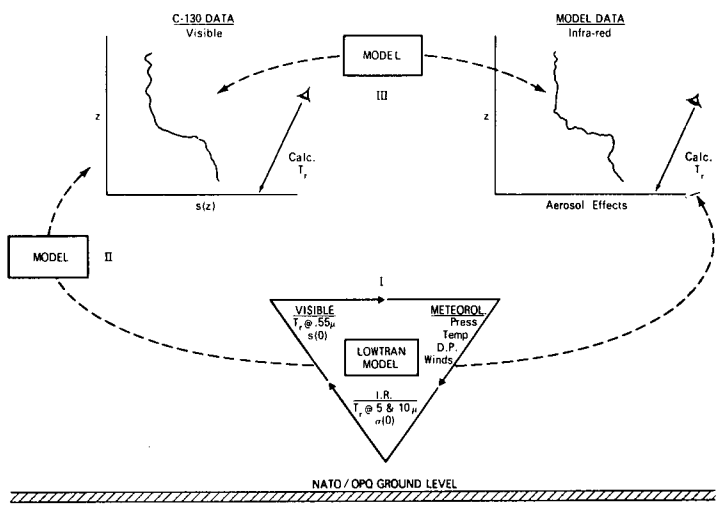

Fig. 1-3. General Experimental Procedure.

2. DATA BASE DESCRIPTION & AVAILABILITY

Neither the OPAQUE flight data nor the OPAQUE surface data are fully available for analysis and interpretation at this time. However, there are adequate amounts from both sets to establish a reasonable methodology and to attempt a variety of preliminary studies. Examples of the primary data available for use during these initial studies are included in this section in conjunction with a selection of brief explanatory comments.

2.1 OPAQUE FLIGHT DATA

The five deployments summarized in Table 1.1 indicate the number of flight profiles that were available for analysis during this initial phase. The profile data for the first three OPAQUE deployments have been available in finished-report format throughout the interval, and the data from the OPAQUE IV deployment have been available in draft form. The general analysis and modelling efforts discussed in Section 4 have used the earlier data, since direct extraction from the report format greatly simplified the procedures and avoided any conflict with the preparation of the OPAQUE IV final copy.

The three reports that provided the flight data were, AFGL-TR-77-0078, AFGL-TR-77-0239, and AFGL-TR-78-0168, Duntley, *et al.* (1977, 1978a and 1978b).

The airborne profile data which are typical of those available from each data sequence listed in Table 1.1 are illustrated in Figs. 2-1 and 2-2. In these plots of measured and derived parameters, the plot format is as described in the three parent reports and thus is only briefly commented upon herein. These data from flight C-418 were abstracted from the OPAQUE III, Summer 1977 report.

In Fig. 2-1 the measured quantities, total volume scattering coefficient, and ambient temperature plus the derived relative humidity are plotted as a function of altitude above ground level.

In Fig. 2-2 the additional derived quantities, Mie volume scattering coefficient, the ratio of total to Rayleigh volume scattering coefficients, and absolute humidity are also plotted as a function of altitude above ground level.

It should be noted, that there is atmospheric temporal variability information also available within these profile plots. Since the elapsed times between each two ascent plots, *i.e.* those coded 2 and 4, and each two descent plots *i.e.* those coded 3 and 5, is approximately

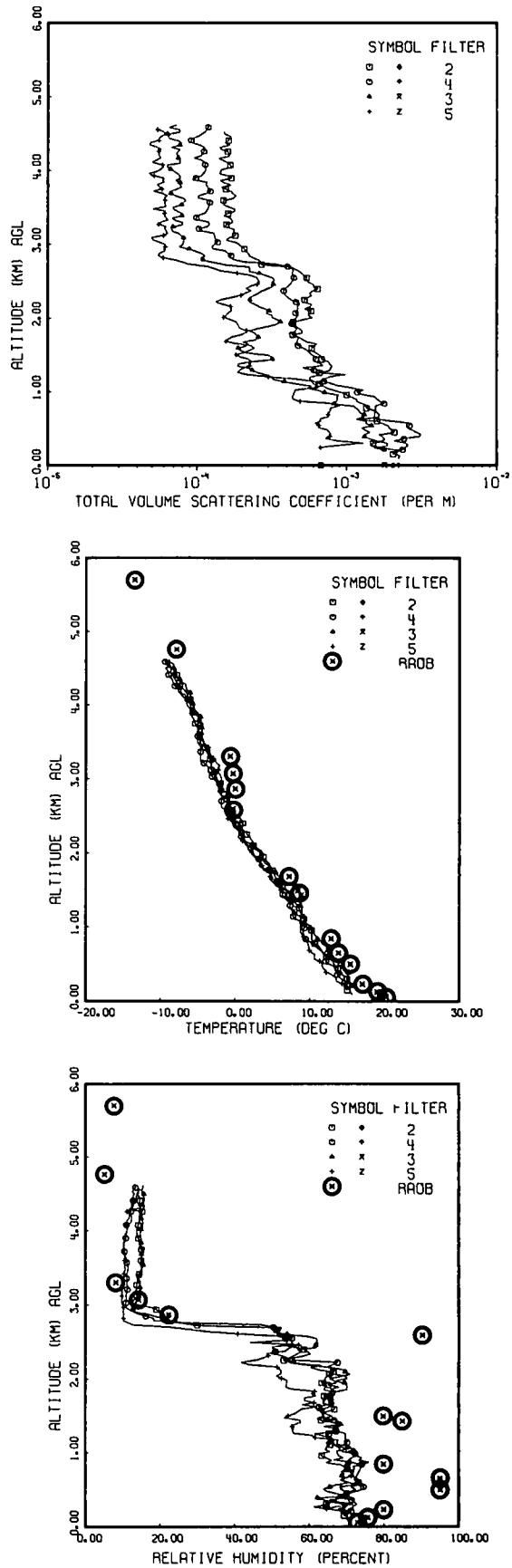

Fig. 2-1. Typical OPAQUE Flight Data, Measured Profiles.

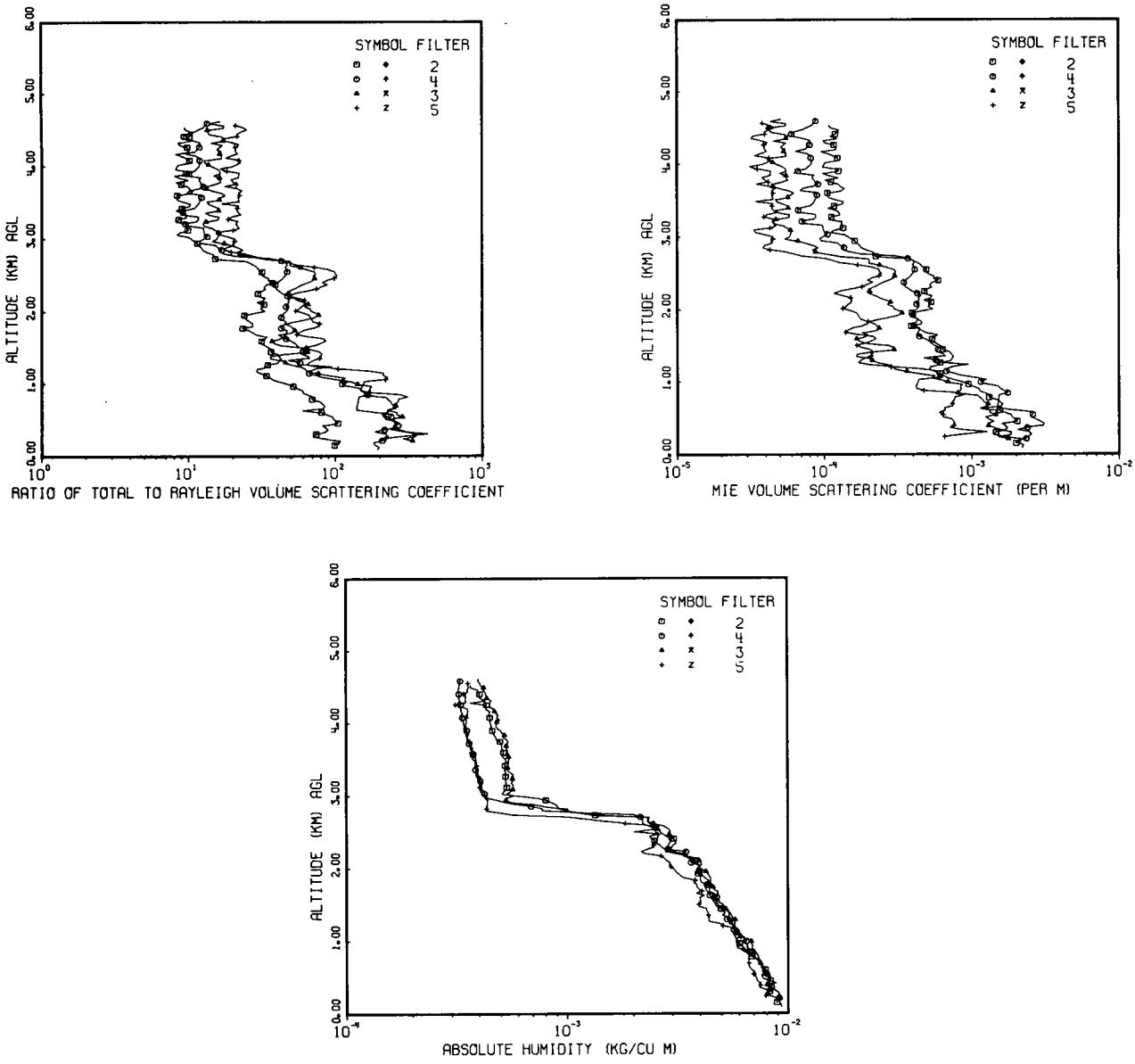

Fig. 2-2. Typical OPAQUE Flight Data, Derived Profiles.

two hours, one may fairly attribute any changes in the inter-filter relationships to small-scale fluctuations in the parameter under measurement. As discussed in Section 4, calculated short-period variability can serve as a baseline for analysis of forecasting accuracy.

Radiosonde data from the reporting station nearest each flight track is also indicated on the OPAQUE profile plots as illustrated in Fig. 2-1. A study of the correlations between these independently acquired measurements and those obtained from the OPAQUE flight profiles provides an additional potential link between the relatively small number of OPAQUE flight samples and the statistically broader European meteorological network.

2.2 OPAQUE SURFACE DATA

The fundamental data base generated at each of the seven OPAQUE experimental stations is fully described in AFGL-TR-78-0011, Fenn (1978). Thus, only a summary of those data evaluated for this study will be included herein. For each data interval examined, a standardized set of graphical displays was produced to aid in the initial assessment of data completeness, reliability and representativeness. In each instance there were fourteen plots illustrating parameter values as a function of time over a 24 hour period. Those "standard time plots" are listed in Table 2.1 and illustrated in Fig. 2-3.

Table 2.1.
OPAQUE Surface Data

STANDARD TIME PLOTS (14)

Plot No.	Measured Quantity			Quantity Description	Units
1..	SMAX & SMIN	vs	Time	Visible Scattering Coefficient (nephelometer)	km^{-1}
2.	SEMAX & SEMIN	vs	"	Visible Extinction Coefficient (transmissometer)	km^{-1}
3.	T1 & T5	vs	"	Infra-red Transmittance (3-5μm, First & Last)	%
4.	T2 & T3	vs	"	Infra-red Transmittance (8-12μm & 8-13μm)	%
5.	TX	vs	"	Infra-red Transmittance (-)	%
6.	PRESS	vs	"	Atmospheric pressure	mb
7.	TEMP	vs	"	Ambient Temperature	°C
8.	RH	vs	"	Relative Humidity (or Dewpoint Temp)	% (°C)
9.	NCLD	vs	"	Cloud Cover	Octals
10.	WS10	vs	"	Wind Speed @ 10m	m/sec
11.	EVN & EVS	vs	"	Illumination (Vertical Surface - North & South)	lux
12.	EVE & EVW	vs	"	Illumination (Vertical Surface - East & West)	lux
13.	EHMAX & EHMIN	vs	"	Illumination (Horizontal Surface)	lux
14.	LPMAX & LPMIN	vs	"	Path Function (Night - East - 100m)	cd/m^2

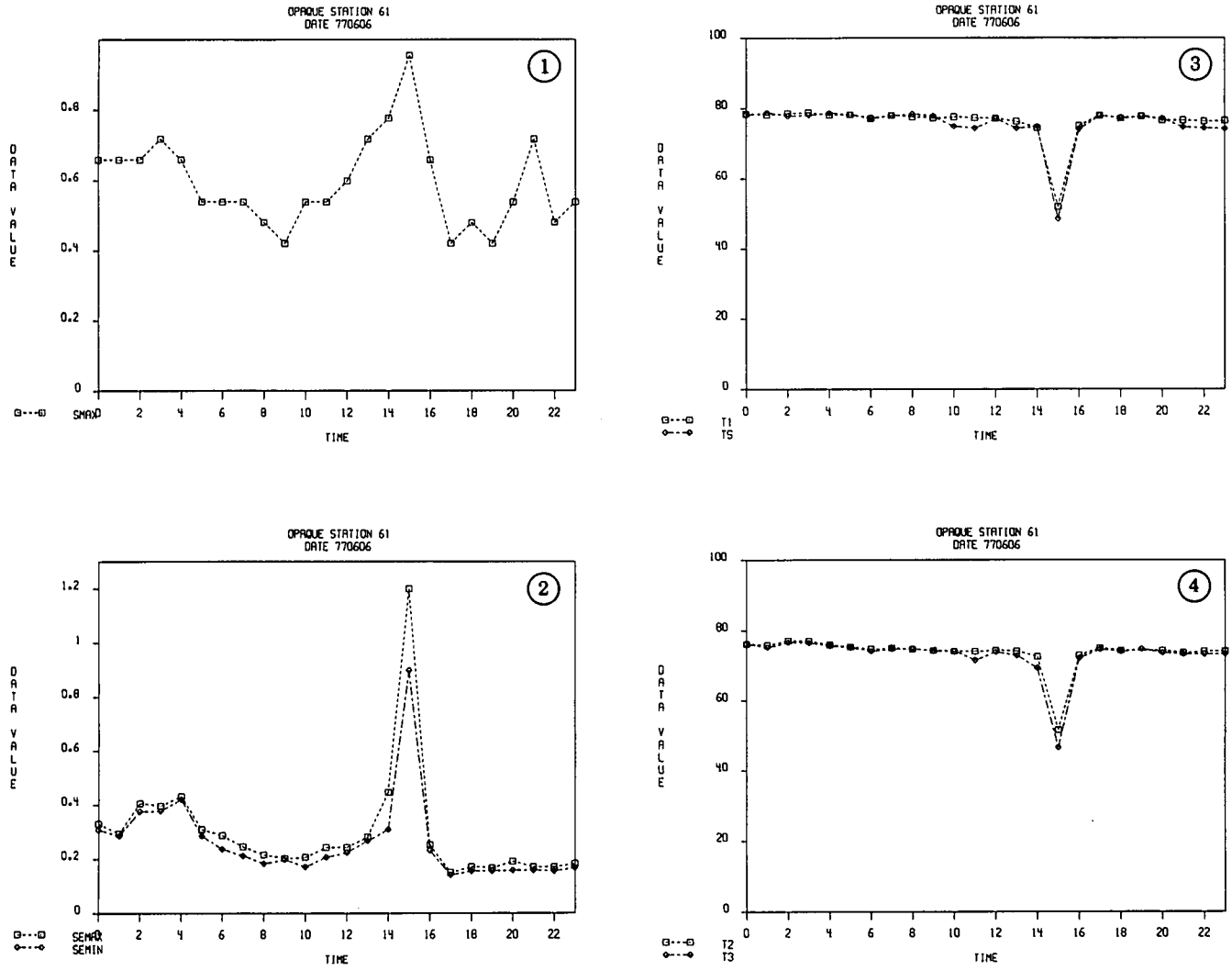

Fig. 2-3. Typical OPAQUE Surface Data, Hourly Time Plots. Station "61" identifies the data as being an initial issue (1) originating from the UK station (6).

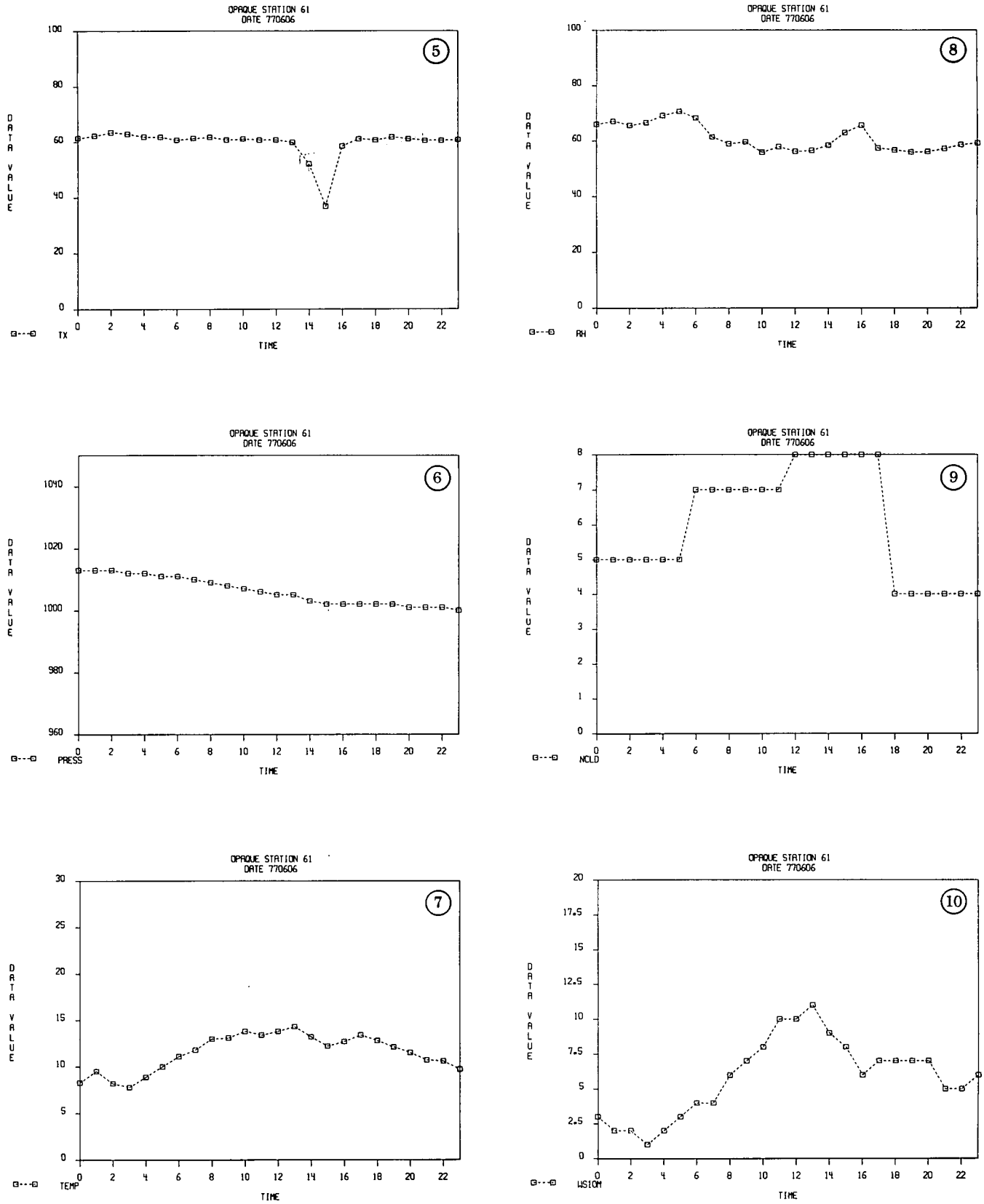

Fig. 2-3. (con't). Typical OPAQUE Surface Data, Hourly Time Plots. Station "61" identifies the data as being an initial issue (1) originating from the UK station (6).

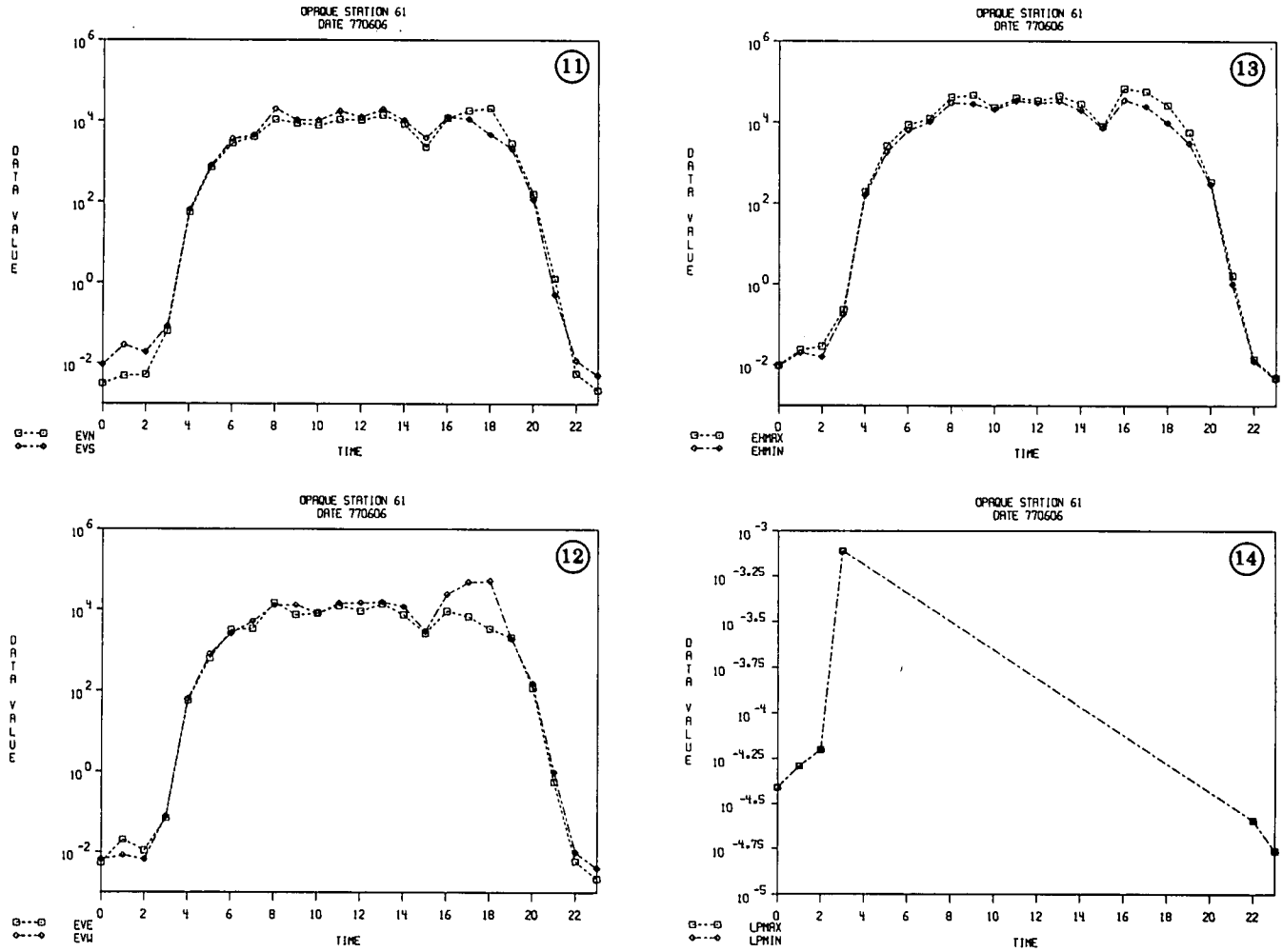

Fig. 2-3.(con't). Typical OPAQUE Surface Data, Hourly Time Plots. Station "61" identifies the data as being an initial issue (1) originating from the UK station (6).

These same data were also displayed as scatter diagrams of selected pairs of measured parameters. There were eleven of these "standard scatter diagrams" produced to accompany the "time plots". They are listed in Table 2.2 and illustrated in Fig. 2-4. As with the "time plots", the scatter diagrams contain data representing a single 24 hour period. Similar displays are available using either shorter or longer time intervals in order to address relationships associated with specific temporal intervals as defined by the analyst.

An early step in establishing an appropriate approach to the analysis of the OPAQUE surface data set, was a case study of the Summer 1977 data from the Netherlands. It was apparent very early in this study that there were an abnormally high number of anomalous data points in the set, particularly in the transmissometer and nephelometer measurements. Consequently, it was decided that the information contained in the two data tapes which were being evaluated would need additional sorting. In order to permit moderate amounts of bulk processing two data tapes were dumped and summarized in order to identify each month's data completeness and reliability. The results of this sorting are illustrated in Figs. 2-5 and 2-6.

Table 2.2.
OPAQUE Surface Data

STANDARD SCATTER DIAGRAMS (11)

Diagram No.	Measured Quantities			Comparison	Remarks
1.	SMAX/MIN	vs	SEMAX/MIN	VIS vs VIS	IR Transmittance is converted to effective extinction coefficient, α, (500m baseline) by the expression $\alpha = \frac{lnT}{r} = \frac{lnT}{0.5}$
2.	SMAX	vs	TEMP		
3.	SMAX	vs	RH	VIS vs MET	
4.	SMAX & MIN	vs	T1 & T5 ($\alpha_{1,5}$)		
5.	SMAX & MIN	vs	T2 & T3 ($\alpha_{2,3}$)		
6.	SEMAX & MIN	vs	T1 & T5 ($\alpha_{1,5}$)	VIS vs IR	
7.	SEMAX & MIN	vs	T2 & T3 ($\alpha_{2,3}$)		
8.	T1 & T5 ($\alpha_{1,5}$)	vs	TEMP		
9.	T2 & T2 ($\alpha_{2,3}$)	vs	TEMP		
10.	T1 & T5 ($\alpha_{1,5}$)	vs	RH	IR vs MET	
11.	T2 & T3 ($\alpha_{2,3}$)	vs	RH		

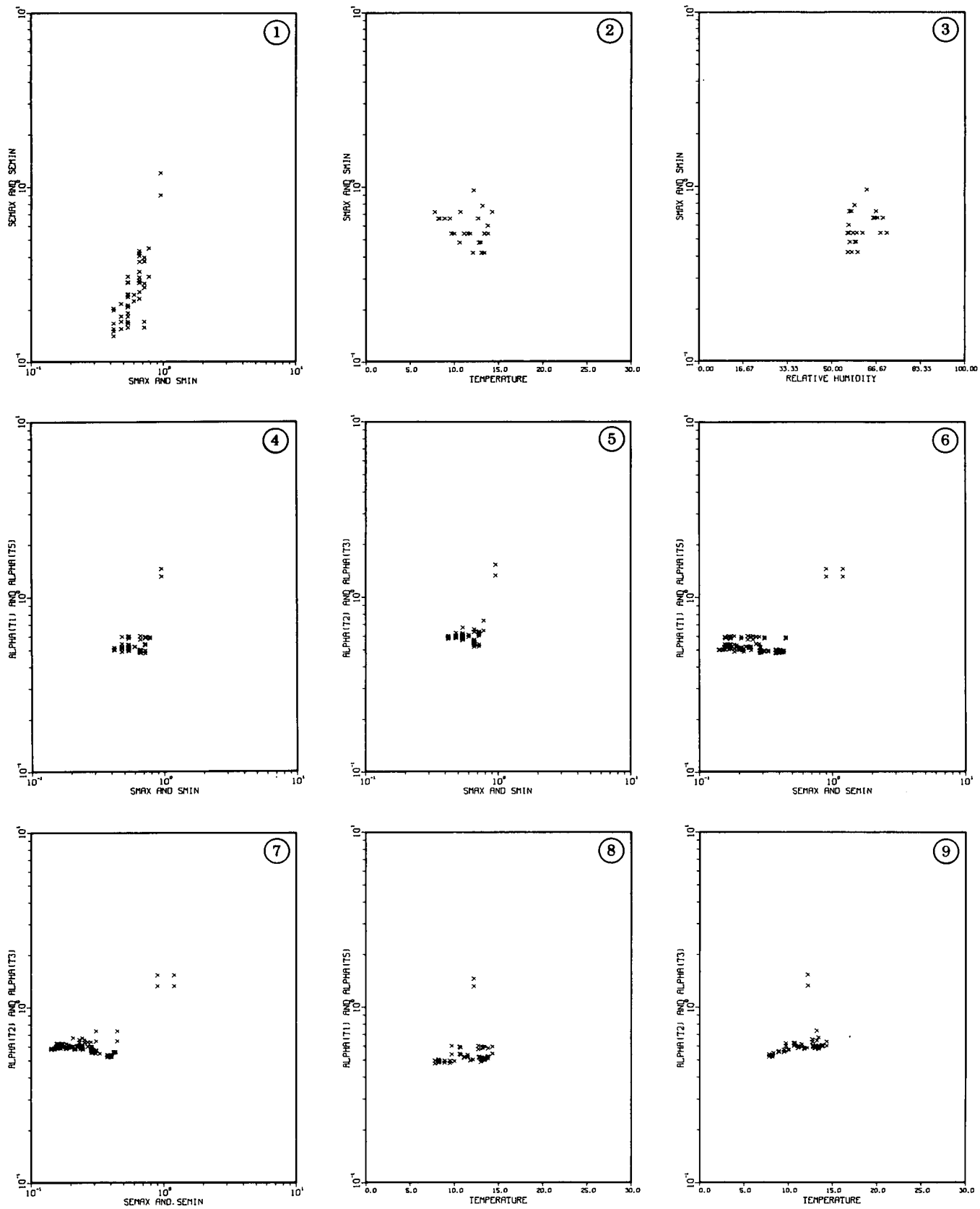

Fig. 2-4. Typical OPAQUE Surface Data, Daily Scatter Diagrams.
Data Station 61 Date 770606.

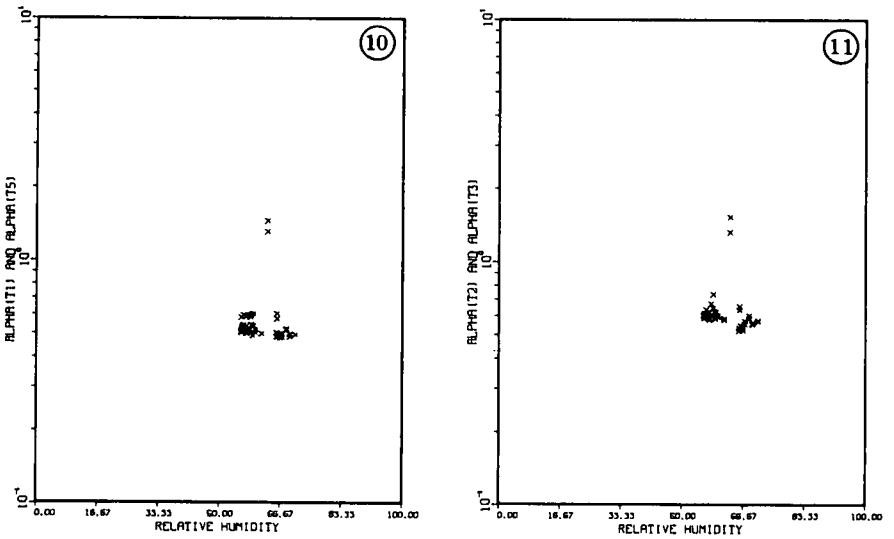

Fig. 2-4 (con't). Typical OPAQUE Surface Data, Daily Scatter Diagrams.

Figure 2-5 represents the degree of completeness associated with each station's monthly measurement of the key optical and meteorological parameters. For each entry, the shading indicates reasonable completeness. In this summary "reasonable completeness" implies that the measured parameter was represented in the monthly set at least 75% of the time. Thus the block associated with the UK/Summer '77 scattering coefficient data (*i.e.* top left entry) indicates that for the first two months the "s" measurements were reasonably complete, but that for the third month they were not sufficiently complete for most analytical purposes. The horizontal dashed lines in the "LP" and "FP" columns indicate significant amounts of data, but an undefined degree of completeness due to the variable nature of the day-night distribution.

Figure 2-6 shows the result of taking the sorting process one step further. In this illustration the data that were at least 75% available had the additional requirement for a reliability of 4 or better imposed. Since significant amounts of these early data were unvalidated, the requirement for reliability 4 severly reduced the overall useable set. Nonetheless, it is this residual body of validated and edited data, *i.e.* that implied in Fig. 2-6 that must be addressed in the studies that follow if one is to hope for reasonable success in establishing reliable optical/meteorological relationships.

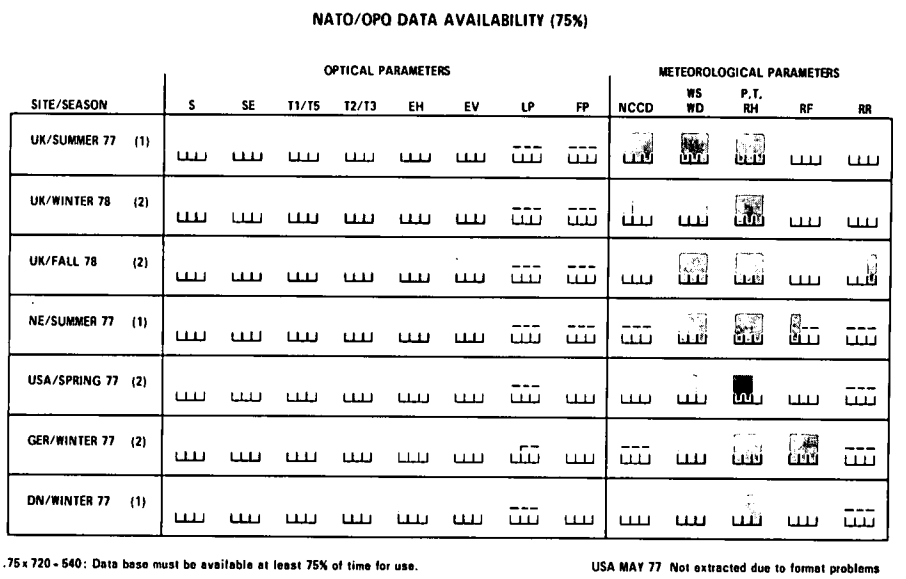

Fig. 2-5. OPAQUE Surface Data Availability (75%).

SELECTED NATO/OPQ DATA : 75% & R ≤ 4

	OPTICAL PARAMETERS								METEOROLOGICAL PARAMETERS				
	S	SE	T1/T5	T2/T3	EH	EV	LP	FP	NCCD	WS WD	P,T, RH	RF	RR
UK / SUMMER 77 (1)													
UK / WINTER 78 (2)													
UK / FALL 78 (2)													
NE / SUMMER 77 (1)													
USA / SPRING 77 (2)													
GER / WINTER 77 (2)													
DN / WINTER 77 (1)													

Fig. 2-6. Selected OPAQUE Surface Data (75% & R≥4).

3. OPAQUE SURFACE DATA

3.1 INTRODUCTION

The initial assessment of the OPAQUE surface data has proceeded in a variety of ways in an attempt to develop a familiarity with the varying quantities and qualities of information that were available on the early initial issue data tapes. It should be recognized at the outset that the development of the surface data set into a clearly defined and readily applicable analytical tool represents a task of significant bulk and complexity. It should therefore not be totally surprising that all aspects of the task have not fallen into line as appropriately as initially might have been wished. The host nation scientific teams, recognizing the complexity and difficulty of building this extensive data base, developed a two stage plan for data submittal that was intended to ease the analytic load and speed the cooperative access. It was agreed that preliminary releases of each data set should be submitted for data validation as promptly as possible, without detailed analysis or editing. Subsequently these initial issue data tapes would be upgraded by a new issue which would contain those data which reflected the corrections and editing deemed necessary by the responsible investigator. Allowance was made for several sequential versions of each issue, each of which could be identified within the two digit station identification code.

Thus, for the data originating from any particular station, the issues numbered 1 through 4 would be understood to be unedited or only partially edited, and issues numbered 5 through 9 would contain data understood to be fully edited and of optimum achievable quality.

The data addressed in this report are all initial issue, unedited data as identified by the various station codes 31, 51, 61, etc., and thus must be evaluated with substantial cautionary caveats. A secondary feature one notices when addressing this preliminary surface data analysis is the relatively limited amounts of data that were utilized. This condition is partially illustrated in Fig. 1-2. If one assumes that data representing a three month interval at any one site constitutes a basic data unit, then the two year program should provide 56 data units, *i.e.* 8 calendar quarters worth of data from each of seven sites. However reducing the selection to include only those stations presently reviewed by the Visibility Laboratory as represented in the distribution of Fig. 1-2, one can appreciate that this analysis has addressed only a small subset of the total potential data base. Since in fact only seven units have been assessed by the Visibility Laboratory so far, the concept of developing a climatology of optical properties from the data base must necessarily be assigned to a longer time frame in order to accumulate a more complete selection of data sets.

Nonetheless, this developing data base represents a research vehicle of major significance that can, with patience, be induced to yield extremely valuable insights into the behavior of the surface optical-meteorological environment.

An initial technical progress plan for the development of the OPAQUE surface data was established relatively early in the program which contained three general areas of activity related to the scheme illustrated in Fig. 1-3. The major subdivisions within this plan were:

I. Determination of Correlations within the OPAQUE surface measurements as related to the three basic data regions.

   a. The Visible Band Photometric Data vs the Meteorological Data

   b. The Infra-Red Band Radiometric Data vs the Meteorological Data

   c. The Infra-Red vs the Visible data

II. Determination of Correlations between the Surface and Profile Data

III. Visible Profile vs IR Profile relationships as related through aerosol characteristics

As will be illustrated in the following several sub-sections, the development of this initial plan has been somewhat altered in emphasis and sequencing. Basically, the procedure has been to de-emphasize the early baseline correlations within the OPAQUE surface data set, and accelerate the development of modelling procedures related to the OPAQUE profile data, and their relationships with the surface directional optical properties. This proposed restructuring of the analytic procedures is an attempt to accelerate the general modelling effort by utilizing a more complete and reliable mix of surface and profile data. Thus although the available sample of surface data does not yet represent all stations, seasons, or parameters, by changing the data mix slightly, it is practical to use carefully selected sub-sets of the surface

data in conjunction with the aircraft's profile data to enhance the development of surface to air models.

Thus, as an immediate and necessary prelude to the analysis of climatological distributions of the surface observables as a function of time, weather, location, etc. we have initiated a general data survey which allows the analyst to select and concentrate on short term sample relationships for evaluating sub-set internal consistency and reliability and to establish requirements for selective data editing within these initial issue data sets. Several samples of these procedures are illustrated in the following sub-sections.

3.2 FIRST CASE STUDY

The first case study addressed the OPAQUE surface data from the site at Christchurch, England. These data were selected from the measurements made during the summer of 1977, and were provided for analysis on the initial data tape. The selection was based upon the desire to examine two sets of data, each representing a relatively short, well-defined and stable meteorological situation, where each of the two situations was distinctly different from the other. At the initiation of this first study, the assumption that the data base had been fully edited was erroneously built in to the selection process. Thus, the resulting early studies were perhaps naively optimistic. The question initially expected to be addressed, upon examining the contemporarily measured optical parameters was in very simplified terms: As the meteorology changed from condition "one" to condition "two", how did the optical properties appear to change, and was there a readily discernible correlation between the optical and meteorological observables? These are in fact complex questions demanding rather comprehensive case studies, in general beyond the scope of this initial attempt. However, it was essential that the methodology be established prior to the expansion of the analysis.

Three pairs of days were chosen for examination. Initially two pairs were chosen, the first representing a stable high pressure good weather condition on the first and second of June 1977, and the second representing a bracketed low pressure frontal passage on the sixth and seventh of June 1977. Subsequent to this initial selection two additional days, the twelfth of June and the ninth of August were chosen to represent conditions of very heavy haze. The primary data displays for one of these six days are illustrated in Fig. 3-1 and 3-2. In these figures only the data representing the visible and infra-red transmittances plus the relative humidity have been selected for illustration, but all of the formats shown in Section 2 were in fact available for analysis.

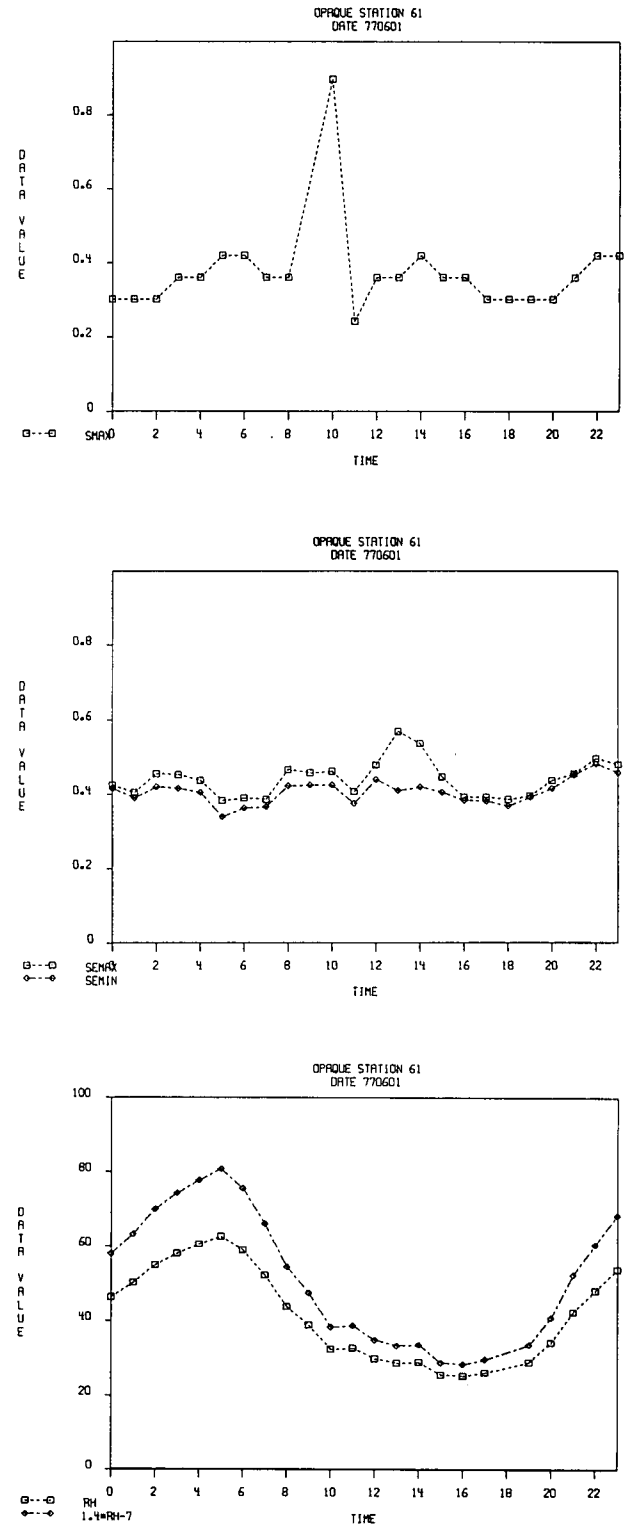

Fig. 3-1. Hourly Plots - 770601 - Station 61.

Several unforseen circumstances contributed to this first case study being rather disappointing in its results. In general, as illustrated in Fig. 3-2, clear, well-defined relationships were not immediately apparent between the various measurements within the visible, infra-red, and meteorological data regimes. Neither the plots for the individual days, as shown in Fig. 3-2, nor supplementary six-day composite plots were illustrative of immediately

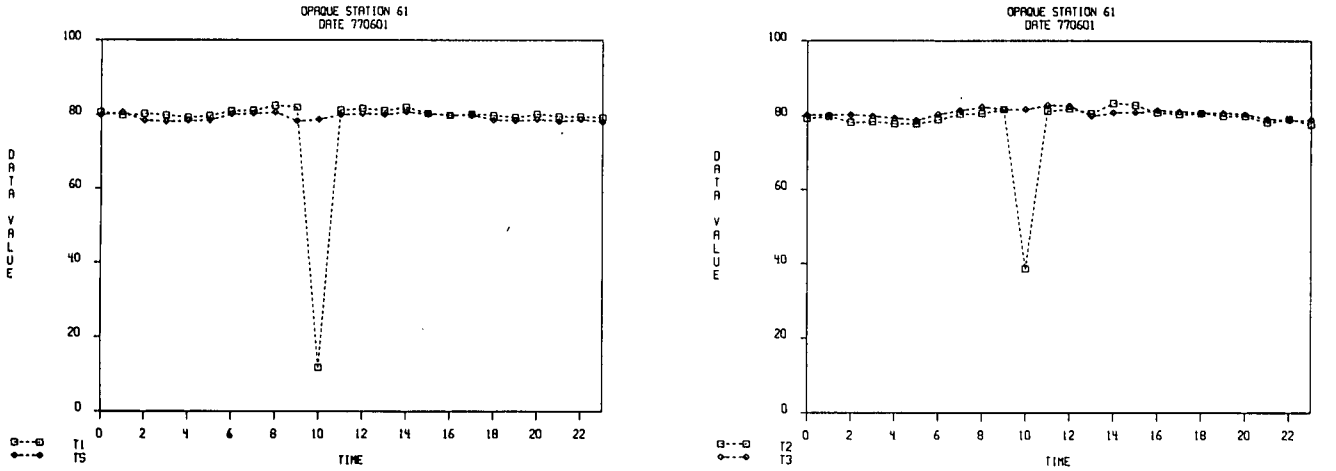

Fig. 3-1 (con't). Hourly Plots - 770601 - Station 61.

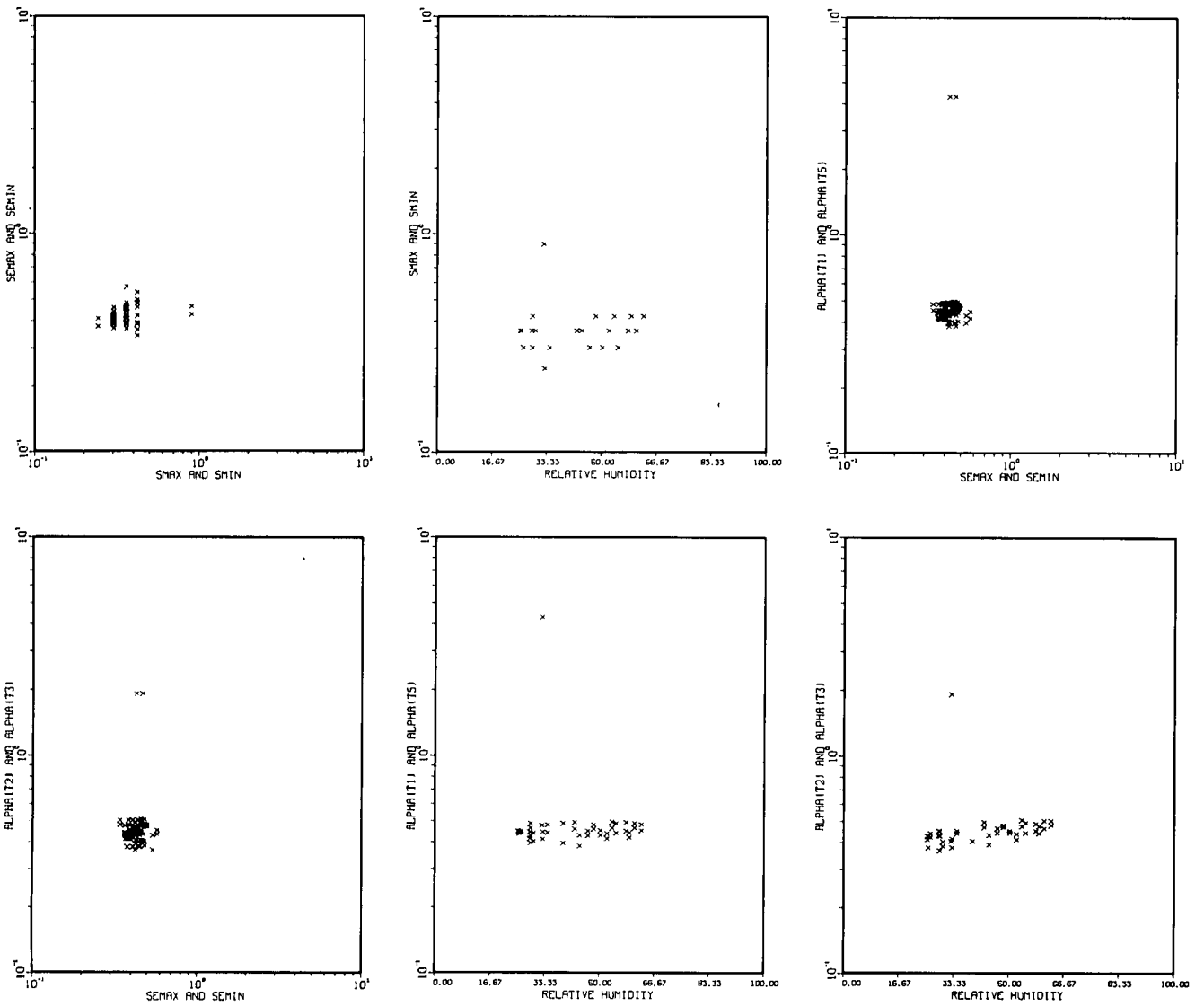

Fig. 3-2. Scatter Diagrams - 770601 - Station 61.

useful relationships. There are perhaps good and sufficient reasons why well-defined optical-meteorological relationships should not always be immediately apparent in an experimental study of real atmospheres such as this. However, beyond the problems normally anticipated in an early data release, there were significant discrepancies found where they were not expected, as in the comparisons illustrated in Fig. 3-3. Several procedural difficulties were however uncovered which helped establish the format for a follow-on study.

The first peculiarity that caused concern, although it might be reasonably anticipated in initial issue data such as these, was a widespread lack of correlation between the two visible band extinction measurements. That is the visible spectrum extinction coefficient as determined by the nephelometer system did not seem to either track particularly well, or match in magnitude with the extinction coefficient as determined by the transmissometer system. To determine how widespread this condition might be, the hourly plots of visible spectrum extinction coefficient were examined for all of the sites and dates (Ref. Table 1.2) included in the first data tape. The results of this visual examination and general classification are illustrated in Table 3.1 and two typical examples of good and poor comparisons are illustrated in Fig. 3-3. With the relatively high percentage of unacceptable comparisons between these two visible spectrum measurements, it became clear that making an initial data sorting based solely upon selected meteorological conditions and initially assigned reliability codes could be very unproductive, and that to insure a reasonably self-consistent set of data a sorting based upon the character of the optical measurements would be required. Thus it was decided to use visual classifications, such as those illustrated in Fig. 3-3, in conjunction with the reliability code associated with each optical measurement as joint sorting indices.

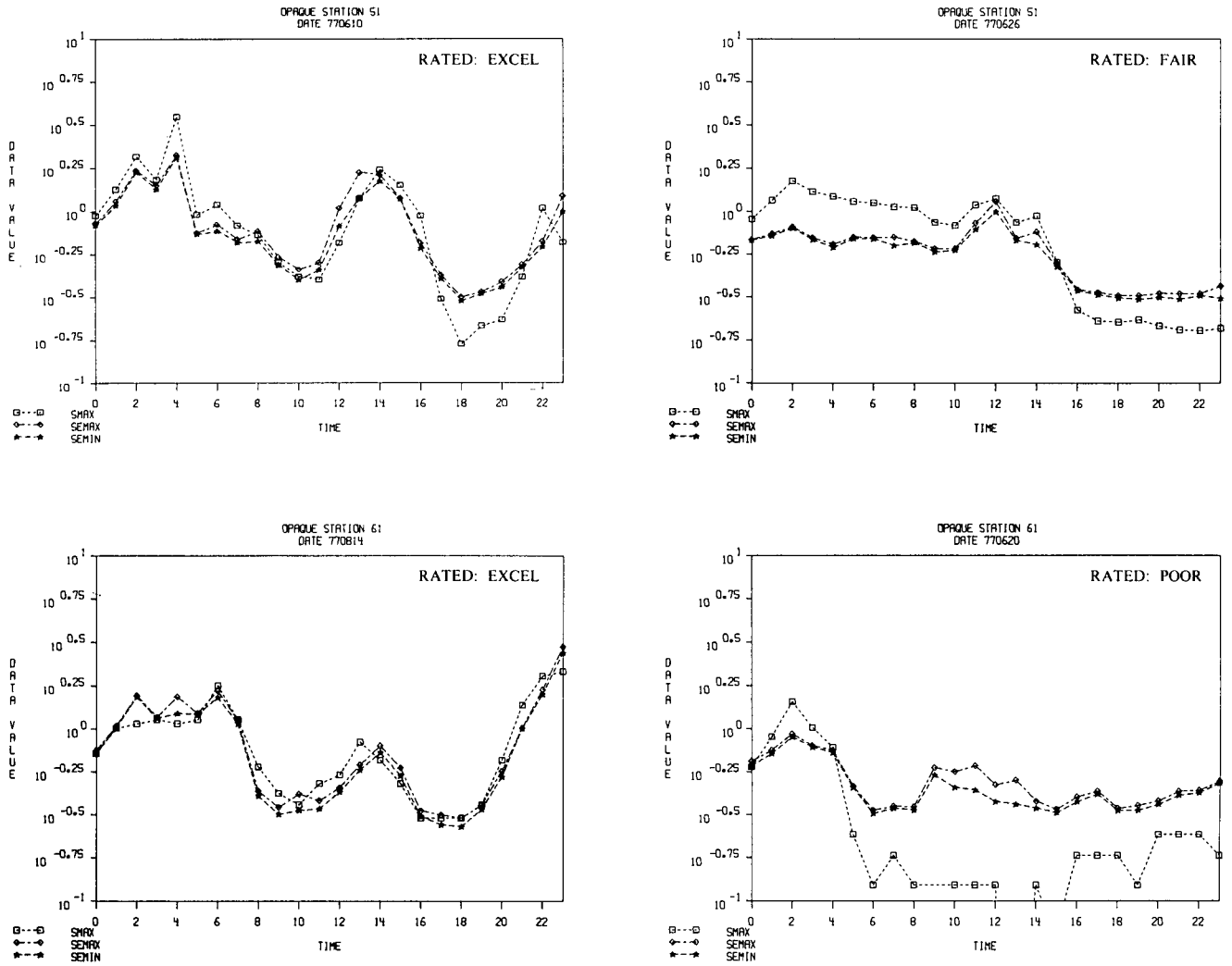

Fig. 3-3. Comparison of Nephelometer and Transmissometer Measurements (Tape I).

Table 3.1

Summary of Comparison Between Daily Nephelometer and Transmissometer Measurements

Site/Time	Comparative Classification				Total	No Data	Excel+Good	% useable
	excel.	good	fair	poor			Total	
Denmark JAN 1977	0	1	2	36	39	3	1/39	2
Netherlands AUG 1977	11	7	5	1	24	1	46/69	67
Netherlands JUN-JUL 1977	10	18	14	3	45	0		
England JUN 1977	1	7	10	10	28	2	43/72	60
England JUL 1977	2	17	6	1	26	5		
England AUG 1977	9	7	2	0	20	12		

Classification Criteria for Hourly Plot Comparisons

excel.: nearly all points in good agreement
good : most points in fair agreement
fair : most points not in agreement (factor of 2 difference)
poor : nearly all points not in agreement

In order to examine only the best of the data, only optical data assigned reliability "4" or better, and having visual comparisons of scattering coefficient measurements rated "excellent" would be selected for detailed analysis. Also, since the data from the English and Danish sites were specifically designated by the respective investigators as being unedited, the selection of the second case study data would be restricted to those data collected at the Netherlands site which had been initially reviewed and edited by the Netherlands experimental team.

In the meantime, in order to preclude serious biasing of the data interpretation, items of the nature illustrated in the following short remarks would be identified and deleted from the initial issue data bases, in anticipation of their eventual correction by the initiating investigators in subsequent data issues.

Spurious Data Points: The daily time plots exhibit intermittent, short term peculiarities such as those shown in Fig. 3-1. At the ten o'clock point, the SMAX nephelometer measurement indicates a high valued spike, which is not reflected in the SEMAX transmissometer data. However the transient condition does occur in the T1 & T2 measurements of IR transmittance, although it is missing from the T3 and T5 measurements. Whereas this perturbation in the hourly trend may in fact be explainable with additional detailed study, it may not represent a valid measurement of the atmospheric condition. In this case, its inclusion along with other similarly ill-defined points in a two parameter scatter diagram can contribute to excessive and possibly misleading scatter.

3.3 SECOND CASE STUDY

The second case study addressed the OPAQUE surface data from the site at Ypenberg, Netherlands. These data were also selected from the measurements made during the summer of 1977. However, prior to the selection of the specific data set that was to be evaluated, a rather extensive preliminary sorting was accomplished in an attempt to concentrate on those data of optimum completeness and reliability.

The general sorting mechanism has been semi-automated by developing several summarizing routines which enable the analyst to rapidly ascertain the completeness of the data in terms of how many entries per day were recorded, the overall range of measured magnitudes, and the anticipated reliability of the measurements. It was from automatic listings such as these that the intervals for the second case study were selected.

The results of the data sorting procedures are summarized on worksheets as illustrated in Table 3.2. On these sheets the three basic assessments of each day's measurements can be made, *i.e.*; 1) Good match between S & SE hourly plots; 2) Completeness of parameter measurements; and 3) Reliability of parameter measurements.

In the last column of Table 3.2, the overall ranking of each day's data is indicated by a three digit series, *i.e.* 2 2 1, 4 3 1, etc. In this numerical series each of the three assessments indicated in the preceding paragraph is ranked on a scale from "1" to "4" where "1" is the poorest assessment and "4" is the best as illustrated in Table 3.3. Thus for a day where the S vs SE plot comparison was excellent, the key Optical and Meteorological data were all complete, and of reliability "4" or better, that day would be ranked 4 4 4. The key parameters are designated as S, SE, T1,T5, T2,T3, RH and Temp. In the Netherlands data set, there are no rankings better than 4 4 1, since all of

Table 3.2

DATA COMPLETENESS AND RELIABILITY SUMMARY

Site NETHERLANDS (51) Month June 1977

Date	Visual Comparison (Hourly Plots) S vs SE	KEY OPTICAL PARAMETERS								Secondary Optical Parameters		KEY MET RH & T	Secondary MET	Overall Ranking
		S		SE		Barnes 1&5		Barnes 2&3						
		Com.	Rel.	Com.	Rel.	Com.	Rel.	Com.	Rel.	Com.	Rel.	Complete	Complete	
01	fair	x	-24	x	-9	-2	-22	-2	-22	x	*	x	x	2 2 1
02	excel	x	-11	x	x	x	-24	x	-24	ES-21		x	WS10-4	4 3 1
03	excel	x	-8	x	x	x	-24	x	-24	ES-21		x	x	4 3 1
04	excel	x	x	x	x	x	-24	x	-24	ES-22		x	NCLD-24 WS10-15	4 3 1
05	good	x	-6	x	-2	x	-24	x	-24	ES-24		x	NCLD-24 WS10-24	3 3 1
06	good	x	-16	x	-6	x	-24	x	-24	ES-24		x	WS10-3	3 3 1
07	excel-good	x	-20	x	-1	x	-24	x	-24	ES-22		x	x	4 3 1
08	fair	x	-24	x	-3	x	-24	x	-24	LP-3		x	x	2 3 1
09	good	x	-4	x	x	x	-24	x	-24	ES-24		x	x	3 4 1
10	excel.	x	-7	x	-1	x	-24	x	-24	ES-24		-2	x	4 2 1
11	good-excel	x	-16	x	-1	x	-24	x	-24	x		x	NCLD-24 WS10-11	3 3 1
12	good	x	-12	x	x	x	-24	x	-24	x		x	NCLD-24 WS10-24	3 3 1
13	excel	x	x	x	x	x	-24	x	-24	x		x	x	4 4 1
14	excel	x	-7	x	x	x	-24	x	-24	ES-22		x	x	4 3 1
15	excel	x	x	x	-1	x	-24	x	-24	ES-23		x	WS10-5	4 3 1
16	good	x	-15	x	x	x	-24	x	-24	ES-24		x	x	3 3 1
17	excel	x	-7	x	x	x	-24	x	-24	ES-23		x	x	4 3 1

*LP all Rel. 3, FP all 3, EV and EH all 4, ES all 4 x fulfills reliability or completeness standards

Entry Codes for Table 3.2:

Com: Parameter Complete, "x" indicates 24 entries/day
Rel: Reliability, "x" indicates all entries "4" or higher
Excel: Excellent match, nearly all points match closely.
Good: Good match, most points in agreement within a factor of two
Fair: Fair match, most points not in agreement by factor of two or more.
Poor: Poor match: nearly all points not in agreement.

Numerical entries, *i.e.* -16, -7, etc. indicate number of exceptions to completeness, or number of reliabilities less than "4".

the Barnes transmissometer data was arbitrarily coded reliability 3 as a caution, since the initial calibration procedure was undergoing revision.

Table 3.3

Data Selection Ranking Indices

Assigned Rank	1st Digit S vs SE Comparison	2nd Digit Data Completeness	3rd Digit Data Reliability
Best: 4	excellent	All there	All ≥ 4
3	good	Key all there	Key all ≥ 4
2	fair	Each key mostly there	Key mostly ≥ 4
Worst: 1	poor	One key mostly not there	One key mostly < 4

Following the selection mechanism outlined in the preceding paragraphs the Netherlands data rankings were examined to select two five day intervals for further study. A ranking of at least 3 3 1 was desired. During the month of June 1977 there were 21 days ranked 3 3 1 or better, during July 1977, 18 days, and during August 1977, 16 days. From these intervals, two new sets of days were chosen for analysis. These two sets were each five consecutive day intervals with rankings as indicated below.

First Interval		Second Interval	
770613 -	441	770815 -	431
14 -	431	16 -	431
15 -	431	17 -	431
16 -	331	18 -	421
17 -	431	19 -	431

These ten days represent optimum intervals where the data appeared to be of better than average quality and quantity, the weather patterns showed significant variations, and there were discrete intervals of very stable optical properties in contrast with intervals where the optical properties underwent large excursions in range. A brief discussion related to the preliminary analysis of these selected data is included in the following paragraphs.

Two types of graphs as illustrated in Section 2, were computer generated for this case study: time plots, which plotted parameter "a" against time for a 24-hour period, and scatter plots, which plotted parameter "a" against parameter "b" for a 24-hour period. In addition, scatter plots for the complete 10-day period were generated manually.

The scatter plots consisted of the following displays: visible spectrum total scattering coefficient, visible spectrum extinction coefficient, and computed visible spectrum aerosol scattering coefficient plotted versus temperature, relative humidity, saturated water vapor pressure at dewpoint temperature, and absolute humidity; visible scattering coefficient (nephelometer) versus visible spectrum extinction coefficient (transmissometer); infra-red radiance transmittance versus temperature, relative humidity, and absolute humidity; and infra-red extinction coefficient versus visible extinction coefficient.

Some of the more interesting 10-day scatter plots for the visible/meteorological data are illustrated in Fig. 3-4. From Fig. 3-4 it is apparent that there is a fairly large spread in the visible/meteorological relationships. The most clearly related parameters shown here are scattering coefficient and relative humidity, and even this graph shows a large spread. It is presumed that this spread is in part due to the normal character of the atmosphere, and should not be attributed entirely to instrumental error. Within the scatter plots of Fig. 3-4, the values of scattering coefficient are seen to range over factors of five or six at any given value of relative humidity. During the same interval, the equivalent time plots for the nephelometer and transmissometer values differed by a factor of only one or two. Since these two instrument responses remained comparable for periods of several days, even as the measurement levels ranged over nearly two orders of magnitude, the absolute error in either instrument can be reasonably assumed to be less than a factor of two. Even errors of this general magnitude however would not account for the significantly greater spreads of five or six shown in the scattering coefficients plots of Fig. 3-4.

Conversely, the scatter plots illustrate relative humidities ranging from about 50% to 90% at any given value of scattering coefficient. This variation is presumed larger than should be attributed to an instrumental error in the humidity indicator, since it would require an error of approximately ±25% in RH to reasonably account for the variation, and this seems extreme.

One interesting feature of the graphs in Fig. 3-4 is the high scattering coefficients at high relative humidities. These points occur at measured relative humidities of about 95%. In several cases, during periods of these high

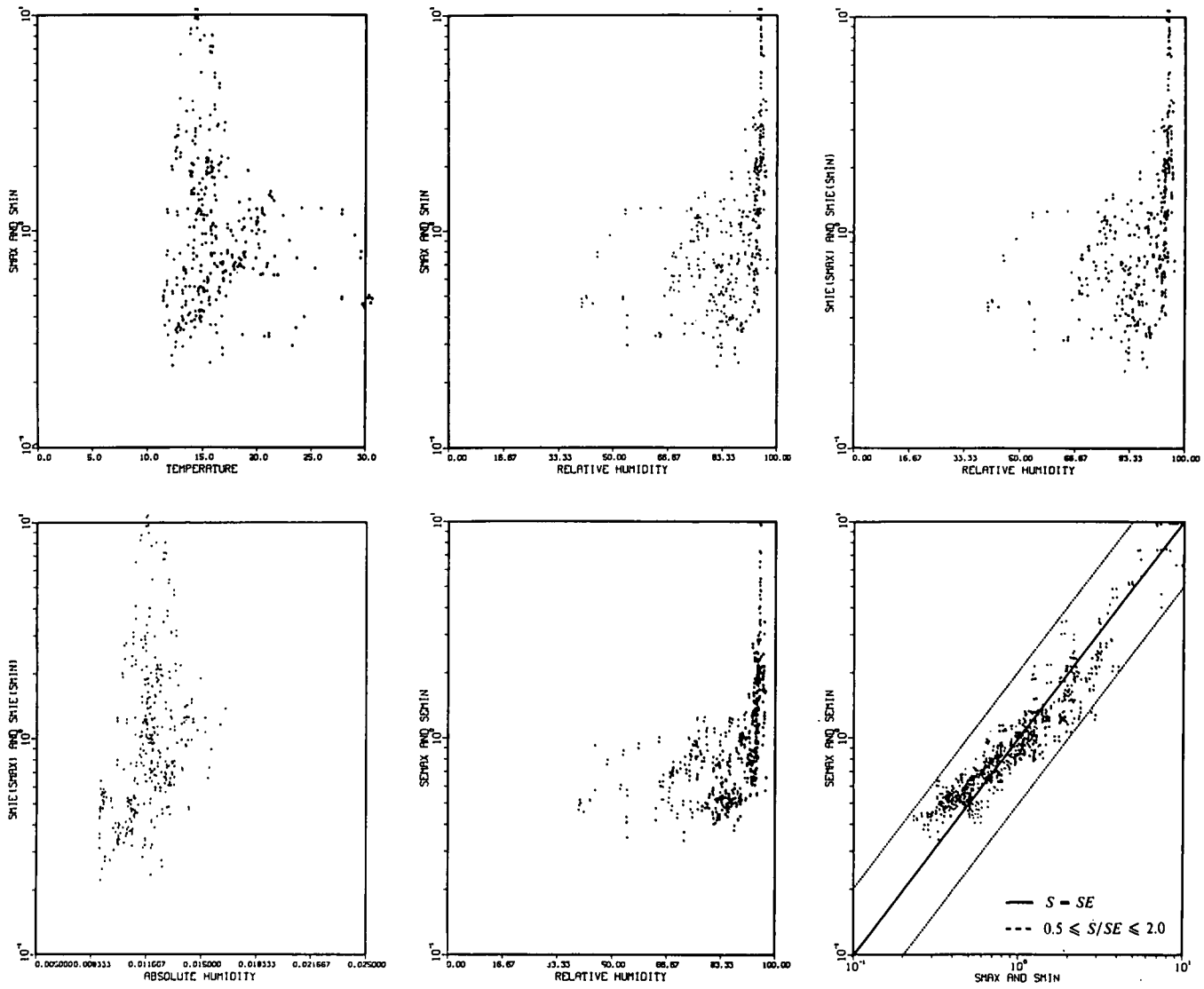

Fig. 3-4. Selected Scatter Diagrams, Visible Spectrum Relationships, Ten Day Interval.

measured relative humidities, the relative humidity reading remained constant at about 95% for several hours. One interpretation of this constant reading would imply an electronic saturation within the transducer which inhibited the devices response beyond the 95% point. In this case then, the true relative humidity would be anywhere between the measured value and 100%. Alternatively, the constant signal could indicate that the transducer was in fact saturated with moisture and an electronic bias caused the system to indicate too low a reading. In this case the true relative humidity would be at 100%, and the environment would be fully in the condensation mode. In light of the relative uncertainty in interpreting these high humidity situations, it may be appropriate to treat them separately, with special attention to attempts in discriminating the appropriate droplet growth mechanism.

Thus, the data in Fig. 3-4 illustrate that: a) high values of scattering coefficient [$s(o)>2$ km^{-1}] occur only in a very narrow range of relative humidities near 100%, b) apparently no similar relationship occurred between scattering coefficient and temperature or absolute humidity, and c) the broad spread on the plots of scattering coefficient versus relative humidity is apparently realistic and not due to experimental error. Of course, this third result has been influenced by the intentional selection of this special data set which has minimal error in the scattering coefficient values. It may be noted from Fig. 3-4 that the spread is not reduced if Mie scattering, rather than total scattering, is plotted.

The conclusion that the spread in the scattering coefficient vs relative humidity plot is realistic, rather than due to experimental error, is an important result, and is expected for theoretical reasons. However, for prediction purposes it is not a particularly desireable result. It is hoped that it may be possible to determine better defined relationships by stratifying the data using such variables as air mass, type of day, etc. Reliable aerosol data and synoptic weather data should be helpful in this attempt at stratifying the data.

Although neither aerosol data nor synoptic weather data were available for this case study, it was possible to classify the scattering coefficient data as a function of several other measured parameters. Three additional plots of scattering coefficient versus relative humidity were generated: one with the data classified by date; one with the data classified by time of day (using different symbols for each 3-hour period of the day); and one with the data classified by temperature (using different symbols for each 2° range of ambient temperature).

The classifications by date and by time of day did not lead to a significant stratification of the data. The classification by temperature did lead to some partial stratification however. The plot is shown in Fig. 3-5. (Note that the relative humidity scale is somewhat magnified). The shading surrounding the 10-11.9 degree, 20-21.9 degree, and 30-31.9 degree data points has been added to help illustrate the separations between the various temperature ranges. Much of this stratification occurs because relative humidity is a function of temperature. However, it is apparent from the curve shapes that one could predict the scattering coefficient from relative humidity much more closely if temperature were also known. That is, the range of SEMAX values at a given relative humidity which fall within a given temperature class, is often much less than the overall range of SEMAX values at that relative humidity. For example, at RH=80 percent SEMAX varies between about 0.4 and 1.2 km^{-1}. However, for RH=80 percent and Temperature = 18-20 degrees, SEMAX varies only between the more limited range of 0.7 to 0.9 km^{-1}. Although this 10-day sample is too small to be statistically significant, it is a valid illustration that the technique of classifying by multiple variables may lead to the ability to predict the scattering coefficient.

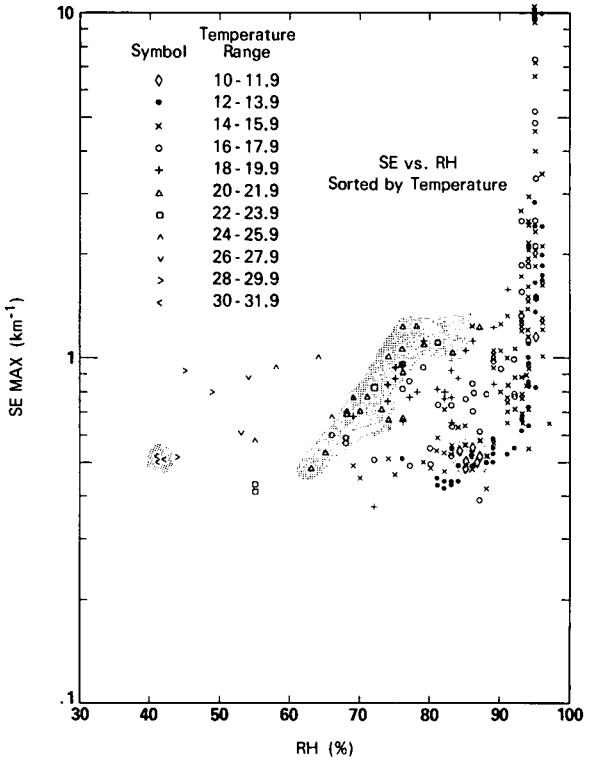

Fig. 3-5. Extinction Coefficients vs Relative Humidity, Classified by Ambient Temperature.

Some of the more interesting scatter diagrams of the infra-red data are illustrated in Fig. 3-6. These data represent total extinction as measured. They have not had any calibration corrections applied.

The infra-red versus meteorological plots may be summarized as follows: in general, the data lie within a very narrow range of transmittances (roughly 80 to 90%), except when relative humidity is very high. In these high

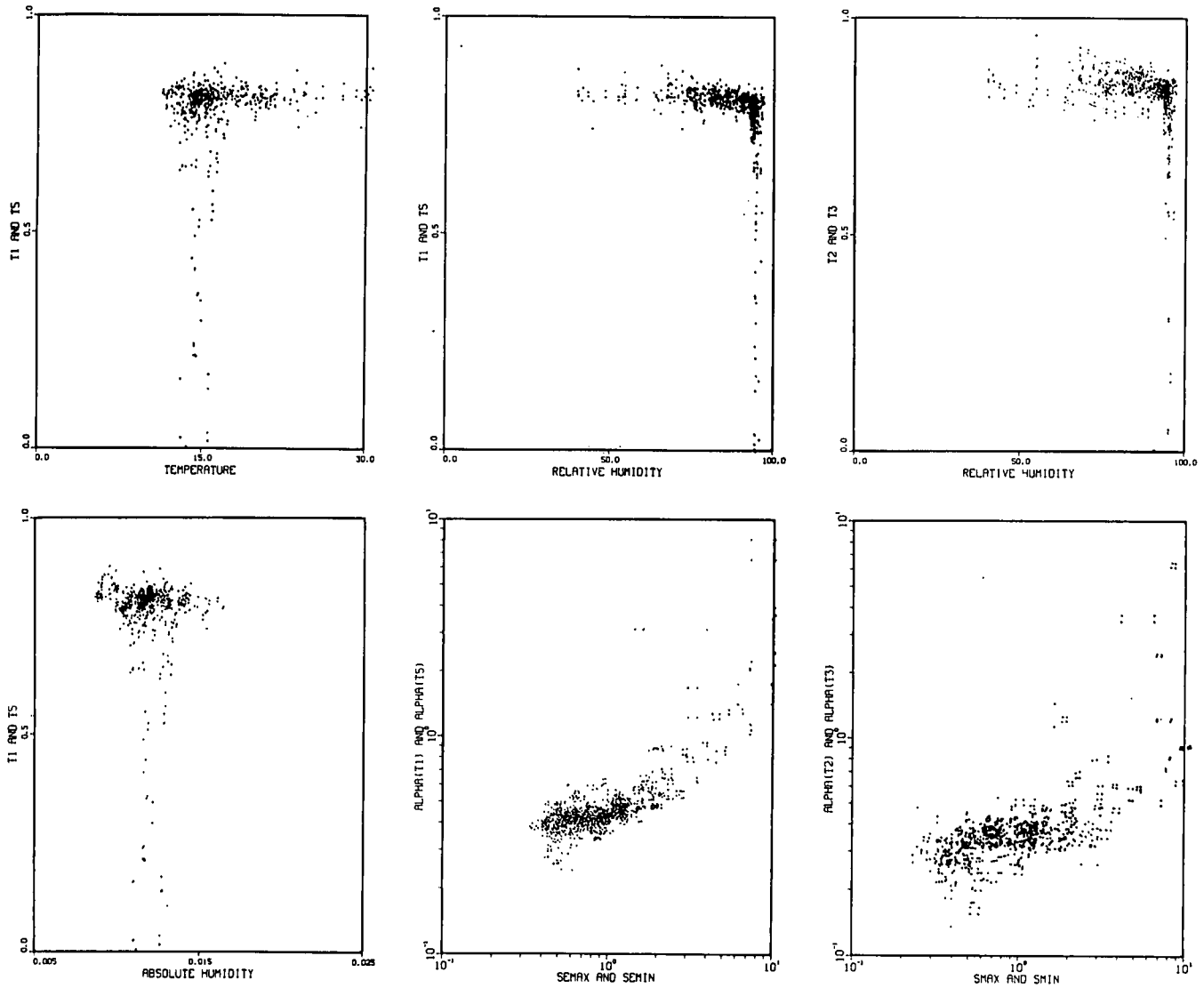

Fig. 3-6. Selected Scatter Diagrams, Infrared Relationships, Ten Day Interval.

relative humidity cases, which may represent the condensation cases, the transmittance varies between roughly 0 and 90%.

It should be noted that the plots of T2&T3 (8-12μm and 8.25-13.2μm) versus the meteorological parameters show the same general features as the plots of T1&T5 (3.4-5.0μm) versus the meteorological parameters. The plot of T2&T3 versus relative humidity is included as an example, in lieu of the fully redundant display of all available combinations.

The last two plots in Fig. 3-6 illustrate the infra-red to visible relationships. These two plots show fairly well defined functional relationship between the infra-red and visible in the 3-5μ band, but as might be expected, a substantially poorer relationship in the 8-12μ band. This is a modestly encouraging development, indicating that through the careful selection of data sets containing minimal experimental uncertainty, tighter interparameter relationships may begin to emerge. It is anticipated that separating the infra-red extinctions into their molecular and aerosol components, and reviewing the data subsequent to multiple parameter classification will aid in the detection of usable functional relationships.

3.4 REVIEW OF SECOND DATA TAPE

Following the review of the surface data contained on the first data tape via the summaries and case studies discussed in the preceding paragraphs, the general consensus was that these initial issue surface data were not fully adequate in either quantity or quality to establish all of the relationships anticipated in the original research plan. It was and is felt however, that the fundamental content of this data base has the potential for application

in many useful modelling efforts once the mandatory edits and verifications can be completed. Thus the review and summarization of the data contained on the second data tape has been addressed and is proceeding in a manner similar to that used for the first. The second data tape contains surface data, also of initial issue quality, from the English, northern German and southern German sites as noted in Fig. 1-2.

The monthly summary sheets have been produced and reviewed for the four quarterly segments indicated in Fig. 1-2. Also the Completeness and Reliability Summaries illustrated in Table 3.2 have been done manually pending the development of a computer subroutine that will do them automatically. An initial sample of the hourly plots of S & SE have been visually compared as summarized in Table 3.4, and thus the ground work for the daily data rankings has been done even though the generation of the formalized ranking sheets has not been completed. Typical comparisons between the S & SE hourly plots are illustrated in Fig. 3-7 and the related scatter diagrams, similar to those shown in Fig. 3-8 are undergoing analysis. The scatter diagrams illustrate a typical hazard one encounters in the analysis of unedited data, that is measurements which have been influenced by the range limitations of the experimental instrumentation.

Table 3.4.

Summary of Comparison Between Daily Nephelometer and Transmissometer Measurements

Site/Time	Comparative Classification				Total	No Data	Excel+Good Total	% useable
	excel.	good	fair	poor				
Birkhof, Germany								
JAN 1977	0	15	11	5	31	0	15/31	48
FEB 1977	1	6	10	11	28	0	7/28	25
Christchurch, England	(Partial Sampling Only)							
DEC 1977	0	0	1	1	5	3	N/A	N/A
JAN 1978	0	9	3	0	13	1	N/A	N/A
FEB 1978	2	4	1	1	13	5	N/A	N/A
SEP 1978	1	1	0	0	3	0	N/A	N/A
OCT 1978	1	1	0	0	3	1	N/A	N/A
NOV 1978	1	3	0	0	6	2	N/A	N/A

Note that since all of the UK data has not been visually screened it is not yet possible to determine the percent useable figures.

Also note that even though all of these data are classified as reliability four, there are broad excursions between the S & SE measurements on many occasions.

In this particular set, attention is drawn to the values of visible extinction as determined by the transmissometer system, SE. In each of the three displays

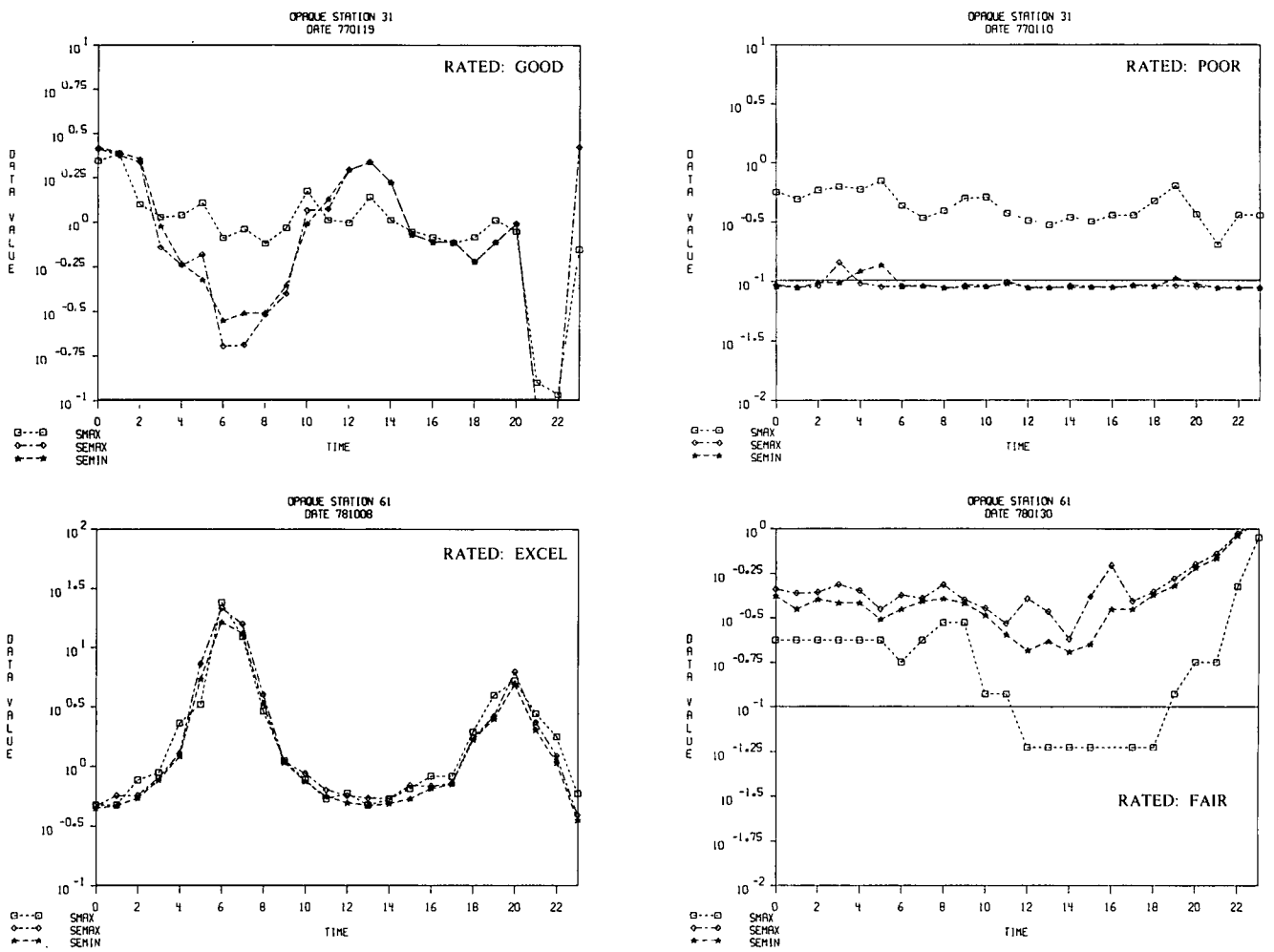

Fig. 3-7. Comparison of Nephelometer and Transmissometer Measurements (Tape II).

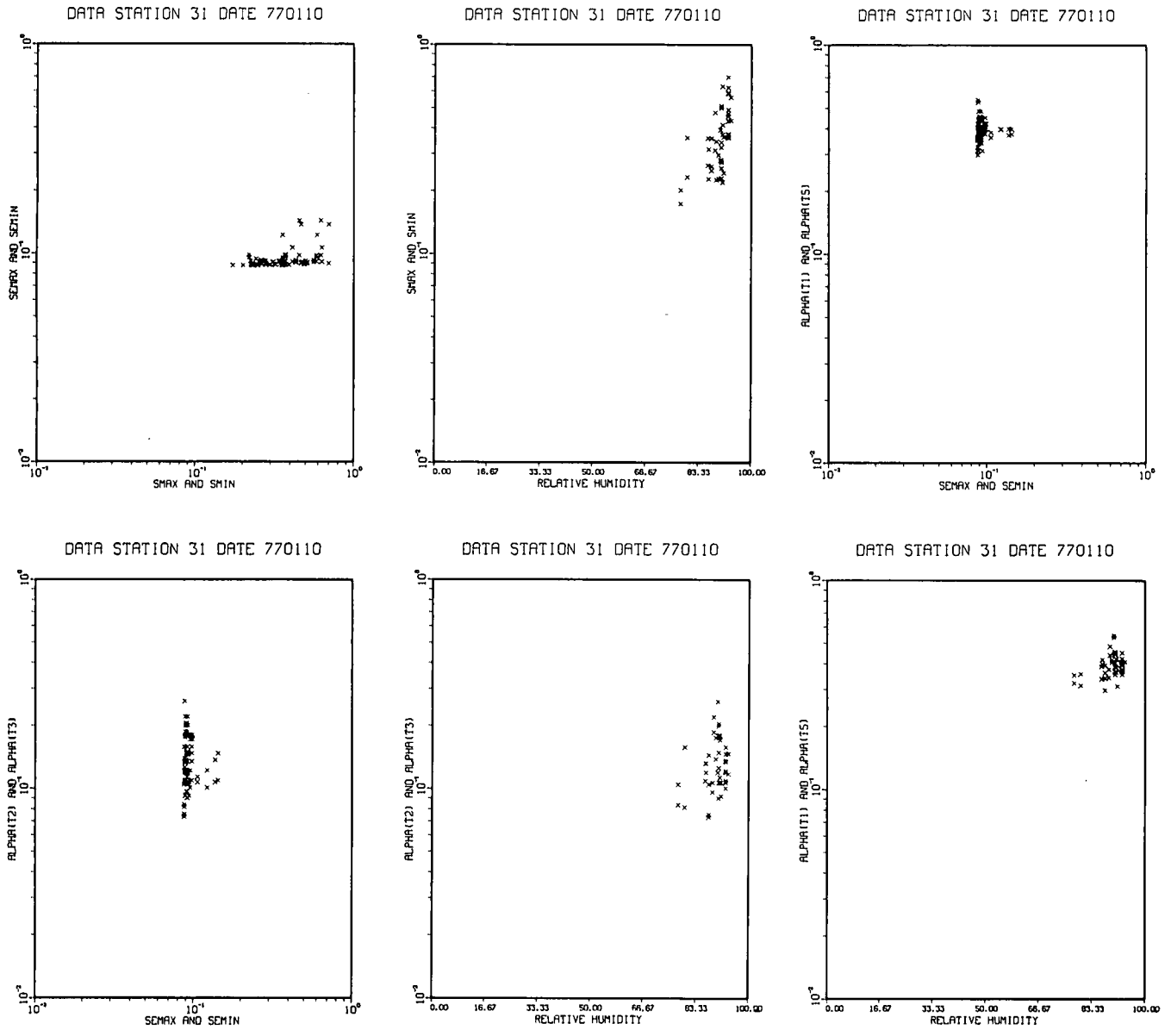

Fig. 3-8. Scatter Diagrams - 770110 - Station 31.

containing the SE data, one immediately notes the bottoming out occurring at 0.10 KM^{-1}. Since these values do not represent valid measurements of the atmospheric conditions, they should be isolated through an editorial sequence and either handled separately or eliminated.

Whereas there are still instances of poor or little correlation between parameters in the three data regimes, the overall data quantities and qualities available even in these initial issue tapes appear to be improving. Thus as editing and analysis methodologies are applied to the newer data sets, and as the earlier data sets are upgraded by the originating investigators, the opportunities for selected application of these surface data to the modelling effort also seem to be increasing.

3.5 RELATED STUDIES

As the short term case studies described in the preceding sections have progressed, similar evaluations have been conducted by several of the originating scientific teams. In many cases, these preliminary studies addressed the statistics of longer time intervals, and were conducted quite early in the program, however since they have provided considerable guidance in developing the short term case study approach described earlier, it is appropriate that they be acknowledged in this report. However, since these studies have in all cases been preliminary in nature, the data displays will not be reproduced and the acknowledging remarks will be kept relatively general in content.

A comprehensive early note was prepared by Ir F.P.H. Engering (1978) of the Physics Laboratory of the National Defense Research Organization TNO, Netherlands. This note OPAQUE N/NL-7806 addressed the development of least square regression lines to several sets of visible and infra-red transmission, rainfall and humidity data. In these studies there were as many as 2076 measurements involved in the regression computations. Computations were continued after applying suitable transforms (*e.g.* by taking the logarithm), and applying selected sorting criteria.

A follow on to Ir Engering's work was produced by A.C. van Tol (1979) of the same organization. This preliminary analysis note, OPAQUE N/NL-7902, contained the work of Engering and contained time plots and histograms of several relevant parameters. This note primarily addressed the infra-red transmittance in the 8-12μ band and its probability of occurrence within pre-specified bounds.

Another preliminary study addressing a relatively early set of measurements similar to that used by van Tol was conducted by Dr. A. Zardecki (1979) of Laval University, P. Q. Canada. In his note OPAQUE N/CAN-7901, thirty day time plots of visible and infra-red transmittances, measured and anticipated illuminance levels, and meteorological parameters were presented in conjunction with the associated frequency and cumulative frequency of occurrence histograms. Scatter diagrams relating the infra-red transmission data with visible transmission, relative and absolute humidity were also included.

A study of the seasonal relationships between the visible and infra-red transmittances for cases of reduced visibilities is presented in OPAQUE N/UK-7905, *Anon.* (1979). In this note, the infra-red transmittance data is converted into extinction coefficient format and reduced by the molecular absorption. The resulting data are compared with theoretical curves as generated by investigators from Royal Signals & Radar Establishment and the Night Vision Laboratory.

While it would be overly presumptious to imply specific conclusions based upon these preliminary studies, some general remarks regarding their influence on our own studies might not be inappropriate. In this context, two generalities appear as a common theme throughout most of the preceding discussions. First, there seems to be rather poor correlation between the visible and infra-red transmittances, a circumstance not totally unexpected and addressed rather directly by Turner, Fenn and Shettle (1979) in their note OPAQUE N/US-7903. And second, the correlations between the various transmittance parameters and the meteorological parameters are generally poor or non-definitive and often show large degrees of scatter. Thus, in an effort to avoid the statistical uncertainties imposed in the handling of these large data sets, we have chosen initially to concentrate on the evaluation of small selected sub-sets, where possible representing five to thirty day intervals, wherein the internal consistency and reliability of each series of measured values can be more clearly assessed. If these sub-sets are chosen to coincide with each series of airborne profile data, then the development of a suitable data base for addressing the air to ground link can be achieved simultaneously with the development of a set of optimum quality ground measurements. As the number of these optimized sets increases either through selected editing of initial issue data, or through the direct utilization of issue 5 sets, then their use in studies of both statistical and phenomenological nature should prove increasingly productive.

3.6 DIRECTIONAL PROPERTIES

An important goal of the OPAQUE data collection program is the development of models to calculate the directional contrast transmittance. In order to calculate the directional contrast transmittance it is necessary to define the angular dependent scattering functions of an atmosphere. Calculations of the angular dependent equilibrium reflectance (See Appendix A for application notes) based on the clear day model atmosphere of Gordon (1969) using the Barteneva scattering functions has been performed [described in Section 2.2 of Duntley, *et al.* (1978)]. Later in this report we will present a comparison of the results of the theoretical calculations with the measured values of equilibrium reflectance obtained from sky radiance measurements. We will demonstrate the need to further explore the derivation of equilibrium reflectance, R_q, based on the existence of a unique relationship between the angular dependent Barteneva scattering functions and the measured total extinction coefficient of an atmosphere. To further explore the possibility of such a relationship an analysis of R_q based on the measurements taken at the OPAQUE ground stations has been undertaken.

A preliminary investigation of the initial issue ground based data set received to date has been conducted using measurements taken at Ypenburg during the periods June 13 to June 17, 1977 and August 15 to August 19, 1977. During the June sample period, data necessary for the computation of R_q were available from sunrise to sunset for all five days. For the August period, however, data was available only for August 18 and 19. During the entire sample period the sky was clear, 0 to 3/8 cloud cover, only on the afternoon of June 13. The other days were overcast with cloud cover of about 6/8 to 8/8.

A cross index between the notations historically used by the Visibility Laboratory, and those used in the OPAQUE surface data set is illustrated in Table 3.5.

The values of R_q are computed using the expression,

$$R_q(z,\theta,\phi) = \frac{B_s(z,\theta,\phi)}{\alpha(z)\ E(z,d)}\ . \qquad (3\text{-}1)$$

Table 3.5.

Notation Cross Index
(Ref Table 2.1)

Quantity	Visibility Laboratory Notation	OPAQUE Notation
Equilibrium Reflectance, (as a function of β)	$R_q(0,\beta)$ or $R_q(0,\theta,\phi)$	-
Path Function (as a function of β)	$B_*(0,\beta)$ or $B_*(0,\theta,\phi)$	FP(β)
Path Function (North)	$B_*(0,90°,N)$	FPN
Path Function (South)	$B_*(0,90°,S)$	FPS
Path Function (East)	$B_*(0,90°,E)$	FPE
Path Function (West)	$B_*(0,90°,W)$	FPW
Downwelling Illuminance	$E(o,d)$	EH
Total Volume Scattering Coefficient	$s(o)$	S
Extinction or Attenuation Coefficient	$\alpha(o)$	SE

where the orientation of the instrument is defined by its altitude above ground (z=0), the zenith angle of the instrument's optical axis (θ=90°), and the azimuth angle, ϕ. The extinction coefficient, $\alpha(o)$ in the photopic was measured with a transmissometer and the total downwelling illuminance, $E(o,d)$, in the photopic was measured with a luxmeter. Measurements of path function, $B_*(z,\theta,\phi)$, made at the four compass directions North, South, East, and West are denoted as $B_*(0,90°,N)$, $B_*(0,90°,S)$, $B_*(0,90°,E)$, and $B_*(0,90°,W)$, respectively. The compass direction indicates the direction from which radiation is received by the instrument sensor (the path of sight of the sensor).

The values of path function measured at each of the four orientations during the day depend on the scattering angle β, the angle between the optical axis of the path function radiometer and the position of the sun, (θ_s,ϕ_s). The expression which defines β is

$$\cos\beta = \sin\theta\cos(\phi-\phi_s)\sin\theta_s + \cos\theta\cos\theta_s \qquad (3\text{-}2)$$

For example, during the morning $B_*(0,90°,E)$ represents a measurement of radiation scattered through a β of less than 90°, at noon β is about 90°, and in the late afternoon β approaches 180°. Therefore, during the early morning hours values of $B_*(0,90°,E)$ should be greater than the values of $B_*(0,90°,W)$, in the late afternoon $B_*(0,90°,W)$ should be larger than $B_K(0,90°,E)$, and at local noon $B_*(0,90°,S)$ should be larger than $B_*(0,90°,N)$. Most of the data in the sample period supports the above three criteria, deviations are probably a result of the changing cloud cover. On June 13, however, none of the three criteria is satisfied even during the clear sky period. The reason for this discrepancy is not known at present, perhaps it was a simple coding error.

The values of R_q as a function of scattering angle, β, for the clear sky period are presented in Fig. 3-9. Remembering, β=0° represents the situation in which the sensor of the path function radiometer is looking directly into the sun. The values of R_q measured with the East facing radiometer are denoted by the symbol (x); the values measured with the West facing radiometer are indicated by (·).. The maximum in the curve of R_q near scattering angles of 0° and 180°, and the minimum near 90° are consistent with Rayleigh and Mie scattering theory and indicate the presence of useful angular information. At local noon (β=90°) the value of R_q measured in the West direction $R_q(0,90°,W)$, should equal the value measured in the East direction, $R_q(0,90°,E)$. This discrepancy, as shown in Fig. 3-9, is caused by the value $B_*(0,90°,E)$ not equaling the value $B_*(0,90°,W)$ at this time. The ratio of the values $B_*(0,90°,E)$ to $B_*(0,90°,E)$ at noon for the days studied are shown in Table 3.6 below.

Table 3.6.

Ratio of the values FPE to FPN at local noon

Date	FPE/FPW
June 13	2.26
June 14	0.85
June 15	2.84
June 16	0.51
June 17	0.62
August 18	0.94
August 19	1.00

The values of the ratio for the June data indicate the presence of a large noise component, however, the trend of improving data quality indicated by the ratios close to 1.0 for the August data is encouraging.

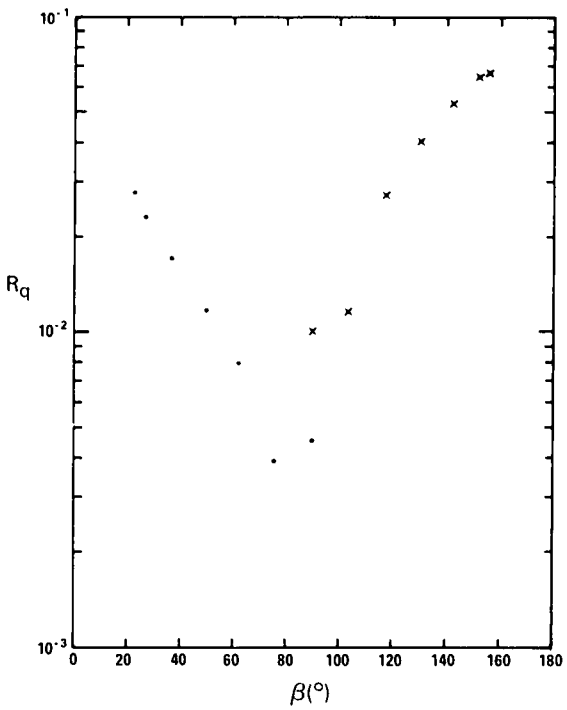

Fig. 3-9. Equilibrium Reflectance versus Scattering Angle, Clear Day.

A day with a constant overcast of 8/8 is represented by the values of R_q shown in Fig. 3-10. The values of

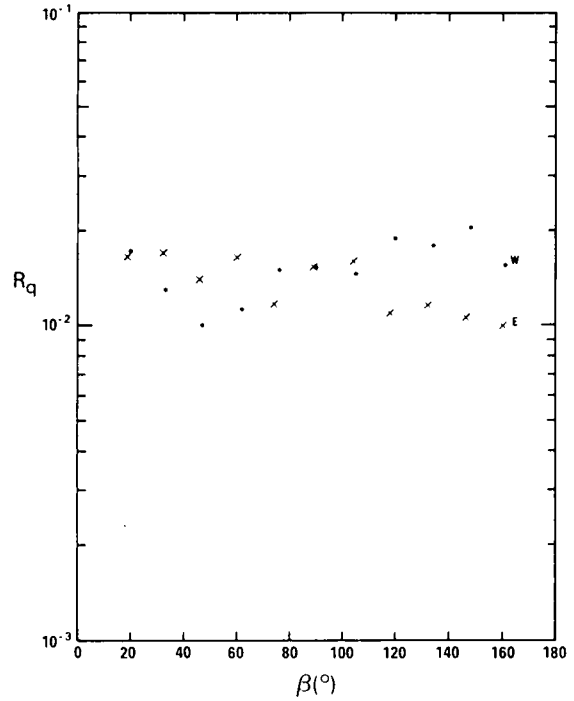

Fig. 3-10. Equilibrium Reflectance versus Scattering Angle, Overcast Day.

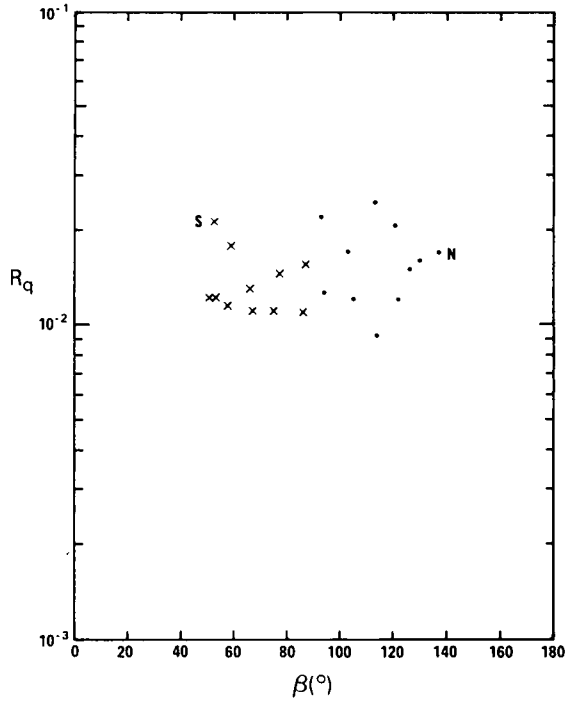

Fig. 3-11. Equilibrium Reflectance versus Scattering Angle, Overcast Day.

$R_q(0, 90°, W)$ represented by the symbol (·) and the values of $R_q(0, 90°, E)$ denoted by (x) cover the time 0700 to 1700 hours local time. At no point during this time span is the solar zenith angle larger than 72°. The lack of any apparent angular dependence is probably due to the near isotropic illumination of the radiometer path by the cloud deck. The lack of agreement between the values $R_q(0, 90°, W)$ and $R_q(0, 90°, E)$ is most likely due to changes in the cloud cover over the time interval studied.

The values of $R_q(0, 90°, N)$ and $R_q(0, 90°, S)$ do not generally cover most values of β, but because of the geometry cluster about a specific value of scattering angle. They, therefore, do not provide as much angular information as the East and West directions, but they do provide an indication of the stability of the instrument and atmosphere during the measurement period. Figure 3-11 presents the values of $R_q(0, 90°N)$ shown by (·) and $R_q(0, 90°, S)$ shown by (x) for the overcast day discussed with Fig. 3-10. The data show, again, the great variability in the values of R_q that can occur for a stable 8/8 overcast condition.

The preliminary analysis indicates that there is useful angular information in the measurements of path radiance for a clear sky, 0 to 2/8 overcast, as shown in Fig. 3-9. The data for an overcast sky appears too noisy to provide any useful information, even when the cloud cover observations indicate a time invariant overcast. The quality of the data appears to improve with time as shown in Table 3.6. Though the data sample investigated so far is small, it is felt that useful information with respect to the directional scattering properties of the surface layer aerosols can be extracted from the OPAQUE surface data base. Thus, the extension of these preliminary studies to the anticipated coincident fully edited data sets will be pursued.

3.7 INFRARED RELATIONSHIPS

A primary goal of the analysis related to the program OPAQUE data base is to derive wherever possible effective forecasting relationships between the optical/IR properties of the atmosphere and the general weather conditions. To this end several measurements of infra-red transmittance are identified in Section 2 that are included within each OPAQUE standard data set. Several examples of relatively simple comparisons between these measured transmittances, their equivalent extinction coefficients and several visual spectrum and meteorological parameters are similarly illustrated in the case study data appearing in the earlier portions of section 3.

The most apparent, yet not unexpected, generalization to be made from rough preliminary examination is that the relationships between visible and infra-red extinction coefficients tend to be weak and highly variable, although the correlations between the two infra-red band extinction coefficients are often quite good. However, an encouraging indication that reasonably well defined visible versus infra-red relationships may emerge from carefully selected sets of data was illustrated by the 3-5μ data displayed in Fig. 3-6. When one considers the atmospheric factors controlling extinction at visible and infra-red wavelengths, the basis for the generalities listed above becomes clear. In attacking the problem of determining well-defined relationships, one must first

separate the total atmospheric extinction into its component parts, the molecular and aerosol scattering and absorption coefficients and then address the individual contributions. When this is done, the complex roles of aerosol scattering and absorption become evident. Thus, eventually the relationships that appear between the meteorological and optical properties, both visible and infra-red, must surely be linked via a definition of the atmospheric aerosol properties.

A variety of studies related to the linkages between the aerosol-optical-meteorological regimes have provided specific guidance in establishing the direction of our proposed investigations. The initial study introducing the character of the infra-red transmittance data was the Pershore intercomparison reported by Shand (1978) in OPAQUE/R7804. Subsequent notes by Shettle (1977,1978), OPAQUE/US7704 and OPAQUE N/US-7805 addressed the predicted performance anticipated from the Barnes system and an example of the LOWTRAN based calibration procedure is discussed by Kohnle (1979) in OPAQUE N/GE-7908.

In pursuing the relationship between atmospheric aerosols and infra-red extinctions, one is led by the discussions of Turner, *et al.* (1979) in OPAQUE N/US-7903 and Nilsson (1979) in his comprehensive paper on the "Meteorological influence on aerosol extinction in the 0.2-40μm wavelength range". From Turner's discussions one notes that with regard to aerosol extinction, "...the contribution of aerosol absorption and scattering to the total extinction varies with particle size...", and that "...predictions of aerosol scattering, especially in the infra-red, are extremely sensitive to aerosol size distribution and refractive index changes...". And from Nilsson, "...it has been shown that the particle number concentration and size distribution have a dominating influence on the relation between the IR aerosol transmission and the meteorological visibility. ...Since different size ranges dominate the particle extinction in different wavelength bands, information on the particle size distribution is also needed before the meteorological visibility can be expected to serve as a useful predictor of the IR aerosol transmission."

It thus seems that a reasonable approach toward extracting the maximum utilization from the infra-red measurements within the OPAQUE surface data would be as follows.

Retain the concept of establishing and working within selected sets of fully edited data. Within these sets, use the AFGL LOWTRAN code where required with the issue 1 through 4 data to verify the application of the most probable calibration constants for the infra-red transmittance measurements, and to compute the aerosol and molecular components of extinction. From this selected library of issue 5 or equivalent data, readdress the relationships between the sample environments short term meteorological history, its aerosol size distribution data, and the derived visible and infra-red extinction properties. Whenever possible, associate these sets of optimized aerosol extinction data with those times and sites when both ground-based and airborne measurements of particle size distribution data are available.

In the context of the general plan outlined above, computer runs demonstrating the essential LOWTRAN computations with the initial issue class data have been accomplished, however the procedures for validating the Barnes calibration via selected LOWTRAN computations have not been established. Also since no surface aerosol data is yet available, only procedural planning has been initiated.

CONCLUSIONS & RECOMMENDATIONS

As discussed briefly in Section 3.1, and illustrated in the remaining body of Section 3, the analysis of the OPAQUE surface data has been conducted as a series of short case studies addressing only selected portions of the available data base. It is appropriate that the results of these studies be assessed within the context of their applicability to the development of the research goals pursued under this current contract effort. The following remarks are therefore directed toward this general assessment and some of its specific aspects. Acknowledging the preliminary nature of the available data issues, it seems that a reasonable course of action is to continue to address the data base in relatively small independent packages which lend themselves adequately to the case study approach, and to temporarily defer the longer range climatological studies.

It is clear also that the basically unedited OPAQUE surface data evaluated to this point is of only marginal value for general application without rather thorough review and editing. It is on this additional basis therefore, that the continuance of case studies of small optimized data sets, which can be easily pre-edited pending the receipt of the issue 5 data, be chosen as the most immediately productive analysis technique.

The short term studies discussed in the preceeding portions of section three have not illustrated any clearly defined relationships between the measured meteorological properties and the measurements of visible and infra-red spectrum scattering and extinction coefficients. They have indicated however that the rather broad scatter observed in the measurement is probably due to the real world characteristics of the environment, and should not be attributed entirely to instrumental error. The studies have also indicated that under selected meteorological conditions, essential information regarding the directional scattering properties of the near surface environment is retrievable from the standard data set. These directional properties are critical to the eventual predictions of contrast transmittance within the visible spectrum, and

may in turn be linkable to the directional scattering at other wavelengths.

There are evidences within the second case study in particular, that with continued effort toward parametric classification of the data some definitive stratifications will occur. This appears to be particularly true with respect to the visible spectrum extinction and relative humidity relationship, and to a somewhat less certain degree to the relationship between the visible and the 3 to 5μ extinction coefficients.

It is recommended that the continued analysis of these surface data be closely associated with the time intervals of coincident airborne and ground based measurements illustrated in Fig. 1-2. There are good evidences discussed elsewhere in this report, that reasonable progress, even in the short term, can be made in modelling the visible spectrum optical properties from selected sets of these jointly conducted measurements. This essential developmental step in the overall research effort need not be deferred nor held in abeyance pending the availability of the completely edited set of surface data.

4. DEVELOPMENT OF OPTICAL FORECASTING MODELS

The OPAQUE flight data gathered over a two-year period in Northern Europe have contributed significantly to our knowledge of the behaviour of aerosol optical properties in the lower troposphere. Under the expanded OPAQUE data analysis program now underway, the high resolution profiles of optical and meteorological parameters provide a basis for the development of improved operational techniques to predict slant path propagation effects from tactical area environmental information. As stated in Section 1, a primary initial task is to establish effective relationships between observed meteorological variables and optical properties in the visible wavelengths. Some preliminary results on the prediction of the vertical profile of photopic scattering coefficient are summarized in the following paragraphs.

4.1 MODEL PROFILES OF TOTAL VOLUME SCATTERING COEFFICIENT

Optical aerosol models included as part of the initial AFGL LOWTRAN Transmission Code (Selby and McClatchey (1972)) linked the vertical profile of photopic aerosol attenuation to surface visibility and specified an exponential decrease of haze density with increasing altitude in the lower troposphere. The aerosol models were later modified (Fenn and Shettle (1976)) on the basis of vertical profile data obtained prior to the OPAQUE flight series in other deployments of the optically instrumented aircraft in Europe and the United States. The revised aerosol models assumed a low-level haze layer of uniform density in the vertical and constant vertical extent (1.5 km). An exponential decrease in aerosol density was assumed above the haze layer. The model parameters were varied with respect to surface visibility and type of environment (*i.e.* urban, rural, marine, etc.)

As a first step in the development of improved techniques for the prediction of slant path transmittance, a more general single-layer haze model is set forth and is subjected to direct test and evaluation with OPAQUE flight data.

For profile model purposes it is important to consider a conservative aerosol property that in the absence of local sources or sinks does not change appreciably following three-dimensional air parcel trajectories. The visible scattering ratio, $Q(z)$, is such a parameter. As the vertical mixing within a given altitude layer becomes more complete, $Q(z)$ becomes more constant with height within the layer. The scattering ratio is defined by

$$Q(z) = s(z)/{}_R s(z) \tag{4-1}$$

where $s(z)$ is the total volume scattering coefficient, which is essentially equal to the extinction coefficient at visible wavelengths, since absorption is small, and ${}_R s(z)$ is the Rayleigh scattering coefficient. Note that

$$s(z) = {}_R s(z) + {}_M s(z) \tag{4-2}$$

where ${}_M s(z)$ is the aerosol scattering coefficient, also referred to as the Mie total volume scattering coefficient. Thus, the aerosol scattering ratio ${}_M s(z)/{}_R s(z)$ is given by

$${}_M s(z)/{}_R s(z) = Q(z) - 1 \tag{4-3}$$

It also would be constant under conditions of complete atmospheric mixing.

A general review of the flight profile data base shows that the top of the low-level haze layer is usually well-defined, and the transition zone between the haze layer and the region of relatively low extinction aloft is confined to a rather shallow transition zone, averaging about 300m in depth. For purposes of the initial tests of a modified single haze layer model, the depth of the transition zone is held constant at 300m. However, the depth of the low-level haze layer, Z, is made variable as a parameter to be specified or predicted from meteorological parameters. Attenuation over slant paths in the lower troposphere is very sensitive to the depth, Z, of the haze layer as well as scattering ratios in the low-level haze layer and in the upper altitude region. In the proposed model, the scattering ratios are assumed constant with height within both the upper and lower layers, and the scattering ratio is assumed to decrease exponentially with increasing altitude in the transition zone between the two layers (*i.e.* $\ln Q(z)$ decreases linearly with height).

4.2 APPLICABILITY TEST OF SCATTER RATIO MODEL

Preliminary tests were made of the accuracy of profile representation with the scattering ratio model. Flight data from the OPAQUE series as described in

Section 2 were selected for initial validation tests. Processed OPAQUE data published to date consist of 32 flights from field deployments in the spring and fall of 1976 and in the summer of 1977. On most but not all flights, scattering coefficient profiles were measured by the integrating nephelometer for each of four wavelength intervals. Three narrow band filters have peak wavelengths of 475 nm (blue), 660 nm (red), and 750 nm (near IR). The fourth is a broad band photopic filter centered near 550 nm. A sample set of profile data are shown in Fig. 2-1 and 2-2. Nine of the flights were of limited vertical extent (<3 km) and were not included in the test series. Also, editing was required to exclude anomalous data resulting from cloud penetrations occurring at the highest levels sampled on a few individual flight profiles.

The scattering ratio model was fitted to the individual filter profiles of scattering ratio by the method of least squares. In the process, we chose initially to minimize the root-mean-square *percentage* error in scattering ratio over all altitude levels. For this reason the form of the dependent variable selected for model fitting was $\ln Q(z)$.

The objective curve fitting procedure determines the specific values of the modelling coefficients which best represent the individual scattering profiles. The three parameters that specify the scattering ratio profile are:

$$(a)\quad \overline{\ln Q_l} = \frac{1}{n_l} \ln \sum_{0}^{Z} \ln Q_l(z) \qquad (4\text{-}4)$$

$$(b)\quad \overline{\ln Q_u} = \frac{1}{n_u} \sum_{Z+300m}^{z_{max}} \ln Q_u(z) \qquad (4\text{-}5)$$

(c) Z = altitude of the top of the haze layer

where $Q_l(z)$ is scattering ratio in the low-level haze layer, $Q_u(z)$ is scattering ratio in the upper region between the transition zone and z_{max}, the highest altitude reached by the flight profile.

Examples of the resultant model fit to individual profiles of scattering ratio are shown in Figs. 4-1, 4-2, and 4-3.

Flight 372 shown in Fig. 4-1 was an afternoon flight in the spring over a rural area in the central Netherlands. Under moderate convective mixing conditions, the haze layer extended to an altitude of 2200m. Flight 390 of Fig. 4-2 was made in the fall season over the shallow water of Femer Bay near Rodby, Denmark. Moderate haze was observed in a marine layer with a well-defined top at 780m. The model fit for each of these two profiles was among the best in the series with a rms specification error of approximation 15 percent for flight 372 and 17 percent for flight 390.

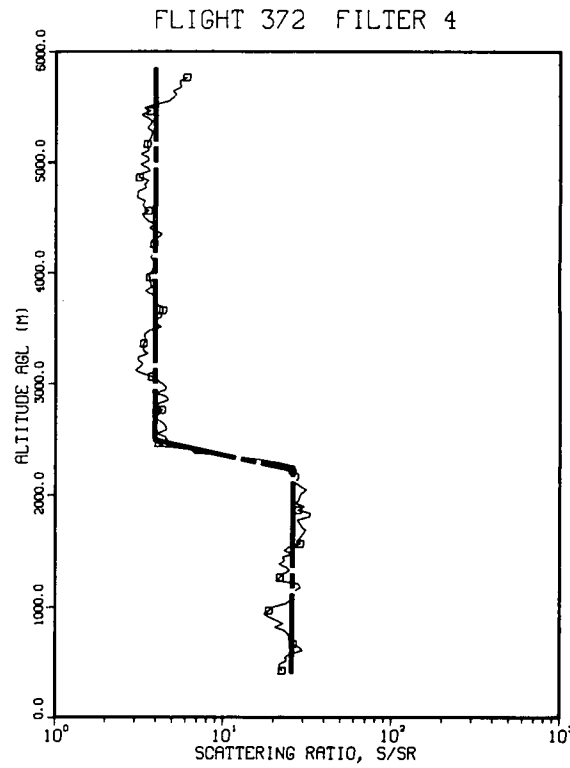

Fig. 4-1. Scattering ratio profile for Soesterberg, Netherlands, 12 April 1976, for the photopic filter. The heavy dashed line is the objective model representation of the profile.

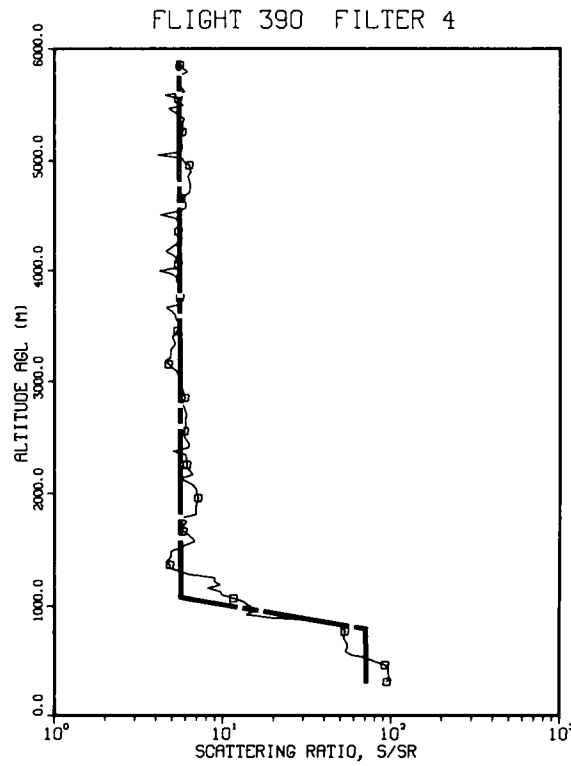

Fig. 4-2. Scattering ratio profile and model representation for Rodby, Denmark, on 25 October 1976 for the photopic filter.

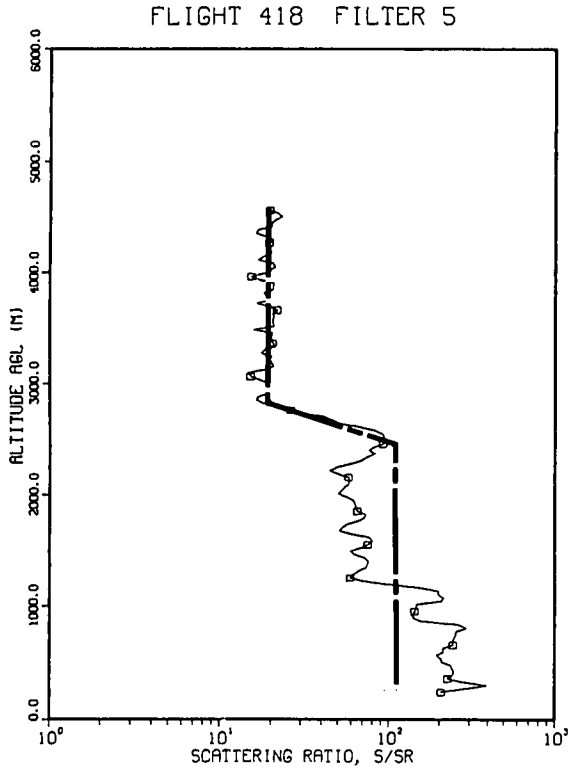

Fig. 4-3. Scattering ratio profile and model representation for Ahlhorn, Germany, on 4 August 1977 for the near IR filter.

In contrast the model representation of the profile of flight 418 shown in Fig. 4-3 has a rms error of 40 percent, one of the worst in the test series. Flight 418 was a morning flight made in summer over open farmland in northwestern Germany. A dense haze layer and an intermediate altitude haze layer of lower density are clearly evident in the $Q(z)$ profile. The least squares solution for a single haze layer model placed the haze top above the second or intermediate layer, although a strong secondary minimum in the calculated residual variance was associated with the top of the lower haze layer. The correspondence between the multi-layered structure of the scattering ratio profile and features of the temperature profile are discussed later in the report.

Calculations were made of the rms percent departure of the measured $Q(z)$ values at 30m-altitude intervals from those specified by the scattering ratio model for all individual filter profiles. The resultant distribution of errors is shown in Fig. 4-4. The results are impressive in that the rms error of the $Q(z)$ profile representation by the single haze layer model was less than 30 percent in 75 percent of the cases examined. As noted above, the largest errors were associated with profiles having an additional and somewhat more dense haze layer near the ground.

4.3 SPECIFICATION OF HAZE LAYER DEPTH

Model representation accuracy is of little consequence unless the model coefficients are of a form

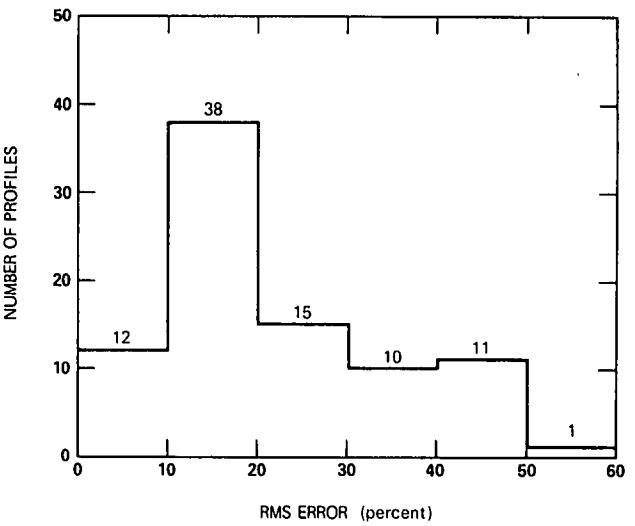

Fig. 4-4. Root-mean-square departure in percent of individual scattering ratio values $Q(z)$ from the single haze layer model representation as calculated by the method of least squares. Histogram represents error distribution as calculated for 87 individual filter profiles.

that can be forecast with acceptable accuracy whenever and wherever needed. The next step in the preliminary test program was to explore techniques for the specification of Z, the depth of the low-level haze layer. The vertical extent of turbulent or convective mixing in the lower troposphere is controlled to a large degree by the temperature lapse rate. Thus, we might expect that the structure of the temperature profile might be the best single predictor of Z. The problem is to establish objective criteria which relate, quantitatively, the temperature lapse-rate structure to mixing depth. In this preliminary study, the temperature profiles measured by the instrumented aircraft in combination with the scattering ratio profiles for each spectral filter were utilized to establish and test such criteria. The data base consisted of the same group of OPAQUE flights which were used for the initial tests of model representations.

Close inspection of the flight profile data suggested that a stable thermal layer of at least 500m in depth was needed to inhibit significant vertical mixing between a low-level haze layer and the relatively clear overlying atmosphere. So as a first trial, the lapse rate, Γ in deg C per km, was calculated by

$$\Gamma = [T(z+510m) - T(z)]/0.510 .$$

Sample calculations of a lapse rate profile and the corresponding temperature profile are shown in Figs. 4-5a and 4-5b. The lapse rate is plotted at the base of the altitude layer over which it was calculated. Values were calculated for overlapping 510m intervals spaced 30m apart. The high frequency fluctuations observed in the lapse rate profiles (as well as in the scattering ratio profiles) are due primarily to noise originating in the aircraft electrical system. The bases of significant stable layers essentially are coincident with the minimum lapse

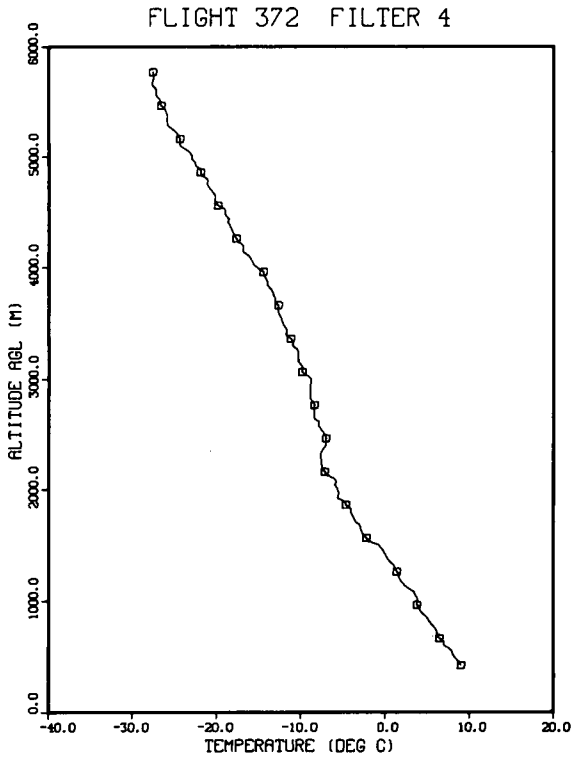

Fig. 4-5a. Temperature profile measured by the instrumented aircraft for Soesterberg, Netherlands, on 12 April 1976. Measurements were made simultaneously with the scattering ratio profile shown in Fig. 4-1.

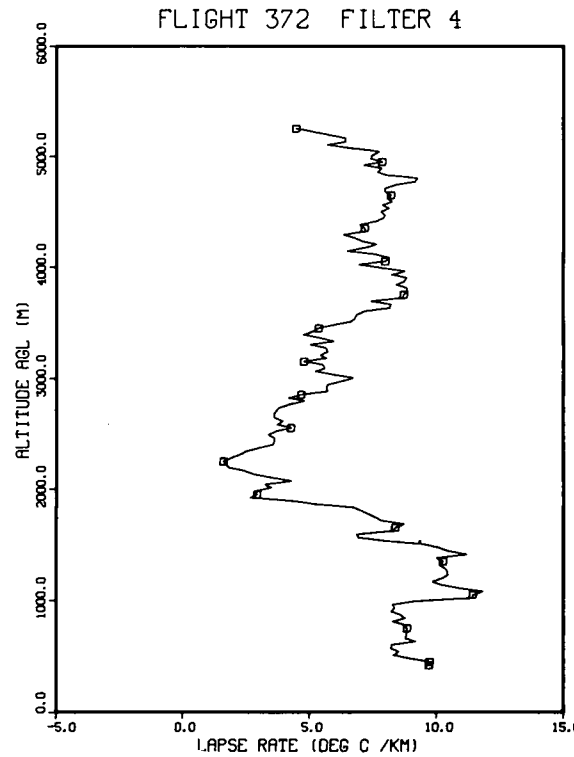

Fig. 4-5b. Temperature lapse rate corresponding to Fig. 4-5a calculated by finite differences over overlapping 510m intervals speed 30m apart.

rate in the stable layer as calculated and plotted in Fig. 4-5b. This definition of the base altitude of the stable layer was adopted for purposes of the analysis.

Individual profiles of temperature lapse rate corresponding to the profiles of scattering ratio depicted above are shown in Figs. 4-6 and 4-7. The close relationship between the base of the stable layer and the top of the haze layers was typical of most flights in the test series. Notice that in the case of the double haze layer shown in Fig. 4-3, a stable layer in Fig. 4-7 was coincident with the top of each layer. The lower haze layer and the associated thermally stable region become prominent in the last of the four profiles (filter 5) measured on this flight.

An analysis of the correspondence between haze layer depth and the base height of the low-level stable temperature layer is shown in Fig. 4-8. For purposes of this comparison, the base of the thermally stable layer was calculated from the average of the temperature profiles measured by the aircraft within the approximately 2-hour period. Similarly, the value of Z was obtained by a simultaneous least-square fit to all of the individual filter profiles of scattering ratio measured on that flight. So that the single value of Z calculated by this method was assumed valid for each of the filter profiles (usually four) measured on that flight; the specified Z yielded the smallest rms departure of all values $\overline{\ln Q(z)}$ from the individual $\overline{\ln Q_l}$ and $\overline{\ln Q_u}$ determined separately for each filter profile.

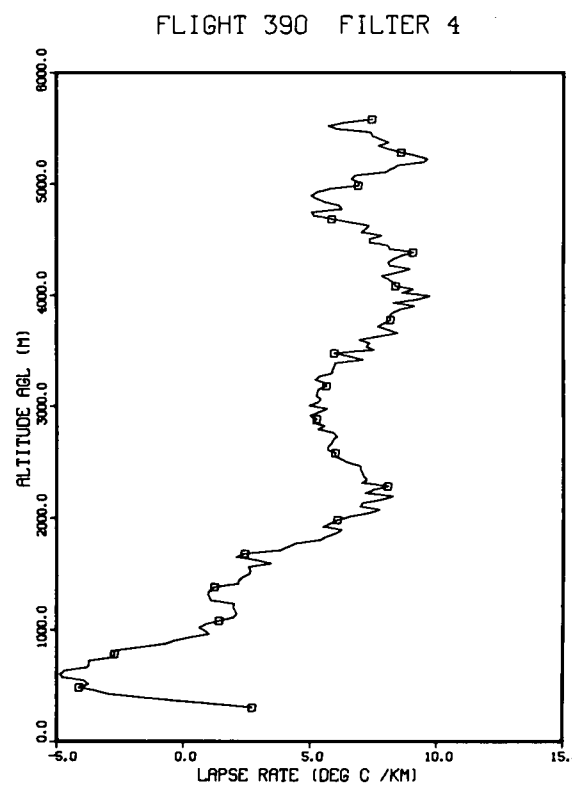

Fig. 4-6. Temperature lapse rate for flight 390 corresponding to scattering ratio profile for Rodby, Denmark, on 25 October 1976, shown in Fig. 4-2.

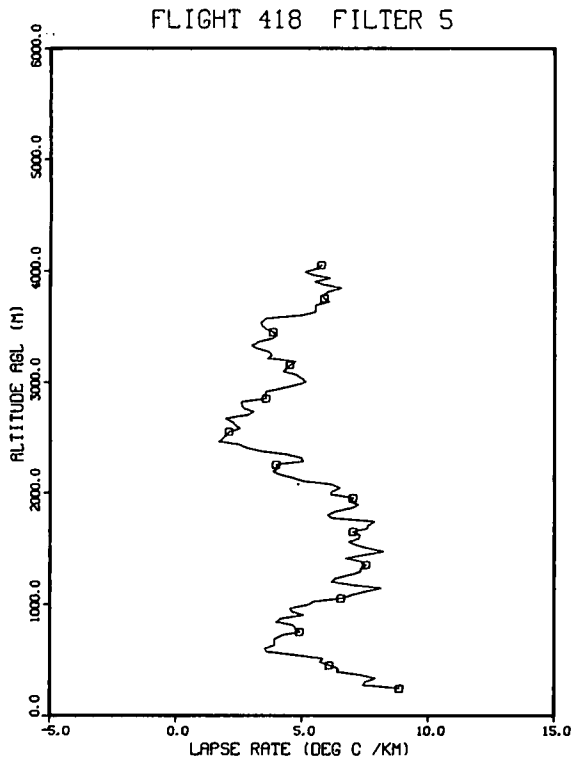

Fig. 4-7. Temperature lapse rate for flight 418 corresponding to scattering ratio profile for Ahlhorn, Germany, on 4 August 1977, shown in Fig. 4-3.

The following criteria were used for the calculation of the base-height of the stable layers as shown in Fig. 4-8. The stable layer was defined as the lowest altitude region where the lapse rate was less than 4.5 deg per km. The base altitude was defined by the minimum value of lapse rate in the stable layer as calculated over overlapping 510m-intervals. If no thermally stable layer with an identifiable minimum of less than 4.5 deg per km is present within the altitude range of the measured profile, the altitude of the minimum lapse rate below 4 km in altitude was selected as the base height of the stable layer. These criteria are straight-forward except that they leave undefined the case where a very low level stable layer is present, and the base of the layer is below the lowest altitude sampled by the aircraft. The importance of ground based inversions in relation to aerosol optical models is discussed in a later section.

The results for this limited data sample shown in Fig. 4-8 are encouraging. The rms departure of the altitude of haze-layer top from the base of the thermally stable layer is 123m. The departures tend to be systematic in that the haze layer top extends somewhat above the calculated base-height of the stable layer at low altitudes and the inverse is true at higher altitudes.

Even more encouraging is the fact that for the test sample the error of profile representation did not increase significantly when Z is obtained from temperature lapse rate criteria instead of the Z calculated from a direct model

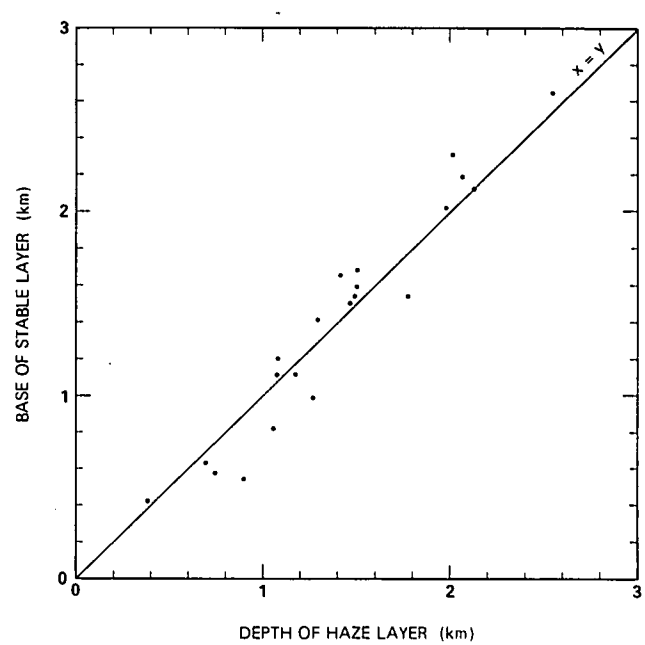

Fig. 4-8. The depth of the low-level haze layer, Z, determined from the model fit of scattering ratio profiles as compared to the corresponding altitude of the base of the stable layer as calculated from the temperature profile.

fit to the scattering ratio data. Figure 4-9 is a histogram of the rms departure of measured $Q(z)$ from the individual model profiles for each flight. It may be compared with Fig. 4-4. Figure 4-9 differs from Fig. 4-4 in that Z was obtained from the temperature lapse rate rather than by direct model fit and the rms error values were calculated for a combined set of all filter profiles for a given flight

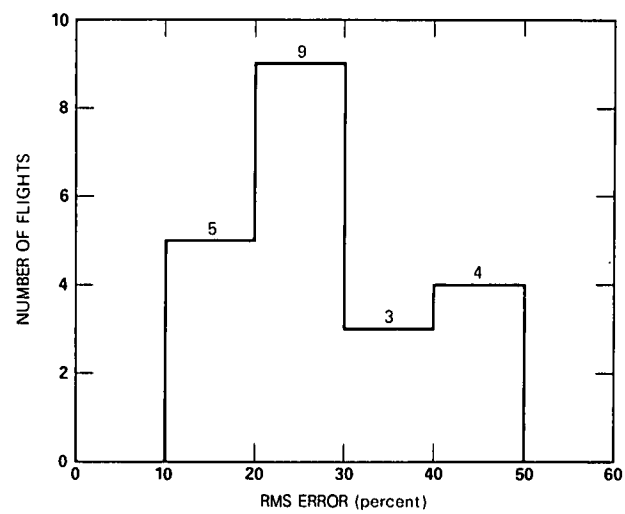

Fig. 4-9. Root-mean-square departure in percent of individual filter values of scattering ratio $Q(z)$ from model representation of the profiles. In contrast with Fig. 4-4, the depth of the haze layer Z was specified from the temperature lapse rate profiles rather than from a direct fit of the scattering ratio profiles. Histogram values represent combined error calculations for all individual filter profiles on a given flight (usually four per flight for a total of 84).

rather than on an individual filter basis. Notice that two-thirds of the cases have rms errors of less than 30 percent in the level by level specification of $Q(z)$ at 30m intervals for the individual filter profiles.

4.4 BEHAVIOR OF MODEL COEFFICIENTS

Let us now examine briefly the behavior of the coefficients $\overline{\ln Q_l}$ and $\overline{\ln Q_u}$ as calculated from the objective fit of the scattering ratio model to the profile data. For the single-layer model, the assumption was made that the scattering ratio is constant with height in the low-level haze layer and is given by $\overline{\ln Q_l}$. To the extent that this assumption is valid, the value of $\overline{\ln Q_l}$ is equal to $\ln Q(o)$ measured near the base of the scattering ratio profile. Figure 4-10 shows the relationship between $\ln Q(o)$ and $\overline{\ln Q_l}$ for all of the filter 4 (photopic) scattering ratio profiles. As was to be expected on the basis of results described earlier, the scattering ratio at the base of the sounding does reflect the average throughout the lower mixing layer. At least for this sample, a systematic trend for either a decrease or increase in scattering ratio with height within the layer is not evident, and the scattering ratio or visual range equivalent in the altitude range 100-300m provides a good estimate of the overall haze layer density. The average error of estimate of $Q_l(z)$ as calculated in Fig. 4-10 is 19 percent.

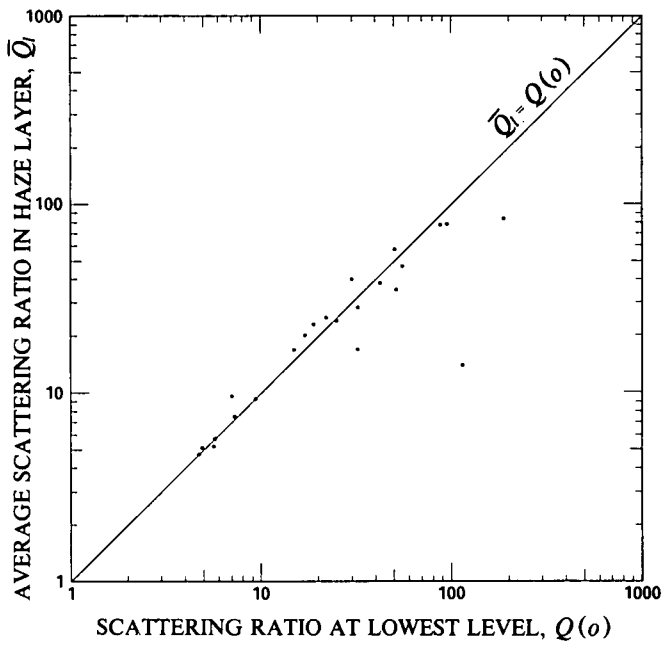

Fig. 4-10. Correspondence between scattering ratio at the base of the profile, $Q(o)$, and the average value of scattering ratio in the low-level haze layer $\overline{Q_l}$ as given by the model.

Values of the average scattering ratio in the low-level haze layer, $\overline{Q_1} = \exp \overline{\ln Q_1(z)}$, for each photopic filter profile in the test series are shown in Fig. 4-11. As indicated in the histogram, a wide range of low-level visibility conditions was sampled in all seasons during the OPAQUE series of airborne measurements. The resultant values of $\overline{Q_1}$ varied from 9 to 82, which correspond at sea level to daytime visibilities of about 29 km and 4 km, respectively, under the assumption of 5 percent threshold contrast.

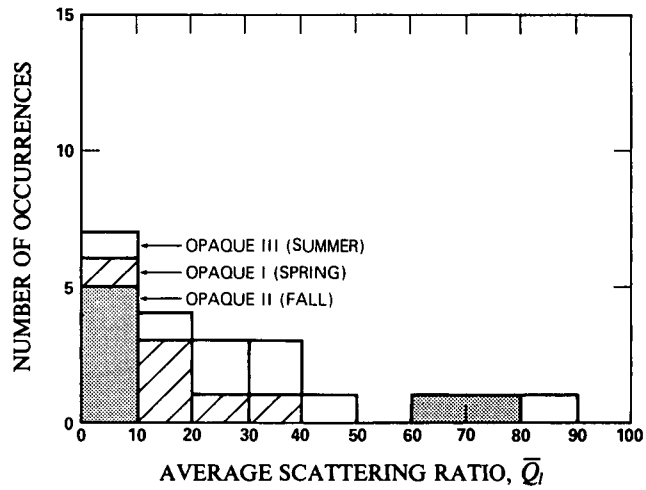

Fig. 4-11. Values of the average scattering ratio in the low level haze layer for the photopic filter. $\overline{Q_1} = \exp \overline{\ln Q_1(z)}$.

As shown in Fig. 4-12, the scattering ratio above the low-level haze layer was consistently low for the spring and fall flight profiles. The values of $\overline{Q_u}$ for the photopic filter for those seasons ranged from a high of 6 times the corresponding Rayleigh scattering coefficient to low of 2. The average scattering ratio above the haze layer for all spring and fall flights was 3.7. For this sample, a small constant value of average scattering ratio $\overline{Q_u}$ could be assumed for modelling purposes during the colder months with relatively small absolute error in computed slant path transmittance. This is not true for the summer flight

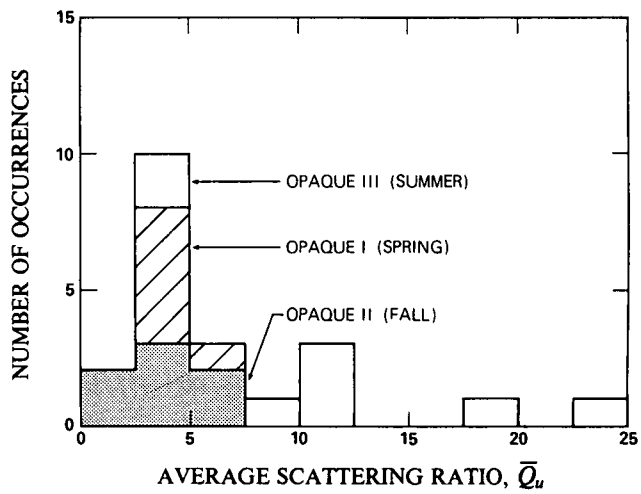

Fig. 4-12. Values of the average scattering ratio in the altitude region above the low-level haze layer for the photopic filter. $\overline{Q_u} = \exp \overline{\ln Q_u(z)}$.

series of OPAQUE data. In contrast, the summer values of $\overline{Q_u}$ ranged from a high of 25 times the Rayleigh scattering coefficient to a low of 4. The summer average was 13.6 times the Rayleigh scattering coefficient. Thus, special attention must be given to the problem of forecasting $\overline{Q_u}$ as well as $\overline{Q_l}$ in the summer months.

The assumption of a fixed depth for the transition zone above the haze layer top may prove to be unnecessarily restrictive and does require additional study. The initial results show that an average depth of 300m is a good approximation for most profiles. However, a tendency is observed, for example, for a deeper zone of transition to occur between the haze layer and the relatively clear region aloft during periods when the surface visibility is less than about 6 km.

4.5 SUMMARY

Preliminary test results suggest that a single haze layer model of variable depth for representation of the scattering ratio profile is a rational approach to the problem of slant path transmittance prediction in the lower troposphere. Additional development, test and evaluation studies are necessary to establish the validity of the model under a wide variety of environmental conditions and to refine and establish criteria for the specification and prediction of the model coefficients Z, $\overline{Q_l}$ and $\overline{Q_u}$.

Although the flight data included in the preliminary test sample were gathered in a variety of locations in northern Europe in all seasons, it is very important to realize that they are very limited in number and somewhat specialized with respect to weather conditions. In particular, all flights were made in the daylight hours in VFR flight conditions and the minimum altitude of the profile test sample was 100m. Accordingly, important complicating factors associated with the formation of ground based temperature inversions or stable layers due to radiational cooling of the ground surface at night did not significantly influence the initial test results. The modelling of the structure and behavior of scattering coefficient profiles within a thermally stable region adjacent to the surface is a prime subject for additional study with specialized high resolution optical and meteorological measurements.

Aside from the significant nocturnal boundary layer effects, we might expect that the relationships revealed by the flight test sample have general applicability. As we proceed with more complete tests based upon substantial additional flight data from Europe and the United States available in our data base, we anticipate the following:

(1) The simple model with a single low-level haze layer of variable depth will represent effectively the vertical profile of photopic scattering ratio in most daytime situations.

(2) A double haze layer model will be required for effective profile representation in some cases as identified by the presence of a significant ground based stable layer.

(3) Haze layer tops can be specified objectively and accurately by temperature lapse rate criteria which identify thermally stable layers in the lower troposphere. The relevant stable layers are of sufficient depth and strength in most cases to be identified with conventional radiosonde observations.

(4) To a good first approximation in the daytime, the optical scattering ratio can be assumed constant with height in a given haze layer and again in the altitude region above the transition zone and below the nominal flight altitude limit of 6 km. It follows, for example, that the average scattering ratio in a given layer may be estimated effectively by an observation or reliable forecast of scattering ratio at the base of the layer.

(5) For many purposes, the scattering ratio above the haze layer in the colder months over northern Europe may be assumed equal to a low average background level. Special forecasting techniques will be required to handle the much greater variability of scattering ratio above the low-level haze layer in the summer months.

5. DETERMINATION OF DIRECTIONAL OPTICAL PROPERTIES

5.1 INTRODUCTION

To calculate the degradation of contrast or the change in radiance of an object due to the attenuating effects of the intervening atmosphere, it is necessary to know the transmittance of the intervening path $T_r(z,\theta)$ and the path radiance $N_r^*(z,\theta,\phi)$. The path radiance may be considered independent of the object radiance ${}_tN_o(z,\theta,\phi)$ or background radiance ${}_bN_o(0,\theta,\phi)$ as long as the relative size of the object and immediate background are small relative to the general terrain. (The general terrain determines the albedo and contributes significantly to the path radiance).

The general equation for apparent radiance is (Eq. (1) Duntley, *et al.* (1957))

$$N_r(z,\theta,\phi) = N_o(z_t,\theta,\phi)\,T_r(z,\theta) + N_r^*(z,\theta,\phi)\,, \qquad (5\text{-}1)$$

and the contrast transmittance $C_r(z,\theta,\phi)/C_o(z,\theta,\phi)$ is (Eq. (2-3), Duntley (1964))

$$\frac{C_r(z,\theta,\phi)}{C_o(z_t,\theta,\phi)} = \left[1 + \frac{N_r^*(z,\theta,\phi)}{{}_bN_o(z_t,\theta,\phi)\,T_r(z,\theta)}\right]^{-1}. \qquad (5\text{-}2)$$

Section 4 dealt with the total volume scattering coefficient profile with altitude which determines the radiance transmittance appropriate for Eqs. (5-1) and (5-2). This section will deal with the determination of visible spectrum path radiance, or the parameters which govern the path radiance, to provide a baseline for developing predictive procedures for the directional properties of the atmosphere.

The airborne data set contains three primary sources of data on the directionality of the scattered light in the troposphere. One source is the measurements made with the three channel integrating nephelometer. These data consist of the volume scattering function at 30 and 150 degrees in addition to the total volume scattering coefficient, all of which were measured during the straight and level flight elements of each data mission. A second source is the data measured by the automatic 2π scanner during cloudless days, since on those days the measured sky radiance is equal to the space-to-earth path radiance. The third source is the measurements of vertical and horizontal path function made during both the vertical and straight and level flight elements of each data mission.

The data related to each of these three sets of measurements and their applicability to the determination of directional tropospheric optical properties is discussed in the following paragraphs.

5.2 DIRECTIONAL ASPECTS FROM NEPHELOMETER DATA

Integrating nephelometer data were taken by the Visibility Laboratory on the ground and in the troposphere during the period 1968 to the present, in Thailand, the continental U.S. and Europe. These data comprise three measurements: the total volume scattering coefficient $s(z)$, and the volume scattering function $\sigma(z,\beta)$ at 30 degrees and 150 degrees. These measurements were made with various narrow and broad band spectral sensitivities in the visible spectrum and very near infra-red, with mean wavelengths ranging from 478 to 765 nanometers.

The pseudo-photopic filter was first used during 1970 for HAVENVIEW I (Duntley, *et al.* (1972a)) and was used in that nephelometer from 1970 to 1974 during four subsequent deployments, ATOM (Duntley, *et al.* (1972b)), METRO (Duntley, *et al.* (1973, 1974)), HAVENVIEW II (Duntley, *et al.* (1976)) and SEEKVAL (Duntley, *et al.* (1975a)). The directional characteristics of these data are depicted in Fig. 5-1. The superimposed curve is based on the data from Barteneva (1960).

For the representation in Fig. 5-1, the measured total volume scattering coefficient and the measured volume scattering function data were first adjusted to sea level density as described in Duntley, *et al.* (1977). A sea level density $\rho(0)$ of $1.225 kg/m^2$ was used which is appropriate for the U.S. Standard Atmosphere (1962). The modification of the flight data to equivalent ground level density values was made in order to enable a more direct comparison with the predominantly sea level data from Barteneva (1960).

Barteneva (1960) provides a catalog of proportional directional scattering functions $\sigma(\beta)/s$ for the photopic sensor based upon 624 measurements made during 1955-1958 at various locations in the USSR and at sea. For each volume scattering function she gives a range of total volume scattering coefficient appropriate to that function. Median values of scattering coefficient were derived for each of the gradual scattering function classes, Nos. 1-10.

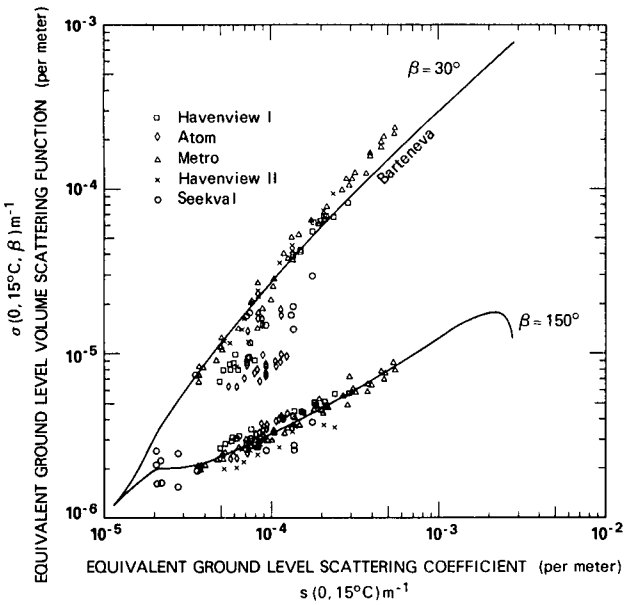

Fig. 5-1. Equivalent sea level volume scattering function at 30° and 150° related to the equivalent sea level total volume scattering coefficient for the pseudo photopic filter mean wavelength 557 nanometers as compared to Barteneva (1960).

Her catalog of gradual functions, classes 1 through 10, are appropriate for very clear to heavy haze, respectively but not fog. This range of functions is applicable to the troposphere under conditions appropriate for flying under visual flight rules, the conditions for the Visibility Laboratory aircraft data missions. Since the Visibility Laboratory ground-based data also were taken in conjunction with the flights, these same conditions are also appropriate for these simultaneous ground-based data.

The values of ${}_B\sigma(0,\beta)$ for the Barteneva curve in Fig. 5-1 were obtained from the Barteneva catalog of $\sigma(\beta)/s$ by multiplying by the median values of total volume scattering coefficient ${}_Bs(0)$

$$ {}_B\sigma(0,\beta) = {}_Bs(0)\ \sigma(\beta)/s\ . \qquad (5\text{-}3) $$

Only a few data values from the Project ATOM flights depart noticeably from the Barteneva curve for ${}_B\sigma(0,30°)$ versus ${}_Bs(0)$ in Fig. 5-1. The relationship of $\sigma(0,150°)$ to $s(0)$ is quite good for all the data.

The nephelometer was redesigned late in 1974 with a folded optical path and subsequently used in this configuration for Project OPAQUE, Duntley, *et al.* (1978c). Since the relationships between the directional scattering and the total scattering in the Barteneva catalog were used to devise a correction applied to the OPAQUE data, it is inappropriate to look at the corrected data in the same form. However, since the corrections applied primarily to the low values of $s(z)$ there may be some uncorrected high-value data that can be so compared. It is planned to proceed to do that comparison.

It was discovered during the analysis of the 1970-1974 data and the OPAQUE data [see Section 8.2, Duntley, *et al.* (1977)] that nephelometer data for the non-photopic filters compared well to the Barteneva median s values and her gradual classes of $\sigma(\beta)/s$ when the Barteneva data and the non-photopic filter data are put in the form of the ratio to the Rayleigh scattering for that filter, ${}_Rs$, or Q, and ${}_R\sigma(\beta)/\sigma(\beta)$. The ratio ${}_R\sigma(z,\beta)/\sigma(z,\beta)$ is equivalent to ${}_R\sigma(0,\beta)/\sigma(0,\beta)$ and $Q(z)$ is equal to $Q(o)$ since both numerator and denominator are multiplied by the same constant, the density ratio. Therefore the altitude designation has been left off those ratios.

The nephelometer data from the period 1970 to 1974 for Filter 2, mean wavelength 478 nanometers have been graphed in Fig. 5-2 in the same form as Fig. 5-1.

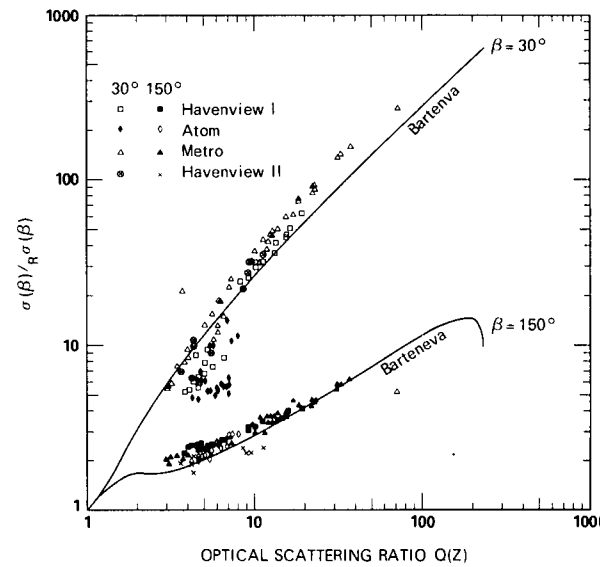

Fig. 5-2. Ratio of measured volume scattering function to the Rayleigh scattering function at 30° and 150° related to the optical scattering ratio $Q(z)$ for Filter 2 mean wavelength 478 nanometers as compared to Barteneva (1960).

The evidence to date is sufficient to suggest that a knowledge of $s(z)$, $\rho(z)$ and ${}_Rs(0,\bar{\lambda})$ will allow one to use the Barteneva catalog to obtain $\sigma(z,\beta)$ for any spectral band within the visible spectrum. Thus a specification of the directional scattering properties of the aerosol can be reasonably deduced from a measurement of the total volume scattering coefficient alone. The degree to which the additional experimental data supports this contention, will determine the degree of generality to which this potentially powerful relationship can be applied.

The next step is to proceed to obtain a statistical measure of the goodness of fit of the nephelometer data to the Barteneva median curves for both the photopic and non-photopic data bases.

5.3 DIRECTIONAL PROPERTIES FROM SKY RADIANCE MEASUREMENT

Although, as yet, no sky radiance data from the OPAQUE deployments have been processed, selected data from deployments previous to OPAQUE can be fruitfully reviewed to determine the potential for using sky radiance measurements as an indicator of the directional scattering properties of the atmosphere. This review will suggest methods to be used for the full exploitation of the OPAQUE sky radiance data base.

EFFECTIVE EQUILIBRIUM RADIANCE

When the sky is free of clouds, the sky radiance is the path radiance for the path of sight from space to the sensor altitude $N^*_\infty(z,\theta,\phi)$. The effective equilibrium radiance $\bar{N}_q(z,\theta,\phi)$ for that path of sight is the path radiance divided by one minus the transmittance of the path of sight $T_\infty(z,\theta)$

$$\bar{N}_q(z,\theta,\phi) = N^*_\infty(z,\theta,\phi)/[1-T_\infty(z,\theta)] \ . \qquad (5\text{-}4)$$

When the effective equilibrium radiance is graphed as a function of angle from sunβ, as in Fig. 5-3, the values cluster as a fairly tight function of β with a characteristic shape similar to the proportional volume scattering function $\sigma(\beta)/s$. [Also see Fig. 1, Gordon (1969) and Fig. 2, Gordon, *et al.* (1973)]. The scattering angle β is a function of the path of sight zenith angle θ, azimuth from the sun ϕ, and the zenith angle of the sun θ_s,

$$\cos\beta = \sin\theta\cos\phi\sin\theta_s + \cos\theta\cos\theta_s \ . \qquad (5\text{-}5)$$

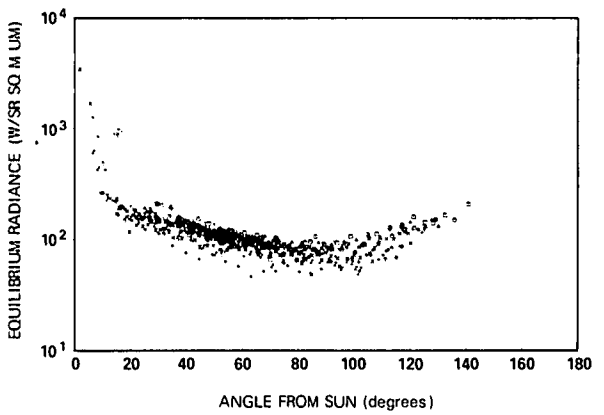

Fig. 5-3. Effective equilibrium radiance derived from sky radiances as a function of angle from sun. For flight C-154, 4.375 km altitude AGL, Filter 2 mean wavelength 478 nanometers. The symbols indicate that the sky radiances were measured at eighteen different zenith angles ranging from 2.5 to 87.5 degrees.

The effective equilibrium radiance graph in Fig. 5-3 is from scanner radiance measurements made during flight 154 at 4.375 km altitude AGL with Filter 2, mean wavelength 475 nanometers during Project ATOM, Duntley, *et al.* (1972). The vertical space-to-sensor transmittance used in Eq. (5-4) was 0.84 as derived from sky radiance ratios, Duntley, *et al.* (1978c). This transmittance is in good agreement with the transmittance as determined by the ground-based Contrast Reduction Meter (CRM) measurements in combination with the airborne measurements of total volume scattering coefficient. Flight 154 was made during the morning of 28 October 1970 over a broad desert valley in central New Mexico. The solar zenith angle during this straight-and-level flight element was 53 degrees. The scalar albedo was 0.14 as computed from the scanner radiances and the transmittance.

POINT FUNCTION EQUILIBRIUM RADIANCE

The point function equilibrium radiance for clear and cloudy skies is also primarily a function of the angle from the principal light source, the sun or the moon. It can be computed from

$$N_q(z,\beta) = {}_sh_0\,T_\infty(z,\theta_s)\sigma(\beta)/s + \int_{4\pi} N(z,\theta',\phi')\sigma(\beta')/s \ d\Omega \ , \qquad (5\text{-}6)$$

where $N(z,\theta',\phi')$ is the 4π radiance distribution and ${}_sh_0$ is the sun irradiance out of the atmosphere. To a first approximation, the second term in Eq. (5-6) which is the diffuse component, can be re-expressed in terms of scalar irradiance quantities (Eq. (21) Gordon (1969))

$$N_q(z,\beta) = {}_sh_0\,T_\infty(z,\theta_s)\sigma(\beta)/s + \frac{h(z,u) + {}_kh(z,d)}{4\pi} \ . \qquad (5\text{-}7)$$

The $h(z,u)$ is the upwelling scalar irradiance and ${}_kh(z,d)$ is the sky scalar irradiance. The sun scalar irradiance at altitude can also be expressed as ${}_sh(z)$.

If we integrate both sides of Eq. (5-7) with respect to β we find that

$$\int_{4\pi} N_q(z,\beta)\,d\Omega = h(z) \qquad (5\text{-}8)$$

where h is the total scalar irradiance. Thus

$$\int_{4\pi} \frac{N_q(z,\beta)}{h(z)}\,d\Omega = 1 \ . \qquad (5\text{-}9)$$

The quantity $N_q(z,\beta)/h(z)$ is the proportional equilibrium radiance function.

PROPORTIONAL VOLUME SCATTERING FUNCTION RECOVERY

Equation (5-7) also gives us the basis for an equation for approximating the proportional volume scattering function $\sigma(\beta)/s$ from sky radiance data for clear days. Rearranging Eq. (5-7) we get (Eq. (23) from Gordon (1969))

$$\sigma(\beta)/s = \left\{ N_q(z,\beta) - \frac{\left[\, h(z,u) + {}_kh(z,d) \,\right]}{4\pi} \right\} / {}_sh(z) \ . \qquad (5\text{-}10)$$

In order to use Eq. (5-10) more easily with sky radiance data, it has been found useful to compute average values of effective equilibrium radiance $\bar{N}_q(\beta)$ for each 5 degrees in scattering angle. An example of just such a calculation is given in Fig. 5-4. The sky radiance data are from the SEEKVAL deployment (Duntley, *et al.* (1975)) flight C-360A, which was a morning flight conducted over flat grassy prairie in western Washington. The sky was clear except for scattered clouds on the horizon, so the sky radiances data used were confined to zenith angles 0 to 82.5 degrees. The sun zenith angle was 66 degrees and the scalar albedo was 0.069.

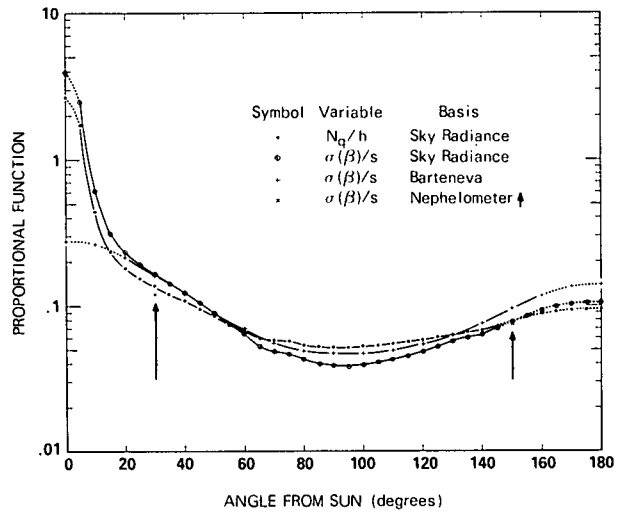

Fig. 5-4. Average proportional equilibrium radiance function and proportional volume scattering function derived from sky radiance data for the pseudo-photopic filter for flight C-360A, 923m altitude AGL.

Figure 5-4 represents the average proportional equilibrium radiance function $\bar{N}_q(z,\beta)/h(z)$ and the derived proportional volume scattering function $\sigma(\beta)/s$ as computed from the sky radiances. The standard deviation of the equilibrium radiance based on each sky radiance from this average curve was 12 percent. The $\bar{N}_q(\beta)$ curve was extrapolated to β=0 and 180 degrees from the last measured values by assuming the function log $\bar{N}_q$ linear with cosβ (the same method used by Barteneva (1960) for her volume scattering functions). The extrapolations are shown as dashed lines. Both $\int_{4\pi} N_q(\beta)/h \, d\Omega$ and $\int_{4\pi} \sigma(\beta)/s \, d\Omega$ should equal one. For these sample data the computed $\int_{4\pi} N_q(\beta)/h \, d\Omega$=1.06 and $\int_{4\pi} \sigma(\beta)/s \, d\Omega$=1.08 which is excellent agreement with theory.

The nephelometer values of total volume scattering coefficient $s(z)$, and volume scattering function at 30 degrees and 150 degrees were used in Eq. (5-7) to obtain the values indicated by an X in Fig. 5-4. The agreement of these nephelometer values with the values from the sky radiances is best for β=150 degrees.

In addition to illustrating the method of recovery of the proportional volume scattering function from sky radiance data, which in itself is an accomplishment addressing significant modelling implications, Fig. 5-4, illustrates the typical relationship of the two proportional functions, $N_q(\beta)/h$ and $\sigma(\beta)/s$. The proportional equilibrium radiance function (which on a semilog graph such as this has the same shape as the equilibrium radiance as a function of β) has a flatter shape, and less variation with β, than the proportional volume scattering function $\sigma(\beta)/s$. This is due to the additive constant component of the secondary scattering, the second term in Eq. (5-7) and (5-10).

The third curve in Fig. 5-4, depicts the values of $\sigma(\beta)/s$ derived from the Barteneva (1960) catalog of proportional volume scattering functions, as described in Section 2.1 of Duntley, *et al.* (1975). The derivation used the nephelometer values of $s(z)$, $\sigma(z,30°)$ and $\sigma(z,150°)$ in conjunction with the Barteneva catalog to obtain a complete function from β=0 to 180 degrees for use in computing equilibrium radiance and path radiance. Since in the Barteneva catalog the values at β=0, 10, 170 and 180 degrees are based on extrapolations, the curve is shown as a dashed line in these regions. There is reasonably good agreement between the two proportional volume scattering functions as denoted by the symbols O and + in the angular region based on direct measurements even though they are derived from radically different data sources, sky radiance and a catalog of nephelometer scattering functions.

This third curve also points out the lack of available information in the forward scattering angles. Although these small forward scattering angles β=0→15 degrees contribute a small portion angularly to the integration to obtain the total volume scattering coefficient s or the equilibrium radiance N_q, the uncertainty in the scattering function $\sigma(\beta)/s$ is large and worthy of further investigation.

Irradiance Effects. The irradiance terms in Eq. (5-7) for computing the equilibrium radiance are scalar irradiances. Scalar irradiance is not easily measured directly, nor is it a commonly reported value but it is readily obtainable from 4π radiance measurements made by the automatic 2π scanner system. The downwelling scalar irradiance is computed from

$$h(z,d) = {}_s h_0 T_\infty(z,\theta_s) + \int_{2\pi} N(z,\theta',\phi') d\Omega \qquad (5\text{-}11)$$

$$= {}_s h(z) + {}_k h(z,d) \, .$$

The upwelling scalar irradiance is

$$h(z,u) = \int_{2\pi} N(z,\theta',\phi') d\Omega \, , \qquad (5\text{-}12)$$

where the zenith angle range is 90→180 degrees. The scalar albedo is

$$A_s = \frac{h(z,u)}{h(z,d)} \, . \qquad (5\text{-}13)$$

The more commonly measured and reported irradiance values are the downwelling irradiance with the added cosine term as follows,

$$H(z,d) = {}_s h_o T_\infty(z,\theta_s)\cos\theta_s + \int_{2\pi} N(z,\theta',\phi')\cos\theta\, d\Omega \ . \qquad (5\text{-}14)$$

The airborne 4π radiance data provide a unique means for obtaining the sky and upwelling scalar irradiances, and scalar albedo as well as the more commonly available downwelling irradiance and albedo. Thus the airborne scanner data can provide the link between albedo and scalar albedo to determine how they differ and thus develop the linking algorithm. Similarly, the link between the more commonly available downwelling irradiance and the scalar irradiance terms can be determined from the airborne scanner data.

The airborne scanner data also may be used to obtain a measure of the variability of the downwelling irradiance with cloud cover for sensors in the visible spectrum. An example of relating cloud cover and the downwelling irradiance as predicted by the clear day illuminances of Brown (1952), is given in Section 2.3 of Duntley, *et al.* (1978c). An alternative approach would be to adapt the total solar radiation equations of Lumb (1964) to visible spectrum radiation using his cloud categories based on cloud type and cloud height.

MEASURED SKY RADIANCE VS MODELLED RADIANCE DETERMINATIONS OF EQUILIBRIUM RADIANCE

The model atmosphere equations of Gordon (1969) assume: a clear sky, no absorption, and equilibrium radiance constant with altitude. These three assumptions are reasonable for clear day sky radiances. The model equations have been used, with the proportional volume scattering functions from Barteneva's classes 1 through 7 to calculate equilibrium radiance for the photopic sensor for a range of sun zenith angle and space-to-earth transmittances.

The equation used was (Eq. (41) Gordon (1969))

$$N_q(z,\beta) = {}_s h(z)\left\{ \frac{\sigma(\beta)}{s} + \frac{A_s}{4\pi} + \right.$$

$$\left. \frac{\frac{1+A_s}{4\pi}\int_{2\pi}\left[\frac{\sigma(\beta')}{s}+\frac{A_s}{4\pi}\right]\left[1-T_\infty(z,\theta')\right]d\Omega}{1-\left(\frac{1+A_s}{4\pi}\right)\int_{2\pi}\left[1-T_\infty(z,\theta')\right]d\Omega} \right\}, \qquad (5\text{-}15)$$

where ${}_s A$ is the scalar albedo. The method of selecting the transmittances appropriate for each proportional volume scattering function was described in Section 2.2 of Duntley, *et al.* (1978c). The equation was evaluated for β=0→180 degrees for sun zenith angles 0, 20, 40, 60, 70, 80, and 85 degrees and a range of albedo.

In the Visibility Laboratory data bank of sky radiances fortunately there are several clear day data sets (for a photopic filter sensor) which contain measurements that are within ±2 degrees of the sun zenith angle, and ±.02 of the transmittances used to evaluate Eq. (5-15). The effective equilibrium radiances based upon the sky radiances in the azimuths from sun 0 and 180 degrees are available in tabular form. These are ground level data sets for which no scalar albedo are available. However, an estimate of 0.10 would not be unreasonable on the basis of a description of the terrain surrounding the data site at the Visibility Laboratory. These equilibrium radiances for the clear day data appropriate to sun zenith angle 70 ±2 degrees and space-to-earth beam transmittance 0.80 ± .02 are graphed in Fig. 5-5. The superimposed curves are evaluations of Eq. (5-15) for Barteneva (1960) scattering function classes 2, 3, 4, and 5 for θ_s=70 degrees, $T_\infty(0,0°)$=0.80 and scalar albedo 0.10. The agreement between data and model is quite good.

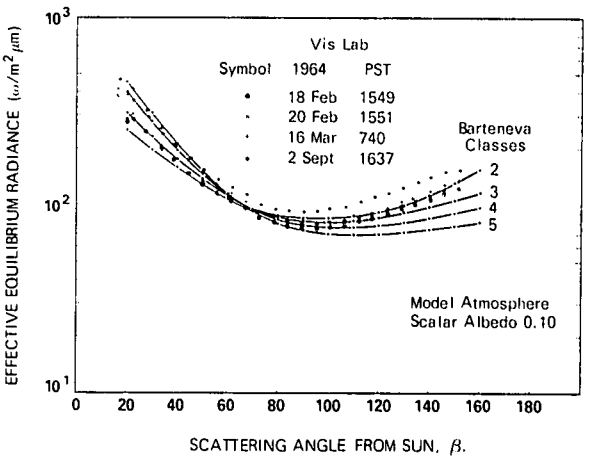

Fig. 5-5. Photopic effective equilibrium radiance from sky radiance data as a function of angle from sun for sun zenith angle 70 ±2 degrees and space-to-earth transmittance 0.80 ±.02, compared to model atmosphere calculations using Barteneva (1960) scattering functions.

The agreement between the equilibrium radiances derived from measured sky radiances and those derived from Barteneva data is sufficiently encouraging to suggest further analysis of the results of the Barteneva model atmosphere calculations for an understanding of the effects of albedo, transmittance, sun zenith angle, etc. on equilibrium radiance.

It also should be fruitful to compare the OPAQUE clear day airborne sky radiance data to calculated values obtained with Eq. (5-15) using the specific values of sun zenith angle, albedo, $s(z)$, and transmittance appropriate to each data set. The $s(z)$ would be used to determine the appropriate Barteneva $\sigma(\beta)/s$ values to be used in Eq. (5-15) as suggested in Section 5.2.

5.4 DIRECTIONAL PROPERTIES FROM PATH FUNCTION MEASUREMENTS

The path function data from the OPAQUE deployments are the first measurements of path function using the OPAQUE version of the airborne variable path function meter. Since the OPAQUE deployments contained a higher proportion of flights under cloudy and generally more marginal flying conditions than previous deployments, it was necessary to investigate more specifically the variability of the point function equilibrium radiance with altitude. The point function equilibrium radiance is equal to the path function $N_\bullet(z,\theta,\phi)$ divided by the attenuation coefficient $\alpha(z)$.. In the absence of smoke, the total volume scattering coefficient $s(z)$ is generally equal to the attenuation coefficient for sensors in the visible spectrum, therefore

$$N_q(z,\theta,\phi) = \frac{N_\bullet(z,\theta,\phi)}{s(z)} . \qquad (5\text{-}16)$$

In general the equilibrium radiance for a given path of sight varies less with altitude than either the path function or the total volume scattering coefficient. However, when the lighting is highly variable, the equilibrium radiance does not stay constant. For the OPAQUE deployment data the point function equilibrium radiance was computed from the vertical-profile flight element data using Eq. (5-16). It was determined that, although the equilibrium radiance varied with altitude under varying cloud conditions, it was generally paralleled in variation by the downwelling irradiance measured concurrently at the same altitudes. See Fig. 5-6 for an example of measured total volume scattering coefficient, measured path function, measured downwelling irradiance, and computed equilibrium radiance. The data are for flight C-390 from the OPAQUE deployment, Duntley, *et al.* (1978a). The flight was near sunset. The dramatic shift to the right of the curve for Filter 4 of path function, irradiance and equilibrium radiance are the result of an interruption in the flight ascent and the lapse of time which occurred during an intervening straight and level flight element.

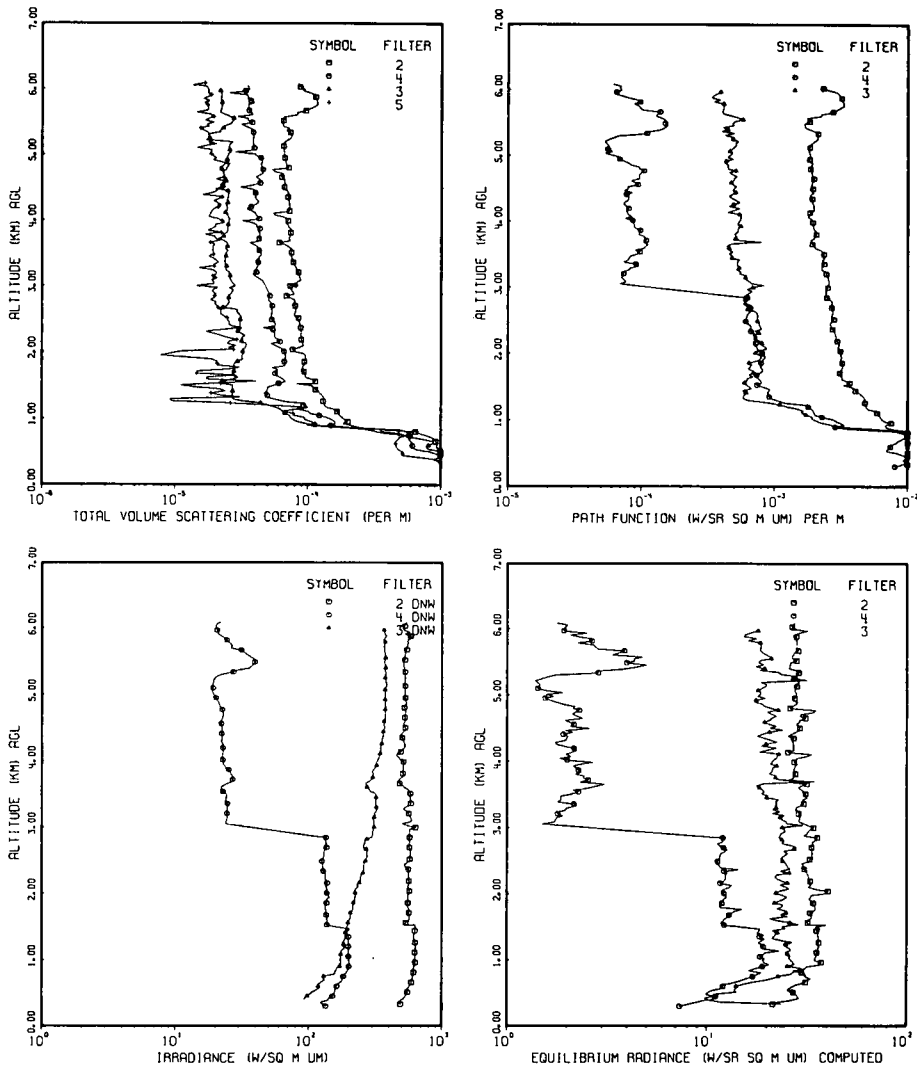

Fig. 5-6. Total volume scattering coefficient, path function, downwelling irradiance, and computed equilibrium radiance as a function of altitude for flight C-390.

The equilibrium reflectance is defined as

$$R_q(z,\theta,\phi) \equiv \frac{N_q(z,\theta,\phi)\pi}{H(z,d)} . \qquad (5\text{-}17)$$

The computed equilibrium reflectance as a function of altitude for flight C-390 is given in Fig. 5-7. The equilibrium reflectance is dramatically more constant with altitude than the equilibrium radiance for the pseudo-photopic Filter 4.

Computed equilibrium reflectance as a function of altitude is in the process of being computed and graphed for all the OPAQUE flights and the standard deviation from the average value determined in order to obtain a clearer picture of the degree of constancy of equilibrium reflectance with altitude over a large variety of lighting conditions for sensors in the visible spectrum.

This constancy with altitude of equilibrium reflectance has theoretical ramifications which lead us to suggest that the sky-ground ratio form of the contrast transmittance equation has more general applicability than to only the clear day, no cloud situation.

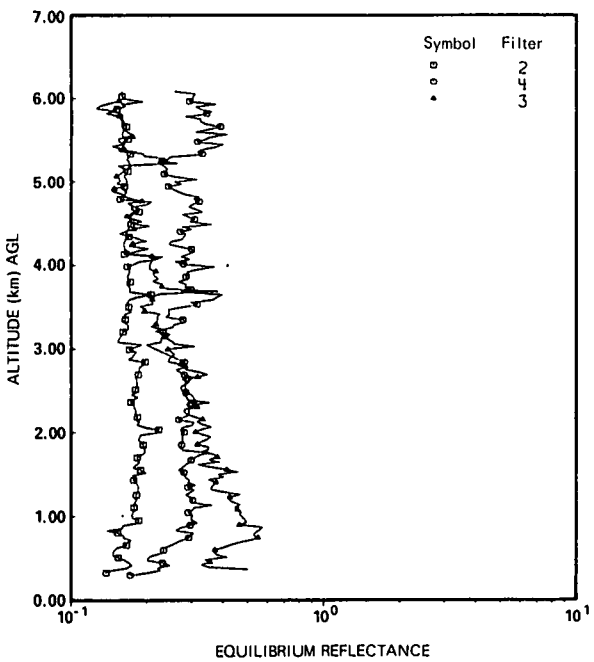

Fig. 5-7. Computed equilibrium reflectance as a function of altitude for flight C-390.

5.5 SKY-GROUND RATIO AS A MODELLING PARAMETER

When the equilibrium radiance is constant with altitude, the path radiance is a simple function of the equilibrium radiance and the radiance transmittance (Eq. (12) Gordon (1969))

$$N_r^*(z,\theta,\phi) = N_q(z_t,\theta,\phi)\left[1-T_r(z,\theta)\right] . \qquad (5\text{-}18)$$

Thus the equation for contrast transmittance Eq. (5-2) can be rewritten as (Duntley (1946) Eq. (36) Section 2 and Duntley (1948) Eq. (20))

$$\frac{C_r(z,\theta,\phi)}{C_o(z_t,\theta,\phi)} = \left[1 + \frac{N_q(z_t,\theta,\phi)\left[1-T_r(z,\theta)\right]}{{}_bN_o(z_t,\theta,\phi)\,T_r(z,\theta)}\right]^{-1} . \qquad (5\text{-}19)$$

The ratio $N_q(z_t,\theta,\phi)/{}_bN_o(z_t,\theta,\phi)$ is often referred to as the sky-ground ratio. Equation (5-19) may also be written in the form of equilibrium reflectance by dividing the numerator and denominator of the second term by $H(z_t,d)/\pi$ as follows

$$\frac{C_r(z,\theta,\phi)}{C_o(z_t,\theta,\phi)} = \left[1 + \frac{R_q(z_t,\theta,\phi)\left[T_r(z,\theta)^{-1}-1\right]}{{}_bR_o(z_t,\theta,\phi)}\right]^{-1} . \qquad (5\text{-}20)$$

where ${}_bR_o(z_t,\theta,\phi)$ is the inherent reflectance of the background.

Equation (5-20) can also be derived directly from assuming equilibrium reflectance constant with altitude. This can be theoretically demonstrated and will be the subject of an ensuing report. Since the equilibrium reflectance is constant with altitude more often than equilibrium radiance is constant with altitude, as was described in Section 5.4, Eq. (5-20) is more generally applicable. Thus Eq. (5-20) can be used for many cloudy as well as clear days for sensors in the visible spectrum.

The ratio $R_q(z_t,\theta,\phi)/{}_bR_o(z_t,\theta,\phi)$ is conceptually equivalent to the sky-ground ratio. It should be used as two separate terms, however, since the equilibrium reflectance and the background reflectance immediately surrounding the target are independent quantities. The albedo affects the equilibrium reflectance but not the background reflectance as long as the background is small in size relative to the general terrain. Similarly, the background reflectance is not the same as the albedo. A target is generally not viewed against the average reflectance of the general terrain.

The concept of sky-ground ratio established in Duntley (1948), and discussed at length by Duff (1972) is an analytically attractive, yet often misused development. Its inherent simplicity of form makes it immediately attractive to the modeller and user alike. Unfortunately, it is this simplicity which is the concept's greatest enemy. It appears so simple that the potential user is lulled into a false sense of security, and is easily led astray by his hopes for an immediate solution to his problem in contrast transmission. The key to the proper application of the concept, is in the full understanding of the sky term, that is, the equilibrium radiance (or reflectance) that appears in the numerator of the ratio.

As defined in Eqs. (5-19) and (5-20) the equilibrium radiance $N_q(z,\theta,\phi)$ or reflectance $R_q(z,\theta,\phi)$ must be determined for the same path of sight (θ,ϕ) as is

the background radiance ${}_bN_o(z,\theta,\phi)$ or reflectance ${}_bR_o(z,\theta,\phi)$. In the event this determination is by computation as implied in Duntley, *et al.* (1976), and similar reports of this series, then the directionalities contained in the 4π radiance distributions and the proportional volume scattering functions are adequately complete and thoroughly enough defined to assure proper compliance with the defining equation. If however the determination of equilibrium radiance or reflectance is attempted from measurements of clear sky horizon radiances,then the opportunity for error is enormously increased. Whereas it is true that a measure of clear sky horizon radiance is equivalent to a measure of horizontal equilibrium radiance for that particular line of sight, it is not true that this value of equilibrium radiance will necessarily be useful in Eq. (5-19) for the calculation of contrast transmittance.

The essential element in using horizon radiances as inputs to Eq. (5-19) is the proper selection with respect to the geometric scattering angle β. As noted in Duntley (1948): "It often happens that some horizontal path of sight bears the same angle with respect to the sun as does the inclined path of sight". What is equally important, and often overlooked, is that for most situations the scattering angles associated with horizontal paths of sight, will not coincide with those of downward inclined paths of sight, and thus horizon radiances cannot be used as the required equilibrium radiance input to Eq. (5-19).

The OPAQUE profile data is in most cases associated with a simultaneously measured set of 4π radiance distributions. Thus for each OPAQUE data flight, there exists a data set suitable for the determination of equilibrium radiances at all upward and downward paths of sight as well as the downwelling irradiance. It is therefore appropriate to develop from these data, a catalog of well-defined equilibrium reflectances for use in the sky-ground ratios based upon real world measurements. This relatively extensive catalog has direct applicability in vastly improving the preliminary modelling efforts reported by Huschke (1976) in the development of the RAND WETTA model algorithms.

5.6 PROMISING PREDICTIVE TECHNIQUES

One of the goals of Project OPAQUE is to develop the capability of predicting contrast transmittance in the visible on the basis of standard meteorological observations of visibility, cloud cover, temperature and pressure as a function of time. Also generally available are radiosonde measurements giving profiles of temperature and pressure as a function of altitude.

Procedures discussed in the previous sections of this report together with key sections from earlier reports, contain the necessary elements of a technique for predicting contrast transmission in the visible on the basis of these standard meteorological observations. They are summarized in the following outline:

(1) A recent report on daytime visibility (Gordon (1979)) describes the relationship between daytime visibility and the total volume scattering coefficient at ground level $s(o)$.

(2) Section 4 describes the development of a technique whereby values of total volume scattering coefficient at the base of the low level haze layer can be used with radiosonde measurements of temperature to produce a profile of $s(z)$ in the troposphere. This profile is expressed in the form of a profile of the visible scattering ratio $Q(z)$.

(3) Section 5.2 indicates that the proportional volume scattering function $\sigma(\beta)/s$ can be reasonably predicted on the basis of the visible scattering ratio $Q(z)$ from the catalog of scattering functions of Barteneva (1960).

(4) Section 5.4 describes the evidence for assuming that equilibrium reflectance can be considered constant with altitude on many cloudy as well as clear days.

(5) Section 5.5 contains the sky-ground ratio form of the contrast transmittance equation, with the sky-ground ratio in reflectance form.

(6) The downwelling illuminance for a standard clear day can be computed from the Brown (1952) illuminance curve for any time of day or night given the time, latitude and longitude. Subroutine ILLUM, developed by Drs. M. Ehrlich and Ir A. C. Van Bochove, The Netherlands, does this computation in full including the effect of moonlight. It also computes the sun and moon zenith angles.

(7) Table 2.5 of Duntley, *et al.* (1978c) indicates a preliminary relationship of cloud cover to the illuminances from Brown (1952) and Lumb (1964) relates total radiation to sun zenith angle and cloud cover, type and height. Techniques must be developed to determine downwelling illuminance for both clear and cloudy days from Subroutine ILLUM in conjunction with cloud type and cover as a function of height. These downwelling illuminances will then be used to obtain equilibrium reflectances from equilibrium radiances.

(8) Prediction of the appropriate scalar irradiances for inclusion in Eq. (5-7), for predicting equilibrium radiance from $\sigma(\beta)/s$ can probably be done from a knowledge of the downwelling illuminance as derived above and the sun and moon zenith angles. This relationship can be developed from the airborne scanner data, and the model atmosphere calculations using the Barteneva scattering functions.

6. GENERAL RECOMMENDATIONS

During the evolution of the various studies discussed in the preceding sections of this report, a consensus has developed among the several participants that are summarized here as general recommendations. The recommendations involve the development of several procedural steps, each related to the general goals outlined in Section 1, but couched within the context of maximizing modelling progress through the utilization of the most available and reliable mix of profile and surface data bases.

A. OPAQUE SURFACE DATA

The existing surface data base, as illustrated in Section 2 and discussed in Section 3, is currently too incomplete to develop broad-scale statistical-climatological studies for the European area. However, as the volume of fully processed and edited data increases, they should be quite adequate for addressing a variety of specific statistical studies as required for the development of optical/IR models. The quality of these early initial issue data sets appears inadequate for direct application to the determination of causual relationships without significant amounts of pre-analysis and editing.

The recommended course of action therefore, is to proceed first with the evaluation and partial editing of selected sub-sets of the surface data needed for meaningful analysis of optical/IR relationships. When practicable, the five to ten day sub-sets selected for analysis will be coincident in time with profile measurements made during the OPAQUE IV and V deployment intervals. The combined surface and flight data sets should then provide the primary base for application to the air-ground modelling and causual relationship studies.

B. VISIBLE-INFRARED RELATIONSHIPS

An ultimate goal of the analysis related to the OPAQUE data bases is the development of models useful in predicting the optical influence of atmospheric aerosols upon infra-red transmittances. Within the data base there are two experimental sub-sets germane to entry into the infra-red regime. They are the infra-red transmittance data and the aerosol size distribution data. Both of these sub-sets are presently extremely limited in both quantity and quality, however a fundamental approach to their use as outlined in Section 3.7 can be recommended. The recommendation is predicated upon the initial premise that atmospheric scattering due to aerosols in both the visible and infra-red regions may be adequately linked through an adequate specification of the aerosol size distribution.

The recommended course of action is therefore to develop a select library of infra-red transmittance data, which has been recalibrated via the LOWTRAN oriented calibration procedure as in the issue 5 data, whose entries are coincident with sets of airborne and surface aerosol size distribution measurements. Subsequently, re-index the library in terms of the aerosol extinction contributions and create the desired data base which associates visible spectrum scattering functions, aerosol size distribution, infra-red aerosol extinctions, and the local meteorological specifications related to aerosol source probabilities.

C. OPAQUE PROFILE DATA

The existing profile data base, as illustrated in Section 2 and discussed in Section 4, represents a statistically much smaller sample of the European environment than does the surface set, however it possesses a compensating advantage. That is, it has already been reasonably well edited and evaluated, and is therefore ready for immediate user applications. The procedures for modelling vertical aerosol scattering properties as presented in Section 4 appear adequate for straight-forward application to the entire OPAQUE profile data base and thus immediately address a primary step in the overall research plan, the prediction of vertical aerosol structure from meteorological parameters.

The recommended course of action therefore, is to proceed with the development of this modelling approach and immediately expand its application to the entire OPAQUE profile library, and subsequently to the overall profile library in order to enhance both the size and generality of the sample.

D. DIRECTIONAL PROPERTIES

The development of predictive models for atmospheric volume scattering coefficient is a

necessary but obviously insufficient accomplishment for the prediction of contrast transmittance. It is essential that the directional scattering properties of the atmosphere also be predicted. As discussed in Section 5, the elements necessary for addressing the prediction of these directional properties, at least within the visible spectrum, appear to exist plentifully within the currently available airborne data base, and to a somewhat lesser degree within the surface set. In both sets, the validation of the quantitative relationships between total volume scattering coefficient and the directional properties specified in the Barteneva catalog is the key initial element.

Assuming that the encouraging initial results on the modelling approximations for the scattering ratio profile and for the angular scattering properties are confirmed by more complete evaluation, it is important to begin parallel investigations of the other factors that determine path radiance and background radiance, as defined by Eq. (5-2). In particular, effective models are required to describe the distribution and variability of illuminance, which in turn depends upon the cloud amount and type as a function of altitude. Here again, the extensive flight data base supplemented with the surface OPAQUE data offer an excellent opportunity for forecasting technique development. In short, the wherewithal now exists for the development and validation of improved predictive models for sky-ground ratio and visible contrast transmittance over slant paths in the lower troposphere.

ACKNOWLEDGEMENTS

The studies conducted prior to and during the preparation of this report have involved talents and skills far in excess of those possessed by the authors alone. We would therefore gratefully acknowledge the contributions willingly and graciously provided by the following individuals.

Air Force Geophysics Laboratory

Dr. Robert W. Fenn, Chief, Atmospheric Optics Branch
Maj. Ted S. Cress, Atmospheric Optics Branch
Mr. Eric P. Shettle, Atmospheric Optics Branch

Visibility Laboratory

Dr. Seibert Q. Duntley, Director Emeritus
Mr. Nils R. Persson, Computer Specialist
Mr. Steven J. Bettinger, Computer Specialist
Ms. Catharine F. Edgerton, Meteorologist

7. REFERENCES

Anon, (1979), "Analysis of Reduced Visibility Data Collected under OPAQUE at Christchurch," OPAQUE N/UK-7905.

Barteneva, O. D. (1960), "Scattering Functions of Light in the Atmospheric Boundary Layer," Bull. Acad. Sci. U.S.S.R., Geophysics Series, 1237-1244.

Brown, D. R. E. (1952), *Natural Illumination Charts,* Report 374-1, Project Ns-714-100, Department of the Navy, Bureau of Ships, Washington, D. C.

Duff, Edward A. (1972), "Atmospheric Contrast Transmission Application to the Visual Detection and Electro-Optical Lock-on Problem," Thesis School of Engineering, Air University, USAF, Wright-Patterson, AFB, Ohio.

Duntley, S. Q. (1946), *Visibility Studies and Some Applications in the Field of Camouflage,* Summary Tech. Rept. Div. 16, NDRC, Columbia Univ. Press, New York, Vol. 2.

Duntley, S. Q. (1948), "Reduction of Contrast by the Atmosphere", J. Opt. Soc. Am. **38**, 179-191.

Duntley, S. Q., A. R. Boileau, and R. W. Preisendorfer (1957), "Image Transmission by the Troposphere I," J. Opt. Soc. Am. **47**, 499-506.

Duntley, S. Q. (1964), "Visibility, I. Introduction and II Summary," Applied Optics **3**, 550-556.

Duntley, S. Q. (1969), "Directional Reflectance of Atmospheric Paths of Sight," Duntley Rep. No. 69-1.

Duntley, S. Q., R. W. Johnson, and J. I. Gordon (1972a), "Airborne Measurements of Optical Atmospheric Properties in Southern Germany," University of California, San Diego, Scripps Institution of Oceanography, Visibility Laboratory, SIO Ref. 72-64, AFCRL-72-0255.

Duntley, S. Q., R. W. Johnson, and J. I. Gordon (1972b), "Airborne and Ground-Based Measurements of Optical Atmospheric Properties in Central New Mexico," University of California, San Diego, Scripps Institution of Oceanography, Visibility Laboratory, SIO Ref. 72-71, AFCRL-72-0461.

Duntley, S. Q., R. W. Johnson, and J. I. Gordon (1973), "Airborne Measurements of Optical Atmospheric Properties in Southern Illinois," University of California, San Diego, Scripps Institution of Oceanography, Visibility Laboratory, SIO Ref. 73-24, AFCRL-TR-73-0422.

Duntley, S. Q., R. W. Johnson, and J. I. Gordon (1974), "Airborne and Ground-Based Measurements of Optical Atmospheric Properties in Southern Illinois," AFCRL-TR-74-0298, SIO Ref. 74-25.

Duntley, S. Q., R. W. Johnson, and J. I. Gordon (1975), "Airborne Measurements of Optical Atmospheric Properties in Western Washington," University of California, San Diego, Scripps Institution of

Oceanography, Visibility Laboratory, SIO Ref. 75-24, AFCRL-TR-75-0414.

Duntley, S. Q., R. W. Johnson, and J. I. Gordon (1976), "Airborne Measurements of Optical Atmospheric Properties in Northern Germany," University of California, San Diego, Scripps Institution of Oceanography, Visibility Laboratory, SIO Ref. 76-17, AFGL-TR-76-0188.

Duntley, S. Q., R. W. Johnson, and J. I. Gordon (1977), "Airborne Measurements of Atmospheric Volume Scattering Coefficients in Northern Europe, Spring 1976," University of California, San Diego, Scripps Institution of Oceanography, Visibility Laboratory, SIO Ref. 77-8, AFGL-TR-77-0078.

Duntley, S. Q., R. W. Johnson, and J. I. Gordon (1978a), "Airborne Measurements of Atmospheric Volume Scattering Coefficients in Northern Europe, Fall 1976," University of California, San Diego, Scripps Institution of Oceanography, Visibility Laboratory, SIO Ref. 78-3, AFGL-TR-77-0239.

Duntley, S. Q., R. W. Johnson, and J. I. Gordon (1978b), "Airborne Measurements of Atmospheric Volume Scattering Coefficients in Northern Europe, Summer 1977", University of California, San Diego, Scripps Institution of Oceanography, Visibility Laboratory, SIO Ref. 78-28, AFGL-TR-78-0168.

Duntley, S. Q., R. W. Johnson, and J. I. Gordon (1978c), "Airborne Measurements of Optical Atmospheric Properties, Summary and Review III," University of California, San Diego, Scripps Institution of Oceanography, Visibility Laboratory, SIO Ref. 79-5, AFGL-TR-78-0286.

Engering, F. P. H. (1978), "The least square regression lines, Vol. I, II and III," Physics Laboratory of the National Defense Research Organization TNO, OPAQUE N/NL-7806.

Fenn, R. W. (1978), "OPAQUE - A Measurement Program on Optical Atmospheric Properties in Europe, Vol. I. The NATO OPAQUE Program," Special Reports No. 211, AFGL-TR-78-0011.

Fenn, R. W. and E. P. Shettle (1976), "Optical Aerosol Models and Light Scattering Programs," Proceedings of the Optical-Submillimeter Atmospheric Propagation Conference, Vol. 1, 209-218.

Gordon, J. I. (1969), "Model for a Clear Atmosphere", J. Opt. Soc. Am. **59**, 14-18.

Gordon, J. I., J. L. Harris, Sr., and S. Q. Duntley (1973), "Measuring Earth-to-Space Contrast Transmittance from Ground Stations," Appl. Opt. **12**, 1317-1324.

Gordon, J. I. (1979), "Daytime Visibility, a Conceptual Review," University of California at San Diego, Scripps Institution of Oceanography, Visibility Laboratory, SIO Ref. 80-1, AFGL-TR-79-0257.

Huschke, R. E. (1976), "Atmospheric Visual and Infrared Transmission Deduced from Surface Weather Observations: Weather and Warplanes VI," Report R-2016-PR RAND, Santa Monica.

Kohnle, A. (1979), "Barnes Calibration via LOWTRAN, some Aspects," Forschungsinstitut für Optik, Tübingen, Germany, OPAQUE N/GE-7908.

Lumb, F. E. (1964), "The Influence of Cloud on Hourly Amounts of Total Solar Radiation at the Sea Surface", Quarterly Journal of the Royal Meteorological Society **90**, 43-56.

Nilsson, B. (1979), "Meteorological Influence on Aerosol Extinction in the 0.2-4.0μm Wavelength Range", Applied Optics, Vol. 18, No. 20, 3457-3473.

Selby, J. E. A. and R. M. McClatchey (1972), "Atmospheric Transmittance from 0.25 to 28.5μm: Computer Code LOWTRAN2," AFCRL-72-0745.

Selby, J. E. A., E. P. Shettle, and R. A. McClatchey (1976), "Atmospheric Transmittance from 0.25 to 28.5μm: Supplement LOWTRAN 3B (1976), AFGL-TR-76-0258

Selby, J. E. A., F. X. Kneizys, J. H. Chetwynd, Jr., and R. A. McClatchey (1978), "Atmospheric Transmittance/Radiance: Computer Code LOWTRAN 4, AFGL-TR-78-0053.

Shand, W. A. Ed. (1978), "Barnes Intercomparison Trial-Pershore, September 1977," RSRE(C) Christchurch, Dorsett, England, OPAQUE R7804.

Shettle, E. P. (1977), "Predicted Transmission for the Barnes Transmissometer, Air Force Geophysics Laboratory, Bedford, Mass, OPAQUE N/US-7704.

Shettle, E. P. (1978), "Theoretical Transmittances for the OPAQUE Barnes Transmissometers," Air Force Geophysics Laboratory, Bedford, Mass, OPAQUE N/US-7805.

Turner, V. D. R. W. Fenn, and E. P. Shettle (1979), "Atmospheric IR Transmittance and Scattering Properties in Europe", Air Force Geophysics Laboratory, Bedford, Mass, OPAQUE N/US-7903.

Tyler, J. E., and R. W. Preisendorfer (1962), "Light," Chap. 8 in *The Sea*, M. N. Hill, Ed., Interscience Publishers, Inc., N.Y., Vol. 1, pp. 397-451.

U. S. Standard Atmosphere (1962), U. S. Government Printing Office, Washington, D.C. 20402.

van Tol, A. C. (1979), "OPAQUE Preliminary Data Analysis," Physics Laboratory of the National Defense Research Organization TNO, OPAQUE N/NL-7902.

Zardecki, A. (1979), "Analysis of the Experimental Data Base of Optical Atmospheric Quantities in Europe (OPAQUE), Laval University, P. Q. Canada, OPAQUE N/CAN-7901.

VISIBILITY LABORATORY CONTRACTS AND RELATED PUBLICATIONS

Previous Related Contracts: F19628-73-C-0013, F19628-76-C-0004

Publications:

Duntley, S. Q., R. W. Johnson, and J. I. Gordon, "Airborne Measurements of Optical Atmospheric Properties in Southern Germany," AFCRL-72-0255, SIO Ref. 72-64 (July 1972).

Duntley, S. Q., R. W. Johnson, and J. I. Gordon, "Airborne and Ground-Based Measurements of Optical Atmospheric Properties in Central New Mexico," AFCRL-72-0461, SIO Ref. 72-71 (September 1972).

Duntley, S. Q., R. W. Johnson, and J. I. Gordon, "Airborne Measurements of Optical Atmospheric Properties, Summary and Review," AFCRL-72-0593, SIO Ref. 72-82 (November 1972).

Duntley, S. Q., R. W. Johnson, and J. I. Gordon, "Airborne Measurements of Optical Atmospheric Properties in Southern Illinois," AFCRL-TR-73-0422, SIO Ref. 73-24 (July 1973).

Duntley, S. Q., R. W. Johnson, and J. I. Gordon, "Airborne and Ground-Based Measurements of Optical Atmospheric Properties in Southern Illinois," AFCRL-TR-74-0298, SIO Ref. 74-25 (June 1974).

Duntley, S. Q., R. W. Johnson, and J. I. Gordon, "Airborne Measurements of Optical Atmospheric Properties in Western Washington," AFCRL-TR-75-0414, SIO Ref. 75-24 (August 1975).

Duntley, S. Q., R. W. Johnson, and J. I. Gordon, "Airborne Measurements of Optical Atmospheric Properties, Summary and Review II," AFCRL-TR-75-0457, SIO Ref. 75-26 (September 1975).

Duntley, S. Q., R. W. Johnson, and J. I. Gordon, "Airborne Measurements of Optical Atmospheric Properties in Northern Germany," AFGL-TR-76-0188, SIO Ref. 76-17 (September 1976).

Duntley, S. Q., R. W. Johnson, and J. I. Gordon, "Airborne Measurements of Atmospheric Volume Scattering Coefficients in Northern Europe, Spring 1976," AFGL-TR-77-0078, SIO Ref. 77-8 (March 1977).

Duntley, S. Q., R. W. Johnson, and J. I. Gordon, "Airborne Measurements of Atmospheric Volume Scattering Coefficients in Northern Europe, Fall 1976," AFGL-TR-77-0239, SIO Ref. 78-3 (January 1978).

Duntley, S. Q., R. W. Johnson, and J. I. Gordon, "Airborne Measurements of Atmospheric Volume Scattering Coefficients in Northern Europe, Summer 1977", AFGL-TR-78-0168, SIO Ref. 78-28 (June 1978).

Duntley, S. Q., R. W. Johnson, and J. I. Gordon, "Airborne Measurements of Optical Atmospheric Properties, Summary and Review III", AFGL-TR-78-0286, SIO Ref. 79-5 (December, 1978).

Gordon, J. I., J. L. Harris, Sr., and S. Q. Duntley, "Measuring Earth-to-Space Contrast Transmittance from Ground Stations," Appl. Opt. 12, 1317-1324 (1973).

Gordon, J. I., C. F. Edgerton, and S. Q. Duntley, "Signal-Light Nomogram," J. Opt. Soc. Am. 65, 111-118 (1975).

Gordon, J. I., "Daytime Visibility, a Conceptual Review", AFGL-TR-79-0257, SIO Ref. 80-1 (November (1979).

Johnson, R. W., and J. I. Gordon, "Airborne Measurements of Atmospheric Volume Scattering Coefficients in Northern Europe, Winter 1978", AFGL-TR-79-0159, SIO Ref. 79-25.

APPENDIX A

GLOSSARY AND NOTATION

The notation used in reports and journal articles produced by the Visibility Laboratory staff follows, in general, the rules set forth in pages 499 and 500, Duntley *et al.* (1957). These rules are:

Each optical property is indicated by a basic (parent) symbol.

A presubscript may be used with the parent symbol as an identifier, e.g., b indicates background while t denotes an object.

A postsubscript may be used to indicate the length of a path of sight, e.g., r denotes an *apparent* property as measured at the end of a path of sight of length r, while o denotes an *inherent* property based on the hypothetical concept of a photometer located at zero distance from an object.

A postsuperscript* or postsubscript$_{*}$, is employed as a mnemonic symbol signifying that the radiometric quantity has been generated by the scattering of ambient light reaching the path from all directions.

The parenthetical attachments to the parent symbol denote altitude and direction. The letter z indicates altitude in general; z_t is used to specify the altitude of an object. The direction of a path of sight is specified by the zenith angle θ and the azimuth ϕ. In the case of irradiances, the downwelling irradiance is designated by d, the upwelling by u.

$_sA(z)$ Scalar albedo at altitude z, defined by the equation $_sA(z) \equiv h(z,u)/h(z,d)$.

$C_o(z_t,\theta,\phi)$ Inherent universal contrast determined for a path of sight of zero length at altitude of the object z_t in the direction of zenith angle θ and azimuth ϕ. This property is defined by the equation

$$C_o(z_t,\theta,\phi) \equiv \frac{{}_tN_o(z_t,\theta,\phi) - {}_bN_o(z_t,\theta,\phi)}{{}_bN_o(z_t,\theta,\phi)} .$$

$C_r(z,\theta,\phi)$ Apparent universal contrast as determined at altitude z from the end of path of sight of length r in the direction of the zenith angle θ and azimuth ϕ. This property is defined by the equation

$$C_r(z,\theta,\phi) \equiv \frac{{}_tN_r(z,\theta,\phi) - {}_bN_o(z_t,\theta,\phi)}{{}_bN_o(z_t,\theta,\phi)} .$$

$H(z,d)$ Irradiance produced by downwelling flux as determined on a horizontal flat plate at altitude z. In this report d is used in place of the minus sign in the notation $H(z,-)$ which appears in Duntley (1969). This property may be defined by the equation

$$H(z,d) \equiv \int_{2\pi} N(z,\theta',\phi')\cos\theta' d\Omega'$$

$h(z)$ Scalar irradiance. This may be defined as the radiant flux arriving at a point, from all directions about that point, at altitude z (Tyler and Preisendorfer, (1962)):

$$h(z) \equiv h(z,d) + h(z,u) .$$

$h(z,d)$ Scalar irradiance produced by downwelling flux. This may be defined as the radiant flux from the upper hemisphere arriving at a point at altitude z.

$_kh(z,d)$ Scalar irradiance defined as the radiant flux from the upper hemisphere sky (flux from the sun is not included) arriving at a point at altitude z.

$_sh(z)$ Scalar irradiance defined as the radiant flux from the sun arriving at a point at altitude z.

$h(z,u)$ Scalar irradiance produced by upwelling flux. This may be defined as the radiant flux from the lower hemisphere arriving at a point at altitude z.

$N(z,\theta,\phi)$ Radiance as determined from altitude z in the direction specified by zenith angle θ and azimuth ϕ.

$_bN_o(z_t,\theta,\phi)$ Inherent background radiance as determined at altitude of the photometer z_t at zenith angle θ and ϕ.

$_bN_r(z,\theta,\phi)$ Apparent background radiance as determined at altitude z from the end of a path of sight of length r at zenith angle θ and azimuth ϕ. This property may be defined by the equation

$$_bN_r(z,\theta,\phi) \equiv {}_bN_o(z_t,\theta,\phi)\,T_r(z,\theta) + N_r^*(z,\theta,\phi)\ .$$

$_tN_o(z_t,\theta,\phi)$ Inherent radiance of an object as determined at altitude of the photometer z_t at zenith angle θ and azimuth ϕ.

$_tN_r(z,\theta,\phi)$ Apparent radiance of an object as determined at altitude z, from the end of a path of sight of length r at zenith angle θ and azimuth ϕ. This property may be defined by the equation

$$_tN_r(z,\theta,\phi) \equiv {}_tN_o(z_t,\theta,\phi)\,T_r(z,\theta) + N_r^*(z,\theta,\phi)\ .$$

$N_q(z,\theta,\phi)$ Equilibrium radiance at altitude z with the direction of the path of sight specified by zenith angle θ and azimuth ϕ. This property is a point function of position and direction.

As discussed by Duntley, *et al.* (1957), many image transmission phenomena are most clearly understood in terms of the concept of equilibrium radiance. This concept is a natural consequence of the equation of transfer which states analytically that in any path segment the difference between the output and input radiances is attributable to a gain term and a loss term, such that some unique equilibrium radiance $N_q(z,\theta,\phi)$ must exist at each point and such that the loss of radiance within the path segment is exactly balanced by the gain, *i.e.* $\Delta N_q(z,\theta,\phi) = 0$.

By virtue of this concept and the equation of transfer, one can show that each segment of every path of sight has associated with it an equilibrium radiance, and that the space rate of change in image forming radiance caused by the path segment is in such a direction as to cause the output radiance to be closer to the equilibrium radiance than is the input radiance. This segment by segment convergence of the apparent radiance of the object field to the dynamic equilibrium radiance was clearly illustrated by the data in the 1957 paper referenced above.

$\bar{N}_q(z,\theta,\phi)$ Effective equilibrium radiance for a path of sight from out of the atmosphere to altitude z in the direction specified by zenith angle θ and azimuth ϕ. This property may be defined by the equation

$$\bar{N}_q(z,\theta,\phi) \equiv N_\infty^*(z,\theta,\phi)/[1 - T_\infty(z,\theta)]\ .$$

This property may also be denoted as a function of angle from light source (sun or moon) β, *i.e.*, $\bar{N}_q(z,\beta)$.

$N_q(z,\beta)/h(z)$ Proportional equilibrium radiance function, where

$$\int_{4\pi} \frac{N_q(z,\beta)\,d\Omega}{h(z)} = 1\ .$$

$N_\bullet(z,\theta,\phi)$ Path function at altitude z with the direction of the path of sight specified by zenith angle θ and azimuth ϕ. This property is defined by the equation

$$N_\bullet(z,\theta,\phi) \equiv \int_{4\pi} \sigma(z,\beta')N(z,\theta',\phi')\,d\Omega\ .$$

This property also is a point function of position and direction.

$N_r^*(z,\theta,\phi)$ Path radiance as determined at altitude z at the end of a path of sight of length r in the direction specified by zenith angle θ and azimuth ϕ.

$N_\infty^*(z,\theta,\phi)$ Sky radiance at altitude z, zenith angle θ and azimuth ϕ. Also the path radiance for the path of sight of length ∞ from out of the atmosphere to altitude z.

$Q(z)$ Optical scattering mixing ratio at altitude z is defined as

$$Q(z) \equiv s(z)/_R s(z)\ .$$

$Q_l(z)$ Optical scattering mixing ratio in the lower haze layer.

$Q_u(z)$ Optical scattering mixing ratio in the upper region; above the haze layer.

$_bR_o(z_t,\theta,\phi)$ Inherent background reflectance as determined at the altitude of an object z_t and viewed at zenith angle θ and ϕ.

$R_q(z,\theta,\phi)$ Equilibrium reflectance $R_q(z,\theta,\phi)$ is defined by the expression $R_q(z,\theta,\phi) \equiv N_q(z,\theta,\phi)\pi/H(z,d)$, and is an outgrowth of the equilibrium radiance concept discussed by Duntley, *et al.* (1957).

During several recent analyses of point function equilibrium radiances, computed from measurements of path function and total volume scattering coefficients, it was noted that variations in the equilibrium radiance profiles were consistently paralleled by similar variations in the measurements of downwelling irradiance. The irradiance variations, which severely influence the magnitude of the path function measurements, were caused most often by changes in the cloud conditions surrounding the flight path, and by changes in sun zenith angle due to several late afternoon flight intervals. The influence of these irradiance variations was removed from the data base by developing the reflectance form for the equilibrium condition, *i.e.* $R_q(z,\theta,\phi)$. Hence for modelling paths of sight composed of cloud free path segments, assuming equilibrium reflectance constant with altitude rather than equilibrium radiance, was shown to provide a more generally applicable concept that was appropriate for both cloudy as well as cloud free real atmospheres. A direct equivalency can be shown between the integrations of the equation of transfer in either the equilibrium radiance form as described in Gordon (1969), or the equilibrium reflectance form illustrated herein. Thus, this more generalized form is being considered as the optimum optical parameter for characterizing the atmospheric component in computations for atmospheric path radiances.

$s(z)$ Total volume scattering coefficient as determined at altitude z. This property may be defined by the equation

$$s(z) \equiv \int_{4\pi} \sigma(z,\beta)\, d\Omega \, .$$

In the absence of atmospheric absorption, the total volume scattering coefficent is numerically equal to the attenuation coefficient.

$_M s(z)$ Total volume scattering coefficient for Mie scattering at altitude z.

$_R s(z)$ Total volume scattering coefficient for Rayleigh scattering at altitude z.

$t(z)$ Ambient temperature °C at altitude z.

$T_r(z,\theta)$ Radiance transmittance as determined at altitude z for a path of sight of length r at zenith angle θ. This property is independent of azimuth in atmospheres having horizontal uniformity. It is always the same for the designated path of sight or its reciprocal.

$T_\infty(z,\theta)$ Radiance transmittance for the path of sight at zenith angle θ from out of the atmosphere to the altitude z.

Z Altitude of the top of low level haze layer.

z Altitude, usually used as above ground level.

z_t Altitude of an object.

$\alpha(z)$ Volume attenuation coefficient as determined at altitude z. In the absence of atmospheric absorption, the attenuation coefficient is numerically equal to the volume scattering coefficient.

β Symbol for scattering angle of flux from a light source. It is equal to the angle between the line from the source to the observer and the path of sight.

β' Symbol for scattering angle of flux from a discrete part of the sky. It is equal to the angle between the direction specified by θ' and ϕ' and the path of sight.

Γ Temperature lapse rate, $\Gamma \equiv -\Delta t/\Delta z$.

θ Symbol for zenith angle. This symbol is usually used as one of two coordinates to specify the direction of a path of sight.

θ' Symbol for zenith angle usually used as one of two coordinates to specify the direction of a discrete portion of the sky.

σ Symbol for volume scattering function. Parenthetical symbols may be added; for example, β may be used to designate the scattering angle from a source. In Gordon (1969) the parenthetical symbols are z and β for altitude and scattering angle.

$\sigma(z,\beta)/s(z)$ Proportional directional volume scattering function. This may be defined by the equation

$$\int_{4\pi} [\sigma(z,\beta)/s(z)]\, d\Omega \equiv 1.$$

ϕ Symbol for azimuth. The azimuth is the angle in the horizontal plane of the observer between a fixed point and the path of sight. The fixed point may be, for example, true north, the bearing of the sun, or the bearing of the moon. This symbol is usually used as one of two coordinates to specify the direction of a path of sight.

ϕ' This symbol for azimuth is usually used as one of two coordinates to specify the direction of a discrete portion of the sky.

Ω Symbol for solid angle.

For a hemisphere: $\Omega = 2\pi$ steradians;

For a sphere: $\Omega = 4\pi$ steradians.

NOTATIONAL EQUIVALENCIES

OPAQUE Notation	OPAQUE Units*	Quantity Description	VisLab **Units	VisLab Notation
σ_E	km^{-1}	Extinction Coefficient	km^{-1}	α
σ_S	km^{-1}	Scattering Coefficient	km^{-1}	$s(z)$
E_h	lux	Horizontal Illuminance	$w/m^2\mu m$	$H(z,d)$
E_v	lux	Vertical Illuminance		-
F_p^E	$Cd/m^2 \cdot m$	Path Luminance (day, east)	$w/\Omega m^2 \mu m \cdot m$	$N_*(z, 90°, \phi)$
L_p^{NT}	Cd/m^{2***}	Path Luminance (night)	$w/\Omega m^2 \mu m \cdot m$	$N_*(z, 90°, \phi)$
T	%	Radiance Transmittance	%	$T_r(z,\theta)$

* OPAQUE optical quantities are measured using photopically corrected sensors and are thus reported in photometric units. Ref: Fenn (1978), AFGL-TR-78-0011

** VisLab optical quantities are measured using a variety of spectrally selective filters and are thus reported in radiometric units. Ref: Duntley, *et al.* (1976), AFGL-TR-76-0188

*** Normalized to 100m path length

Additional abbreviations commonly utilized within this report are defined in Tables 2.1, 2.2 and 3.5